Intensification of Liquid-Liquid Contacting Processes

By

Zheyan Qiu

Submitted to the Department of Chemical and Petroleum Engineering and the Faculty of Graduate School of the University of Kansas in partial fulfillment of the requirements for the degree of Doctor of Philosophy

Committee Members

Dr. Laurence Weatherley, Committee Chair

Dr. Cory Berkland

Dr. Aaron Scurto

Dr. Kyle Camarda

Dr. Belinda Sturm

08/20/2010
Date defended

The Dissertation Committee for Zheyan Qiu certifies that this is the approved version of the following dissertation:

Intensification of Liquid-Liquid Contacting Processes

Committee Members

Dr. Laurence Weatherley, Committee Chair

Dr. Cory Berkland

Dr. Aaron Scurto

Dr. Kyle Camarda

Dr. Belinda Sturm

08/20/2010
Date Defended

Abstract

In order to improve mass transfer rate and efficiently employ energy in liquid-liquid contacting processes, especially in biodiesel production through transesterification, two process intensification technologies were addressed based on two different energy sources and were investigated in this dissertation. They include electrostatic liquid spraying based on electric field and a two-disc spinning disc reactor based on high gravity field.

Interfacial turbulence plays an important role in electrically enhanced mass transfer. One specific aspect of this work was to investigate interfacial turbulence which can occur at the interface between two phases because of interfacial tension gradients resulting from the change of charge density across droplet surface. Firstly, a Schlieren optical technique was developed and the experimental setup was built for the visualization of electrically induced interfacial phenomena in the ethanol-water-1-decanol system. Two Schlieren cells were designed and fabricated, and were successfully used for the interrogation of interfacial disturbances in pendant droplets and at plane interfaces. The mechanism of interfacial turbulence was further understood by study of these Schlieren images. Additionally, interfacial mass transfer in the ethanol-water-1-decanol system was investigated in the presence of electric fields and mass transfer coefficients were measured from the pendant droplets. Initial results show that a time-dependent nature was presented and mass transfer was intensified by the application of electric fields.

As an alternative biofuel, biodiesel is produced through transesterification of vegetable oils, fat and algae lipids and alcohol with the help of acid or base. Transesterification is a liquid-liquid two phase reaction, whose rate is limited by mass transfer between oil and alcohol due to their immiscibility. This work firstly applied electrostatic liquid-liquid

contactors to improve biodiesel synthesis. The reaction rate of transesterification of canola oil with sodium methoxide was investigated in the plane interface contactor. A fourfold enhancement was observed at an applied voltage of 10kV DC. A compact electrostatic spraying reactor based on simple tubular geometry with horizontal injection of an electrostatic spray of sodium methoxide was developed to achieve continuous biodiesel production. Preliminary data demonstrate it is a promising technology.

A novel two-disc spinning disc reactor was developed as another alternative for biodiesel synthesis. It comprises two flat discs, located coaxially and parallel to each other with a very small gap between the discs. A grooved rotating disc was integrated to increase residence time allowing relatively slow transesterification reaction to be as complete as possible. The reaction performance was investigated widely. The conversion achieved in the reactor was significantly influenced by the size of inter-disc gap, the rotational speed, the canola oil phase flowrate, the surface topography of the rotating disc, and the reaction temperature. The experimental conditions were optimized. Finally, the new reactor was also compared with the stirred tank reactor according to the data of conversion rates and droplet size distribution of the emulsions.

Acknowledgements

I would like to offer thanks to my advisor, Dr. Laurence Weatherley, for providing continuous support and guidance in research and study. His mentorship and insight will continue to inspire me both personally and professionally.

I would like to acknowledge Drs. Cory Berkland, Jerzy Petera, Aaran Scurto and Kyle Camarda, Belinda Sturm for serving on my dissertation committee and for their valuable time, helpful guidance and critical of this Ph.D. dissertation. A special acknowledge also goes to Dr. Cory Berkland for his encouraging and supporting me to take comprehensive exam. I would also like to thank those who have provided guidance and assistance toward this dissertation project over the years, which include Mr. Alan Walker and Mr. Scott Ramskill for their assistance in building experimental setups, Dr. Trung Van Nguyen for providing space in his lab during the early period of my projects, Dr. Michael Michnik for his earnest help in experiment, Dr. Russ Ostermann and Dr. Jenn-Tai Liang for providing access to the facilities in their labs.

I greatly acknowledge funding from the Transportation Research Institute. I would like to thank Staya Aravind Gangu for the exchange of ideas and his assistance with the experiment equipment purchase.

Finally, I want to thank my mother, my parents-in law and my sister for the unconditional support over the past years. My special thanks go to my wife, Lina Zhao, for her unselfish love and support over ten years. None of this could be accomplished without her encouragement and care. I also would like to thank my daughter, Emma Qiu, who offers so much happiness to my life. I love them deeply.

Table of Contents

List of Figures

Chapter 1

Chapter 2

Chapter 3

Chapter 4

Chapter 5

Chapter 6

Chapter 7

No Figures

Appendix

List of Tables

Chapter 1 Introduction

1.1 Liquid-Liquid Contacting

Many chemical processes including solvent extraction and liquid-phase reactions involve liquid-liquid systems. The efficient contact between two immiscible liquid phases is of importance for these processes to improve production capacity, and reduce process cost and equipment size. The mixing intensity and mixing rate determine the degree of contacting of the two phases. The performance of liquid-liquid contacting in mixers, extraction devices and chemical reactors can play key roles in mixing, transport (momentum, mass and heat transfer) across the phase boundary, and the rate of chemical reaction. For solvent extraction, separation is achieved by the transport of a desired component from one liquid phase into the other, known as interphase mass transfer [1]. Contact area or interfacial mass transfer area of two liquid phases is a key factor in determining mass transfer rate. This is in addition to the magnitude of the concentration gradient of the extracted component between the two phases and the magnitude of mass transfer coefficient. In addition, interfacial turbulence or convection driven by interfacial tension gradients can make a significant contribution to mass transfer rate [1]. To ensure good performance it is important to enhance contact and contact area between the two phases and decrease resistance to mass transfer in extraction devices. In liquid-liquid reactions, immiscible reactants must be transferred from one phase to another or contact intimately with each other before reaction happens, and this mass transfer can become the limiting step. It is desired that mass transfer rate can be increased to a level allowing the reactions to be limited only by intrinsic-reaction kinetics [2]. Therefore, it is very important for liquid-liquid two phases to obtain good contacting and mixing in solvent extraction processes as well as in chemical reactions.

Physical contact and mass transfer between liquids are greatly enhanced when the liquids are intimately mixed together. Conventionally, mixing can be realized by mechanical stirring or dispersion. Bulk stirring is able to provide the chance for liquid molecules to contact one another after sufficient time has elapsed. However, the process is very slow. These contacts can be improved by establishing small-scale liquid structures or eddies within which molecular diffusion becomes significant [2]. Creating these small-scale liquid structures (micromixing) is the role of the mixing and mass transfer equipment and the reactors associated with it.

Moreover, in order to generate and improve mixing or mass transfer, these mixing and mass transfer devices or the reactors must therefore direct energy into a liquid system in the correct way [2]. In a stirred tank reactor (STR) the energy input clearly comes from an impeller, but this arrangement suffers from high energy losses through friction and macro-agitation, mere recirculation of liquids, and other factors. The energy employed is focused mainly upon the liquid in contact with the impeller, particularly with its leading edges. Forced, molecular inter-diffusion can only occur along the leading edges. This means that the majority of the liquid is not undergoing forced molecular inter-diffusion, and the average power input across the whole tank producing conversion is low(e.g. 0.1-1W/kg) [2].

Numerous studies have been done to improve mixing or mass transfer process in liquid-liquid systems. For example static mixers may involve pipework fitted with fixed internal flow diverters and obstacles to promote mixing [3]. The large amount of energy that can be supplied by pumps goes into the whole of the liquid. In this way, higher average power inputs (100W/kg) can be achieved [2]. In rotor-stator mixers, the proportion of the liquid volume in contact with the rotor surface is much higher [2]. The mixing process occurred in

the above mixers is relatively fast compared with that in stirred vessels, where the mixing times (the time to achieve a predefined level of homogeneity of a tracer in a mixing vessel) of these mixers are estimated in the range of ~10 to ~100 milliseconds. To further decrease the mixing time, the mixing scale between the liquids must get smaller to allow less time for the liquids to smooth the segregation between each other [4]. In the last ten years, micro mixer has been proposed to promote the mixing and mass transfer process, in which the mixing of the reactants occurs in ~10 to ~100 micrometer wide channels [5]. In a micro mixer, due to the reduced spatial scales or diffusional path the mixing times can reach milliseconds and mass transfer is accelerated. All of the above equipment lies within the scope of process intensification technologies, which are discussed in detail below.

1.2 Process Intensification

Process Intensification (PI) is a strategy which aims to accomplish process miniaturization, reduction in capital cost, improved inherent safety and energy efficiency and often improved product quality [6]. The concept was pioneered in Imperial Chemical Industries (ICI) during the late 1970s, when the primary goal was to reduce the capital cost of a production system. ICI developed HiGee technology, which employs rotating equipment as a replacement for much larger separation systems [7]. Ramshaw, one of the pioneers of the field, first defined process intensification as a strategy for making dramatic reductions in the size of a chemical plant so as to reach a given production objective when the 1st International Conference on Process Intensification in the Chemical Industry opened in 1995[8]. While cost reduction was the original objective for PI, it quickly became apparent that there were other important benefits, particularly in respect of improved intrinsic safety, reduced environmental impact and energy consumption. Given the anticipated plant volume

reductions, the toxic and flammable inventories of intensified plant are correspondingly reduced, thereby making a major contribution to intrinsic safety. The most telling environmental influence of PI could well be in the development of new reactor designs which give high selectivity. This would facilitate delivery of a high quality product with a marked cut in wastes or byproduct formation. Improved performance of PI technologies could achieve high energy efficiency and decrease in energy consumption by the enhancement of transport rates and the combination of reaction and separation. Process intensification can lead to compact, safe, energy-efficient, and environmentally-friendly sustainable processes.

Process intensification consists of two areas: engineering methods and equipment as shown in Figure 1.1 [9]. Process-intensifying equipment is composed of novel reactors or apparatus for non-reactive processes. The former include spinning disc reactors, static mixer reactors, monolithic reactors, microreactors, rotating packed-bed reactors and jet-impingement reactors. The latter includes some intensive mixers (static mixers and rotor/stator mixers) and mass/heat transfer devices (compact heat exchangers, rotating packed beds). Static mixers which combine mixing and transport of fluids through pipelines, were first patented by Shell and later commercialized by Sulzer and others [10]. Process-intensification methods are relevant to many applications including multifunctional reactors, hybrid separations, and techniques using alternative energy sources and supercritical fluids. Multifunctional reactors enhance the chemical conversion and aim to integrate reactions and downstream operations into a single unit. Examples of multifunctional reactors include membrane reactors, reactive distillation, reactive extraction, reactive crystallization, etc. Reactive distillation is an early type of process intensification. It was used by Eastman Chemical Co. for the esterification of methanol to methyl acetate in a tower reactor with a

liquid-phase catalyst [11]. Many of the developments in hybrid separations involve combination of membranes with another separation technique. These PI technologies include membrane absorption and stripping, membrane distillation. Absorptive distillation is a type of hybrid separation technology not involving membranes.

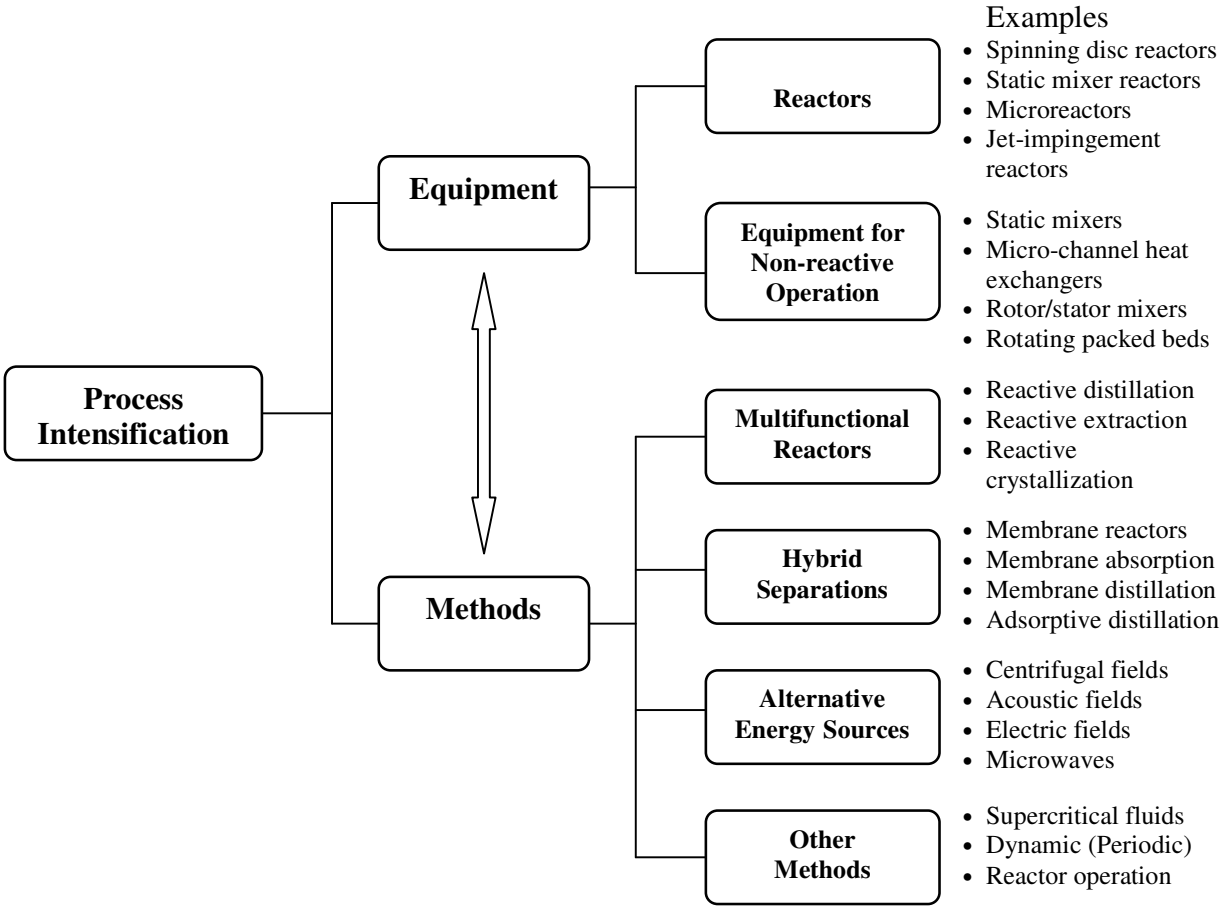

Figure 1.1 Process intensification and its components [9]

Alternative energy sources, which some PI technologies rely on include centrifugal fields, acoustic and flow fields, microwaves, solar energy, electric fields and plasma. Table 1.1 gives a summary of these alternative energy sources [12]. HiGee technology uses high centrifugal forces which greatly accelerates mass transfer of a two-phase system (liquid/liquid or liquid/vapor). This allows large distillation columns to be replaced with much smaller equipment. The first known example of commercial use was reported in 1997

in the Shengli oil field in China, where 1.5-m-dia. rotating strippers replaced 30-m-high vacuum towers for the deaeration of water [13]. In 2001, Dow Chemical Co. used the HiGee

Table1.1 Alternative energy sources of process intensification [12]

Energy sources	Application	Intensified element	Possible magnitude of intensification (Approx.)
High gravity field	Spinning disc reactor	Liquid-side mass transfer	10 times
		Liquid-side heat transfer	15 times
		Reaction time	1000 times
		Equipment size	100 times
		Impurities level	>90%
	Rotating packed bed	Liquid-side mass transfer	200 times
		Gas-side mass transfer	9 times
Electric field	Liquid-liquid extraction	Mass transfer	10 times
		Heat transfer	3 times
		Interfacial area	500 times
	Boiling liquids, evaporator	Heat transfer	10 times
Microwave	Liquid-phase catalytic reaction	Reaction time	1250 times
		Product yield	10%
	Gas-phase catalytic reaction	Product yield	Several times
	Distillation	Distillation time	20 times
Light	Photocatalytic reaction	Product yield/selectivity	Several times, in some cases 100% selectivity can be achieved
Acoustic field	Ultrasonic irradiation	Reaction time	25 times
		Product yield	In some cases 100% yield of product can be synthesized
		Gas liquid mass transfer	5 times
	Low frequency acoustics	Liquid solid mass transfer	20 times
		Gas solid mass transfer	3 times
		Gas liquid mass transfer	2 times
Flow	Hydrodynamic cavitation	Reaction time and product yield	Similar as with ultrasound, however 10 times higher cavitational yield for same energy input
	Supersonic flow	Gas liquid mass transfer coefficient	10 times
		Fluid bed reactor capacity	2.25 times

concept in a rotating packed-bed reactor in its hypochlorous acid process [14]. Centrifugal force produced in spinning disc reactors produces a very thin wavy film (typically 100 μm) resulting in high transfer rates [15]. Cavitational reactors have been developed based on the use of acoustic fields and flow in order to intensify chemical processes [16]. Electric fields can also augment process rates and control droplet size for a range of processes, including painting, coating, and crop spraying. In these processes, the electrically charged droplets exhibit much better adhesion properties. Electric fields also can enhance processes involving liquid/liquid mixtures, in particular liquid/liquid extraction [17] where rate enhancements of 200–300% have been reported [18].

Application of the new methods outlined above may require novel types of equipment to be developed and vice versa, while novel apparatuses already developed sometimes make use of new, unconventional processing methods. My interest will focus on spinning disc reactors and electrically intensified technologies, especially electrostatic liquid spraying.

1.3 Motivation and Goals

Biodiesel is a renewable fuel, which is mainly produced by transesterification of vegetable oils with alcohol in the presence of base or acid catalysts. The reaction takes place in a liquid-liquid two phase system and its reaction rate is limited by mass transfer due to immiscibility of oils and alcohol. The efficiency of the contact between the feed oil and the alcohol/catalyst reaction mixture is crucial to achieving a high rate of reaction and achievement of an economic reactor size. In view of this, process intensification technologies can be applied to enhance liquid-liquid contacting, increase mass transfer rate during transesterification processes. Hence, the overall objective of this dissertation was to develop novel intensive liquid-liquid contacting processes, and to explore the feasibility of these

novel process intensified technologies for efficient biodiesel production through alkai-based catalyzed transesterification. Two novel technologies were addressed to intensify contact between liquid-liquid two phases based on two different energy sources. They include electrostatic liquid spraying based on electric field and a two-disc spinning disc reactor based on high gravity field.

First, Chapter 2 reviews the current situation with respect to biodiesel production in the world, and the technical background to the alkali-based transesterification reaction, including the reaction mechanism, reaction kinetics, and phase behavior. A detailed review of some of process intensification technologies being developed for intensive biodiesel synthesis is also presented. These technologies include various novel reactors and relevant coupled reaction/separation processes.

One of the process intensification techniques which are the focus of the thesis is enhancement of liquid-liquid contact in the presence of electrostatic fields. One specific aspect studied is the promotion of interfacial turbulence (Marangoni phenomena) which can occur at the interface between two phases because of interfacial tension gradients resulting from the change of charge density across droplet surface [19, 20]. Interfacial turbulence is one of the important factors involved in electrically enhanced mass transfer. Therefore, the first aim was addressed to validate experimentally the intensified mass transfer for a real liquid-liquid system. One task is to visualize the interfacial turbulence which is anticipated in the vicinity of the liquid-liquid interfaces. The liquid-liquid interfaces being investigated involve pendant droplets and plane interfaces. The other is to investigate the mass transfer from a pendant electrically charged droplet and occurred at the plane interface in the presence of electric fields. In order, Chapters 3 and 4 serve to address the aim. In Chapter 3, a

Schlieren optical system was designed, fabricated and used to record visibly electrically induced interfacial turbulence happened in the acetone-water-1-decanol system. In Chapter 4, experimental methods were developed to measure interfacial mass transfer from a pendant liquid droplet and across a plane interface when electric fields were applied.

Chapter 5 focuses on the exploration of feasibility of a novel intensification technology based on electrostatic liquid spraying for efficient biodiesel production. In this chapter, a novel intensive electrostatic contactor was developed and its performance was investigated initially, some existing problems about the electrostatic spraying process for biodiesel production were also mentioned.

Chapter 6 highlights a modified spinning disc reactor used for intensified biodiesel synthesis. The performance of the new reactor was evaluated and the experimental parameters affecting transesterfication reaction and biodeisel yield were studied and optimized. A comparison between the new spinning disc reactor and stirred tank reactor was present.

Chapter 7 is the conclusion, where summarizes some results in a global context. Some possible correct direction and further works can be pursued in the future are discussed.

1.4 References

1. J.D. Thornton, Science and practice of liquid –liquid extraction, Volume 1, Phase equilibria; mass transfer and interfacial phenomena; extractor hydrodynamics, selection and design, Clarendon Press, Oxford, (1992).
2. A. Green, B. Johnson, A. John, Process intensification magnifies profits, Chemical Engineering, Dec., (1999) 66-73.

3. W.F.C. Van Wageningen, D. Kandhai, R.F. Mudde, H.E.A. van den Akker, Dynamic flow in a kenics static mixer: an assessment of various CFD methods, A.I.Ch.E. Journal, 50 (2004) 1684.
4. J. Baldyga, J.R. Bourne, Turbulent mixing and chemical reactions, Wiley, New York, (1999).
5. V. Hessel, H. Lowe, F. Schonfeld, Micromixers-a review on passive and active mixing principles, Chem. Eng. Sci. 60 (2005) 2479.
6. M. Vicevic, R.J. Jachuck, K. Scott, Process intensification for green chemistry: rearrangement of α-pinene oxide using a catalysed spinning disc reactor (SDR), BHR Group process intensification, (2001) 201-213.
7. C. Ramsha, HiGee distillation- an example of process intensification, Chem. Engr. – Lodon, 389 (1983) 13-14.
8. The incentive for process intensification, Proceedings, 1st Intl. Conf. Proc. Intensif. For Chem. Ind., BHR Group, London, 18 (1995) 1.
9. A. I. Stankiewicz, J.A. Moulijn, Process intensification: transforming chemical engineering, Chem. Eng. Pro., 96 (2000) 22-34.
10. Mixing and reaction technology, Sulzer Chemtch, Winterthur, Switz, (1997).
11. J.J. Siirola, An industrial perspective on process synthesis, AIChE Symposium Series, 304 (1995) 222-233.
12. A. Stankiewicz, Energy Matters: Alternative sources and forms of energy for intensification of chemical and biochemical processes, Chem. Eng. Res. Des., 84 (2006) 511-521.

13. C. Zheng, Industrial practice of HIGRAVITREC in water deaeration, Proceedings of the 2nd international conference on process intensification in practice, BHR Group, London, 28(1997) 273-287.
14. D. Trent and D. Tirtowidjojo, Commercial operation of a rotating packed bed (PBR) and other applications of PBR technology, Proceedings of the 4th international conference on process intensification for chemical industry, BHR Group, Cranfield, UK, (2001) 11-19.
15. S. Thomas, A. Faghri, and W. Hankey, Experimental analysis and flow visualization of a thin liquid film on a stationary and rotating disk, ASME J. Fluids Eng., 113 (1991) 73.
16. P.R. Gogate, A.B. Pandit, Hydrodynamic cavitation: a state of the art review, Rev. Chem. Eng. 17 (2001) 1-85.
17. L. R. Weatherley, Electrically enhanced mass transfer, Heat Recov. Sys. & CHP, 13 (1991), 515-537.
18. M. Yamaguchi, Electrically aided extraction and phase separation equipment, in liquid-liquid extraction equipment, J. C. Godfrey and M. J. Slater, eds., Wiley, New York,(1994) 585-624.
19. G. Stewart and T.D. Thornton, Charge and velocity characteristics of electrically charged droplets. Part I. Theoretical considerations, Int. Chem. Engng. Symp. Ser., 26(1967a) 29-36.
20. G. Stewart and T.D. Thornton, Charge and velocity characteristics of electrically charged droplets. Part II. Preliminary measurements of droplet charge and velocity, Int. Chem. Engng. Symp. Ser., 26(1967b) 36-41.

Chapter 2 Biodiesel Production and its Process Intensification Technologies

2.1 Worldwide Biodiesel Production and Capacity

In order to reduce the dependency on imported oil and deal with high oil price, in recent years more countries are focusing interest on biofuels production from biomass. Biodiesel is a clean alternative diesel fuel and can reduce air pollution [1]. What's more important is that it can be used without modification in engines currently in use [2]. In view of these advantages, biodiesel has experienced a major surge worldwide in the 21st century. Figure 2.1 shows worldwide biodiesel production and installed capacity from 2002 to 2008. Global biodiesel installed capacity has been increased from 2.2 million tons in 2002 to 32.6 million tons in 2008. Accordingly, the annual production capacity has risen from 1.8 million tons in 2002 to 11.1 million tons in 2008. The worldwide biodiesel market is estimated to reach 37 billion gallons by 2016 growing at an average annual rate of 42 percent [3]. The European Union has been the global leader in biodiesel production. Its production capacity occupies over 50% of worldwide production totals as shown in Figure 2.2. The United States is secondary to the E.U. in biodiesel production. Figure 2.3 presents the U.S. biodiesel production data over the 10 years from 1999 to 2009. The United States has increased its production from 0.5 million gallons in 1999 to 545 million gallons in 2009 although there was a reduction in 2009. The most notable growth was between 2004 and 2006 when sales increased ten-fold to 250 million gallons. The annual production capacity has reached 2.69 billion gallons per year in 2009 [6].

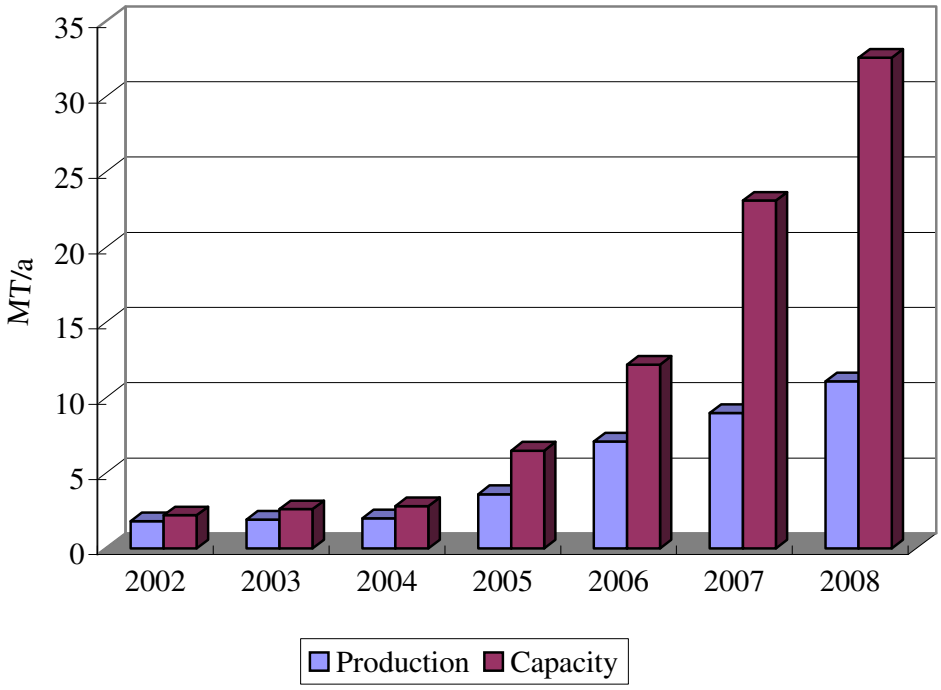

Figure 2.1 Worldwide biodiesel production and installed capacity from 2002 to 2008[3]

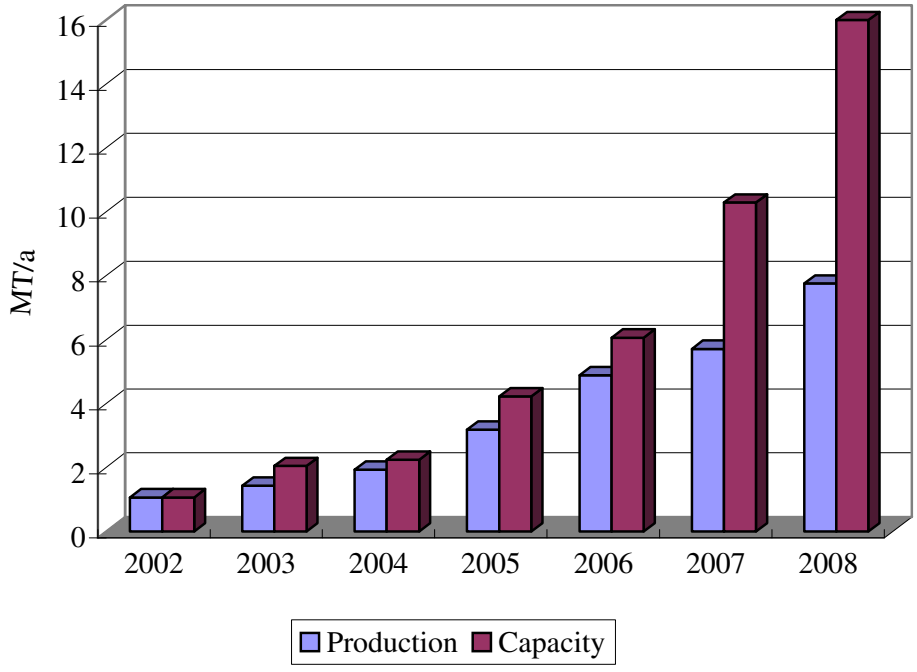

Figure 2.2 E.U. biodiesel production and installed capacity from 2002 to 2008 [4]

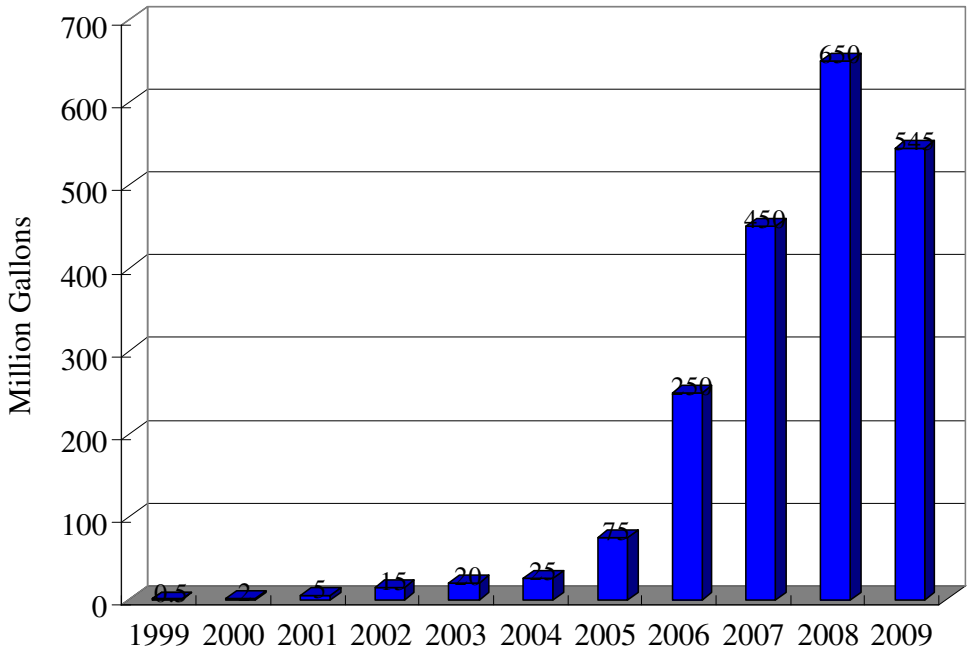

Figure 2.3 U.S. biodiesel sales between 1999 and 2009[5]

2.2 Alkali-based Transesterification Reaction

Biodiesel is a mixture of fatty acid alkyl esters. It is biodegradable, nontoxic, and essentially free of sulfur and aromatics. The majority of commercial biodiesel is made by transesterification of vegetable oils and animal fats with methanol or ethanol in the presence of base or acids catalysts. First, transesterification is a liquid-liquid two phase reaction. Reaction rate can be limited by mass transfer between the oils and alcohol because they are immiscible. Second, vegetable oils and animal fats are typically made of triglycerides which are esters of free fatty acids with the trihydric alcohol, glycerol. During the transesterification of triglyceride (TG), there are three stepwise and reversible reactions with intermediate formation of diglycerides (DG) and monoglycerides (MG) resulting in the production of 3 mol of methyl esters (ME) and 1 mol of glycerol (GL) per mole of triglyceride as follows [7]. Hence, there is an upper limit to conversion in the absence of product removal and excess

alcohol. These reactions are shown in Figure 2.4 and Figure 2.5. The molar ratio of alcohol to triglyceride, catalyst type, reaction time and reaction temperature can affect the transesterification at the different levels [8]. For oil feedstock, rapeseed and soybean oils are most commonly used today, though other crops such as mustard, palm oil, hemp, jatropha, and even algae show promise. In the USA, soybean oil is the primary resource used to produce biodiesel. In Europe, rapeseed oil and sunflower oil are the main feedstocks for biodiesel. The relatively high prices of these vegetable oils make the resulting biodiesel unable to compete with petroleum-based diesel. Their use for biodiesel synthesis might drive up their prices. Additionally, the growing of crops for biodiesel feedstocks requires substantial agricultural land areas. Recycled cook oils and animal fats can be used for the biodiesel feedstock, but they are limited in quantity and cannot meet the requirement for the increased scale of production required to make a significant impact on overall supply. Algae is a very good candidate because it has a much higher oil yield per acre, (as high as 10,000 gallons per acre) than other plant-oil crops including soybean (48 gallons per acre) and its culturing does not compete with these crops in farmland [9, 10]. However, it takes a long time before it can be feasible for the biodiesel feedstock because there are some challenges with large-scale production including effective growing, and economically feasible extraction of lipids from algae, etc.

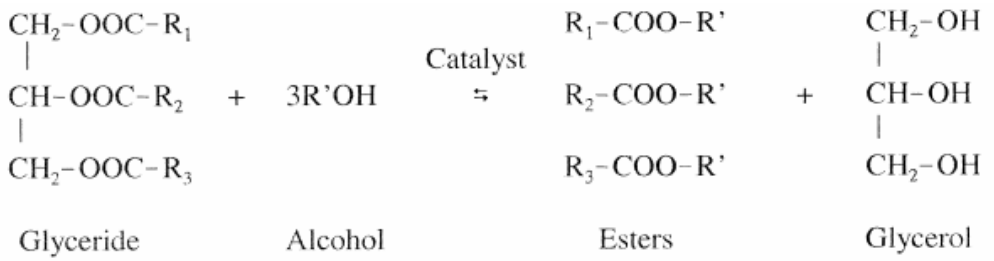

Figure 2.4 Overall transesterification reaction of triglycerides with alcohol, where R´OH-alcohol; R_1, R_2, and R_3-long chain alkyl groups

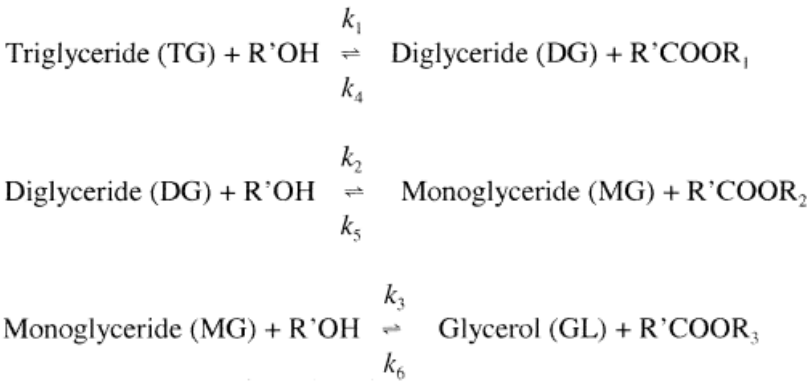

Figure 2.5 Stepwise transesterification reactions of triglycerides with alcohol [7]

2.2.1 Reaction Mechanism of Alkali-catalyzed Transesterifcation

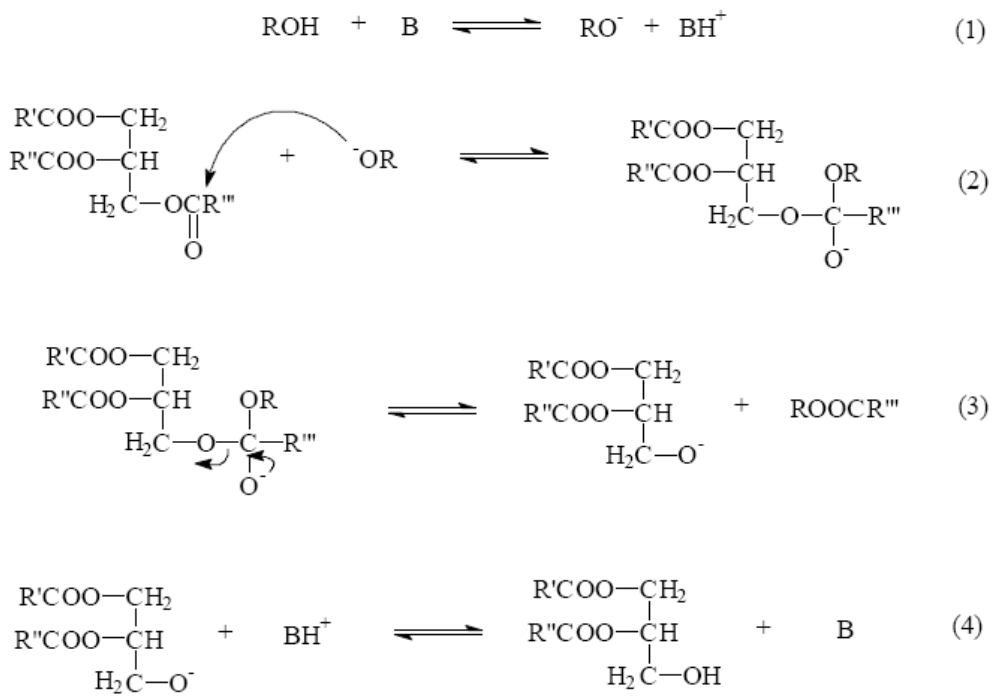

Figure 2.6 Mechanism of the base-catalyzed transesterification of vegetable oils, where B-base; ROH-alcohol; R´, R˝, and R˝´-long chain alkyl groups [11,12]

The mechanism of the base-catalyzed transesterification of vegetable oils is shown in Figure 2.6[11, 12]. The first step (Eq. 1) is the reaction of the base with the alcohol, producing an alkoxide and the protonated catalyst. The nucleophilic attack of the alkoxide at

the carbonyl group of the triglyceride generates a tetrahedral intermediate (Eq. 2), from which the alkyl ester and the corresponding anion of the diglyceride are formed (Eq. 3). The latter deprotonates the catalyst, thus regenerating the active species (Eq. 4), which is now able to react with a second molecule of the alcohol, starting another catalytic cycle. Diglycerides and monoglycerides are converted to a mixture of alkyl esters and glycerol by the same mechanism.

2.2.2 Kinetics of Alkali-catalyzed Transesterification of Vegetable Oils

There are three consecutive and reversible reactions during transesterification. Freedman *et al.* [7] first investigated the kinetics of the transesterification of soybean oil (SBO). They determined how some variables including type of alcohol, molar ratio of alcohol to SBO, catalyst type and reaction temperature affected kinetic order, reaction rates and energies of activation. Simultaneously, rate constants were determined for each reaction with a computerized kinetic program. Forward reactions appear to be pseudo-first order or second order depending upon conditions used. Reverse reactions appear to be second order. At a molar ratio of MeOH/SBO of 6:1, a shunt reaction was observed where 3mol MeOH directly attacked 1mol TG resulting in rapid appearance of esters without the appearance of intermediate DG and MG. The values of energy activation ranged from 8 to 20 kcal/mol.

Darnoko *et al.* [13] studied the kinetics of transesterification of palm oil with methanol in a batch reactor in the presence of potassium hydroxide. The rate of transesterification in a batch reactor increased with temperature up to 60°C. Higher temperatures did not reduce the time to reach maximal conversion. The conversion of TG, DG and MG appeared to be second order up to 30 mins of reaction time. Reaction rate constants for TG, DG and MG hydrolysis reactions were 0.018 -0.191 (wt % @ min)-1, and were higher at higher

temperatures and higher for the MG reaction than for the TG hydrolysis. Activation energies were: 14.7, 14.2 and 6.4 kcal/mol for the TG, DG and MG hydrolysis reactions, respectively. The optimal catalyst concentration was 1% KOH.

TG and alcohol phases are immiscible and form two liquid layers upon their initial introduction into the reactor. Mechanical mixing is normally applied to increase the contact between the reactants, resulting in an increase in mass transfer rate. Therefore, it is very important to study how the mixing intensity affects the kinetics of the transesterification reaction. Noureddini and Zhu [14] investigated the effects of variations in the mixing intensity and temperature on kinetics of transesterification of SBO with methanol. During the reaction, the molar ratio of methanol to triglycerol (6:1) and the concentration of catalyst (0.2wt% of SBO) were held constant. The variations in mixing intensity appeared to affect the reaction similar to the variations in temperature. A reaction mechanism consisting of an initial mass transfer-controlled region followed by a kinetically controlled region was proposed. The experimental data of Noureddini and Zhu for the latter region seemed to fit a second-order kinetic mechanism.

2.2.3 Phase Behavior of Alkali-catalyzed Transesterification

During the transesterification, the reaction mixture passes from a biphasic (methanol and oil) system to a biphasic (methyl ester-rich and glycerol-rich) system. These phase transitions affect the kinetics and steady-state position of the reactions, which are critical for making standard biodiesel fuels. There is little available information on the phase behavior during transesterification, and hardly any studies are available on the effect of phase transitions on the reaction kinetics. One reason is that the glycerol-rich phase is relatively small and colorless and is not easy to be observed, particularly in stirred reactions.

Zhou and Boocock [15] investigated the phase behavior during transesterification by visualization of the different stages of the transesterification of TG in the form of soybean oil (SBO) using a polar dye. Simultaneously, they studied the effect of the initial mixing time on the phase behavior of transesterification. For methanolysis, the minimum mixing time that was required to achieve a rapid and sustained reaction was approximately 3 min. After 3 min of mixing in methanolysis, the glycerol-rich phase continued to settle, resulting in a distinct phase at the bottom of the tube in 10 min. The settling was essentially complete after 40~60 min. In methanolysis, the MG and DG appeared to be reacting faster than the TG, such that the TG concentration stayed above those of the other two. They proposed that the MG and DG, which carry –OH groups, could more easily access the polar glycerol-rich phase, which contained most of the catalyst as well as some methanol. The TG, on the other hand, preferred to be in the less polar ester-rich phase where reaction was negligible.

Phase distribution of methanol, glycerol, and catalyst in the transesterification of soybean oil was investigated by Zhou and Boocock [16]. At 23°C, for methanolysis it was found that 42.0% of the alcohol, 2.3% of the glycerol, and only 5.9% of the catalyst were present in the ester-rich phase at steady state starting with an initial condition of 6:1 alcohol/oil molar ratio and catalyst concentration (1.0 wt% sodium methoxide).

2.3 Process Intensification Technologies in Continuous Biodiesel Production

Most of the biodiesel produced today uses the base-catalyzed transesterification reaction, which needs low temperature and pressure, yields high conversion with minimal side reactions and reaction time. However, the vegetable oil and alcohol must be substantially anhydrous [17] and have a low FFA content because the presence of FFA promotes soap

formation. The soap formation partially consumes the catalyst, lowers the yield of esters and renders the downstream separation of the products difficult [8]. A conventional biodiesel production process is shown in Figure 2.7.

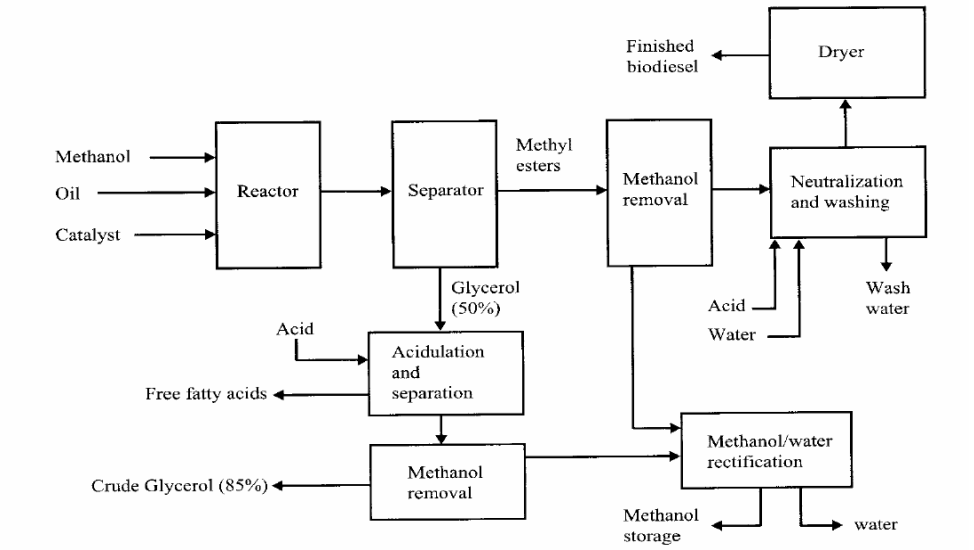

Figure 2.7 General process flow schematic for biodiesel production via base catalyzed transesterification [18]

The whole process consists of reaction followed by downstream processing. Reaction usually takes place in a continuous stirred tank reactor (CSTR) where the alcohol and catalysts are added into oil in a predetermined molar ratio and catalyst concentration. Following the reaction, the glycerol is removed from the methyl esters. Generally, this separation may be accomplished with either a settling tank or a centrifuge due to the low solubility of glycerol in the esters. Water may be added to the reaction mixture after the transesterification is complete to improve the separation of glycerol. Then, the excess methanol is recycled from methyl ester and glycerol phases for reactant by a vacuum flash process. In order to obtain the desired products, methyl ester and glycerol streams need additional processing procedures including neutralization and water washing in the end. The current conventional

techniques involve long residence time, high molar ratio of alcohol to oil and catalyst concentration, and most of them are run in a batch mode and thus do not gain some of the advantages of continuous operation. Long residence times and downstream processing time incur low production efficiency. High cost and energy consumption are involved in order to recover excess amounts of alcohol and catalyst, and to deal with the resulting significant amounts of toxic waste water during downstream processing. In recent years, some process intensification technologies have been developed and applied to improve mixing and mass/heat transfer between the two liquid phases. These technologies either utilize novel reactors or coupled reaction/separation processes. Reaction rate is greatly enhanced and thus residence time may be reduced.

2.3.1 Novel Reactors

- **Static Mixers**

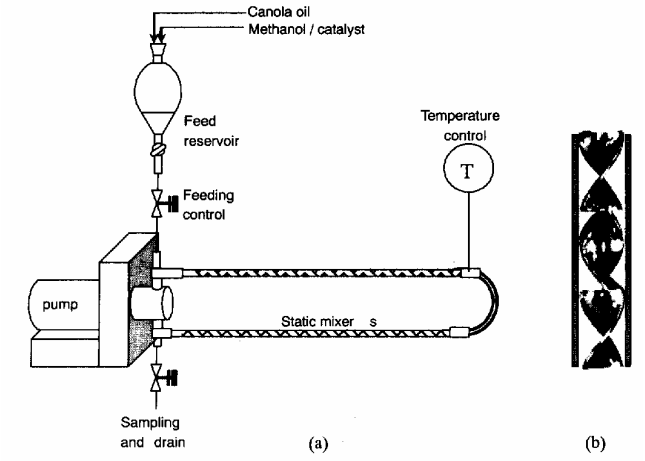

Figure 2.8 Experimental setup: (a) static mixer closed-loop system, and (b) internal structure of static mixers [21]

Static mixers consist of specially designed motionless geometric elements enclosed within a pipe or a column and create effective radial mixing of two immiscible liquids as they

flow through the mixer. Recently, they have been used in continuous biodiesel synthesis in combination with other equipment [19, 20].

Thompson *et al.* [21] used a stand-alone closed-loop static mixer system as a continuous flow reactor to produce biodiesel from canola oil with methanol when sodium hydroxide was used as catalyst. The experimental setup is shown in Figure 2.8. The system is composed of two stainless steel static reactors (4.9mm ID $\times$300 mm long) including 34 fixed right- and left-hand helical mixing elements. High quality biodiesel which met the ASTM D6584 specification was obtained after optimization of experimental conditions. The most favorable conditions for completeness of reaction included operation at a temperature of 60^{o}C and using a concentration of 1.5% sodium hydroxide catalyst and a reaction time of 30 min. The total glyceride content was lower than 0.24%wt when the molar ratio of methanol to oil is 6:1. Boucher *et al.* [22] also reported a reactor/separator design involving a static mixer for continuous biodiesel production and product separation as shown in Figure 2.9. Pretreated waste canola oil and the solution of potassium hydroxide in methanol flow into a static mixer, which was exploited as an injector into a reaction chamber with no moving parts. Emulsified reactants were released into the chamber from the mixer with decreasing bulk velocity and separated into two phases under laminar flow conditions in the main body of the reactor. The less dense biodiesel phase separated as an upper layer. The glycerol phase, which had a higher density, settled as the lower layer. This required that the bulk flow velocity be set to a value which was lower than the settling velocity of glycerol. The new reactor system obtained conversions greater than 99% with simultaneous removal of 70-99% of the glycerol after 6 hr continuous running. This was achieved at slightly elevated temperatures (40-50^{o}C), using an overall feed rate of 1.2 L/min, a 6:1 molar ratio of methanol to vegetable oil

triglycerides, and a 1.3 weight % catalyst. Static mixers present the advantage of low maintenance and operating cost and low space requirement because they have no moving parts. However, the mixing process relies mainly on slow, unforced molecular inter-diffusion in the laminar regime and therefore reactions are still slow.

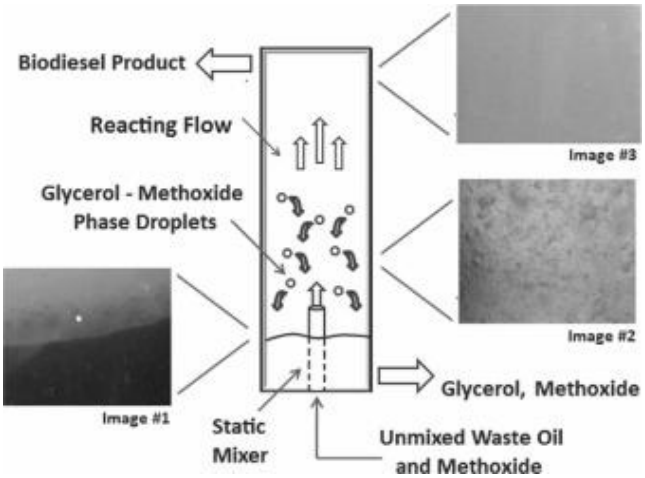

Figure 2.9 Diagram of a laminar flow reactor/separator [22]

- **Microchannel Reactors**

Microchannel reactors achieve rapid reaction rates by improving the efficiency of heat and mass transfer and utilizing high surface area/volume ratio and short diffusion distance [23]. Canter *et al.* [24] reported that biodiesel could be produced in a microreactor at mild conditions. Yields of greater than 90% biodiesel after a residence time of 4 minutes were reported. Sun *et al.* [25] studied KOH-catalyzed transesterification of unrefined rapeseed oil and cottonseed oil with methanol in capillary microreactors with inner diameters of 0.25 mm. At a 5.89 minutes residence time, they obtained a 99.4% yield of methyl esters at a catalyst concentration of 1wt% KOH and using a 6:1 molar ratio of methanol to oil and at a temperature of 60^{o}C. Finally, Wen *et al.* [26] investigated zigzag microchannel reactors for continuous alkali-based biodiesel synthesis. The configuration of zigzag microchannel reactors with narrower channel size and more turns is shown in Figure 2.10. This type of

reactor was shown to intensify the biodiesel production process by obtaining smaller droplets compared to those microchannel reactors with T- or Y- flow structures. At a residence time of 28s and a temperature of 56^{o}C, the yield of methyl ester reached 99.5% in an optimized zigzag micro-channel reactor using a 9:1 molar ratio of methanol to oil and a catalyst concentration of 1.2wt% sodium hydroxide. Under these conditions it was reported that less energy consumption was needed for the same amount of biodiesel than in the case of a conventional stirred reactor. This was attributed to the high heat transfer rates achieved in the micro-channel reactor. The micro-channel reactor is smaller in size offering reductions in footprint requirements, construction and operating costs. Another advantage of microchannel reactors is ease of scale-up which may be readily achieved by adding more reactors of the same proven dimensions in parallel. This approach can reduce the risks associated with scaling up of conventional reactors.

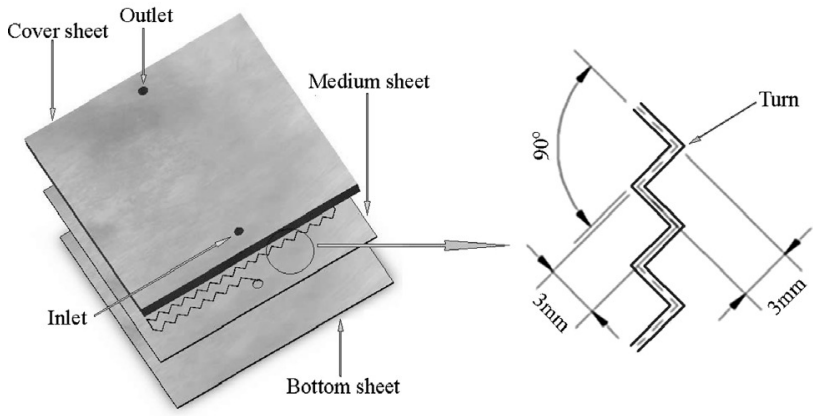

Figure 2.10 Representative configuration of a zigzag micro-channel reactor [26]

- **Oscillatory Flow Reactors**

Oscillatory flow reactors are tubular reactors in which orifice plate baffles are equally spaced and produce oscillatory flow using a piston drive as shown in Figure 2.11. When a bulk fluid is introduced into the reactor, an oscillatory motion interacts with it and intensifies

radial mixing, with enhancements in mass and heat transfer whilst maintaining plug flow. The reactor can achieve long residence times because the degree of mixing is not directly dependent upon the Reynolds number of the bulk flow through it, but is mainly related to the oscillatory conditions. Hence the oscillatory flow reactor can be designed with a short length-to-diameter ratio and improves the economy of biodiesel production due to smaller "footprint", lower capital and pumping cost, and easier control. Harvey et al [27] developed a continuous oscillatory flow reactor (OFR) to produce saleable biodiesel from rapeseed oil in a pilot-scale plant shown in Figure 2.12. The reactor is composed of two vertically positioned jacketed QVF tubes of 1.5m length and 25mm internal diameter. Conversions of biodiesel up to 99% were achieved after 30 min at 50^{o}C using a molar ratio of methanol to rapeseed oil of 1.5 and in the presence of a sodium hydroxide catalyst. Another biodiesel pilot plant using an oscillatory flow reactor was demonstrated by the Polymer Fluids Group in the University of Cambridge [28]. It has been in operation since 2004 and producing at a rate of 25liters/hour.

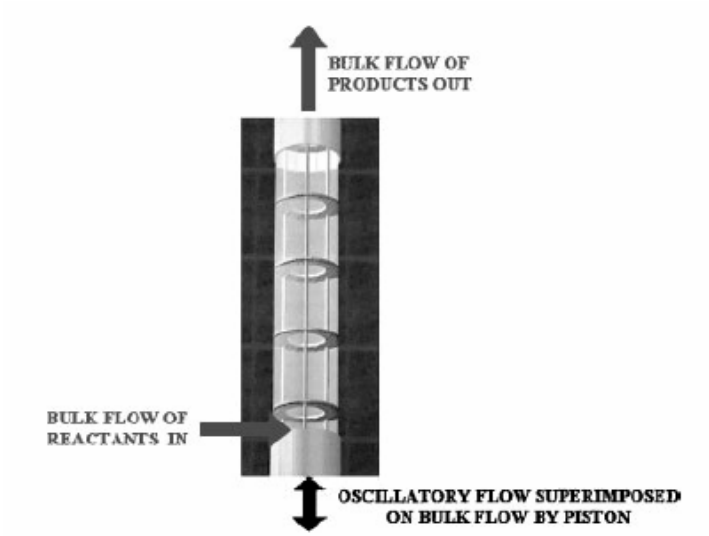

Figure 2.11 Configuration of an oscillatory flow reactor [27]

One of the advantages of this technology is the very low molar ratio of methanol to oil they applied. It is lower than the stoichiometric ratio (3:1) required and reduces significantly the operating cost. The short length to diameter of this reactor decreases capital cost and allows it to be scaleable.

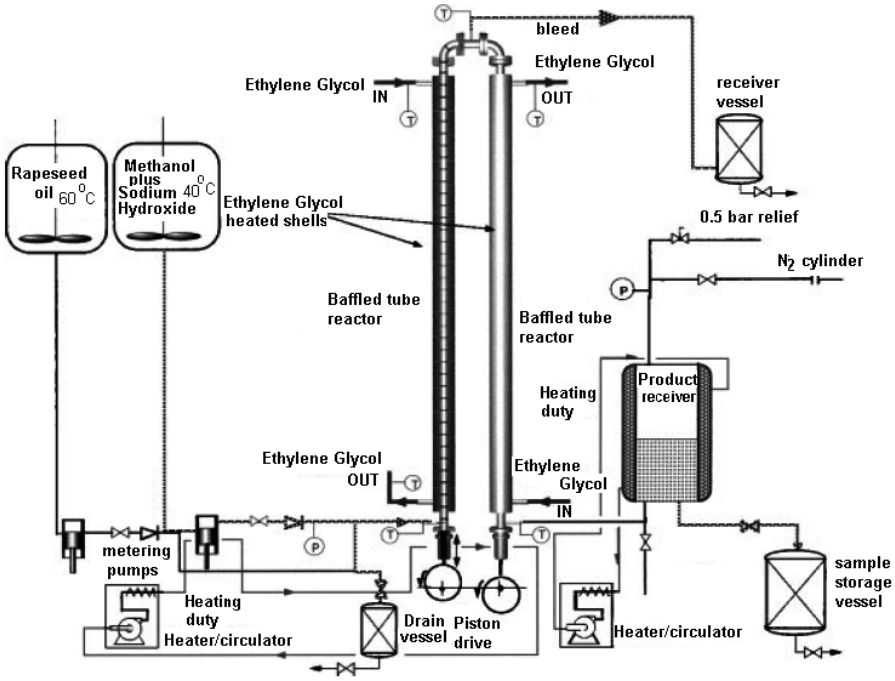

Figure 2.12 Schematic of an oscillatory flow reactor for biodiesel production [27]

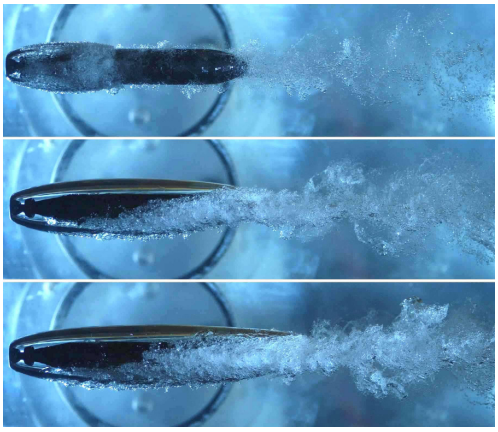

Figure 2.13 Picture of hydrodynamic cavitation [30]

- **Cavitational Reactors**

Cavitational reactors use acoustic energy or flow energy to generate cavitation phenomena, which results in process intensification. During the process of cavitation, the violent collapse of the cavities produced by the pressure changes from sound and flow energy releases large magnitude of energy over a small location, and brings about very high temperatures and pressures [29]. A picture of hydrodynamic cavitation is shown in Figure 2.13. Cavitation also intensifies the mass transfer rate by generation of local turbulence and liquid micro-circulation in the reactor [31, 32]. All of them contribute to the intensification of processes which under other conditions are limited by mass transfer and heat transfer. Kelkar *et al.* [33] investigated two different reactors based on acoustic and hydrodynamic cavitation and compared their performance in biodiesel synthesis from vegetable oils. At a reaction time of 15 min, more than 90% yield of biodiesel was obtained during transesterification of vegetable oils with methanol in the presence of sodium hydroxide in these two reactors. From the point of view of energy efficiency of mixing, hydrodynamic cavitation (1×10^{-4} to 2×10^{-4} g/J) is about 40 times more efficient than acoustic cavitation (5×10^{-6} to 2×10^{-5} g/J) and 160–400 times more efficient than conventional mixing methods [33]. Moreover, it is difficult for sonochemical reactors to be scaled up because acoustic cavitation relies on a source of vibrations. The scale-up of the hydrodynamic cavitation reactors is relatively easier and thus they provide potential for commercial scale applications because extensive information about the fluid dynamics downstream of the constriction is readily available [34, 35].

Arisdyne System, Inc. [36] used controlled flow cavitation (CFC) technology to produce higher grade ASTM 6751 B100 biodiesel as shown in Figure 2.14. The reactor consisted of

one or more controlled flow cavitation zones or flow constrictions achieved by a diaphragm with one or more orifices. The pressure drop across the constrictions is controlled by the size of orifices, the flow rate of reaction mixture and, by a localized hydraulic resistance downstream of the constriction. Precise process control ensures a tightly controlled, repeatable droplet size distribution by cavitation during the process. The conversion of fatty acids to fatty acid alkyl esters reached 99% after passing through four cavitation constrictions in series with 1:6 molar ratio of fatty acids to methanol at 60^{o}C only in residence time of microseconds.

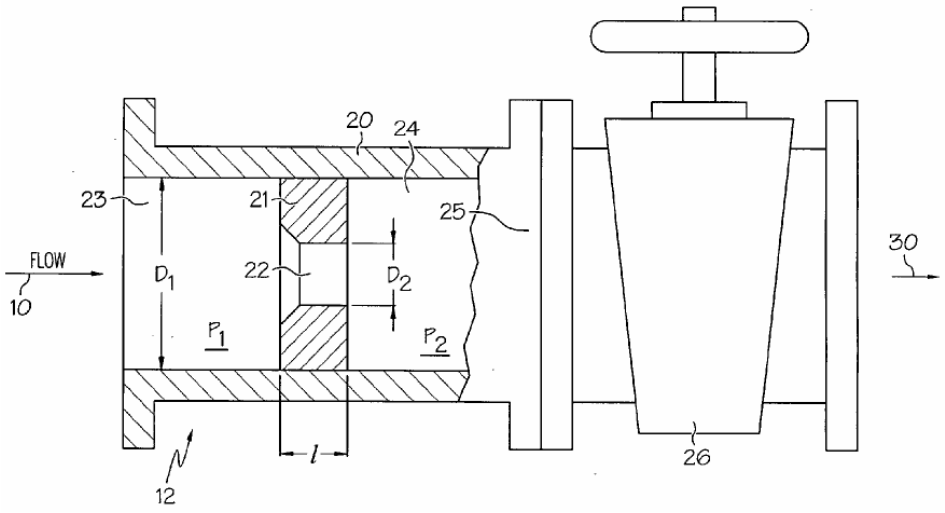

10 reaction mixture; 12 controlled cavitation apparatus; 20 flow-through channel; 21 localized flow constriction; 22 orifice; 23,24 chamber; 25 outlet; 26 localized hydraulic resistance; 30 reaction production

Figure 2.14 Schematic of a biodiesel process using a controlled flow cavitation apparatus [36]

Another reactor design which uses the principle of cavitational mixing is described by Hydro Dynamics, Inc. [37]. Here a ShockWave Power Reactor (SPR) based on “controlled cavitation” is described for process intensification of the transesterification reaction in

biodiesel production. A commercial SPR is shown in Figure 2.15. One difference between the SPR and above the controlled flow cavatiation reactor is the mechanism of producing flow cavitation. The ShockWave Power Reactor works by taking a feedstock, methanol and catalyst, into the machine housing, where it is passed through the generator's spinning cylinder. The specific geometry of cavities in the cylinder and rotational speed creates pressure differences within the liquids where tiny bubbles form and collapse. The cavitation is controlled so that the bubbles collapse only inside the cavities and away from the metal surfaces and therefore reduce the risk of damaging the material of construction. The shock waves increase the surface area of the compounds being mixed so that a higher mass transfer rate occurs. It takes only several seconds to complete transesterification of vegetable oils or animal fats. Hence, the reactor allows the use of a variety of feedstocks with a broader range of free fatty acid concentrations because short reaction time leads to less saponification and emulsification.

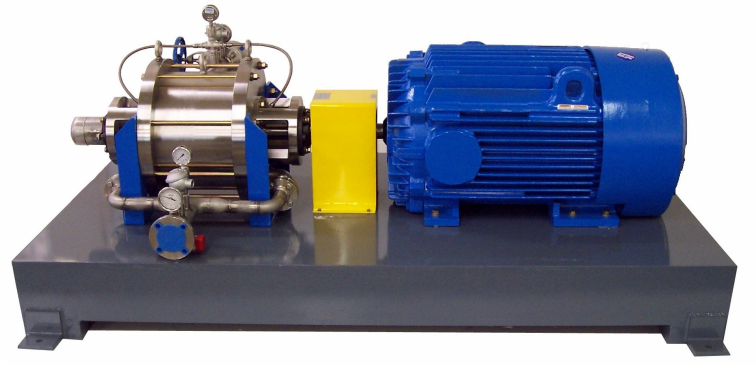

Figure 2.15 A commercial SPR reactor for biodiesel production developed by Hydro Dynamics, Inc. [38]

- **Rotating/Spinning Tube Reactors**

The Rotating, or Spinning tube reactor is a shear reactor consisting of two tubes. A scheme of the rotating tube reactor is shown in Figure 2.16. One inner tube rotates rapidly

within another concentric stationary outer tube. There is a very narrow annular gap between the outer tube and the inner tube. Once reactants are introduced into the gap, Couette flow is induced and the two liquids are mixed instantaneously and move through the gap as a coherent thin film due to the high shear rate. Couette flow leads to high mass transfer rate and very short mixing time. The thin film presents a very large interfacial contact area. Hence, the rate of reaction between reactants is enhanced. Less reaction time and mixing power input are required compared to conventional reactors.

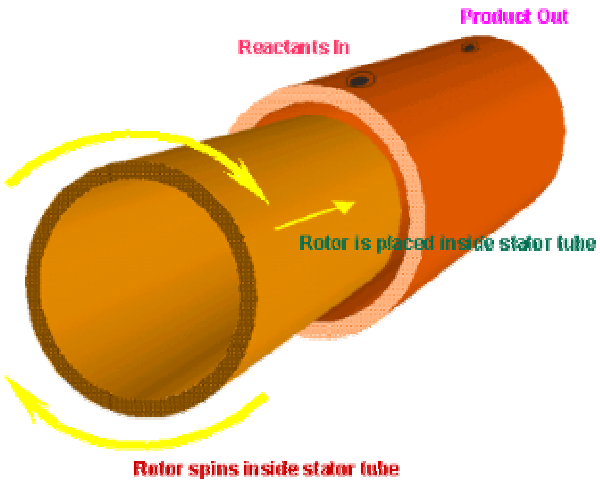

Figure 2.16 Schematic of a spinning tube reactor [39]

Four Rivers BioEnergy Company, Inc [40] utilized the technology and developed a commercial Spinning Tube in a Tube (STT) system for biodiesel production as shown in Figure 2.17. The STT reactor accelerates the rates of chemical reactions by up to three orders of magnitude. The transesterification reaction of soybean oil and methanol for biodiesel production is conducted at a residence time of 0.5 seconds.

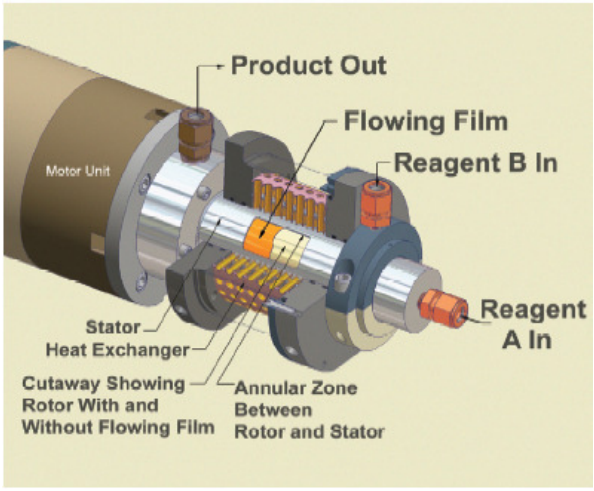

Figure 2.17 Spinning Tube in a Tube (STT) system developed by Four Rivers BioEnergy Company, Inc [40]

Lodha *et al.* [41] investigated a rotating tube reactor to produce biodiesel from canola oil with sodium hydroxide as catalyst. Within 40 seconds, conversions to biodiesel greater than 98% were attained under mild operating temperatures in the range 40-60^{o}C, and at atmospheric pressure. The short residence time allows this reactor to handle feedstocks with high free fatty acid content. The size of the reactor is relatively small and it is easy to scale up.

- **Microwave Reactors**

Microwave reactors are units that utilize microwave irradiation to transfer energy directly into reactants and thus accelerate the rate of chemical reaction. Thus conversions are achieved in less time compared with similar reactors using conventional thermal heating. Recently, microwave reactors have been developed for biodiesel synthesis. Because the mixture of vegetable oil, methanol, and alcohol contains both polar and ionic components, microwave irradiation can play an active role in heating reactants to the required temperature quickly and efficiently [42]. Breccia *et al.* [43] studied the transesterification of commercial

seed oils with methanol under microwave irradiation. In the presence of a variety of catalysts, yields greater than 97% were achieved with reaction times of less than 2 minutes. Leadbeater *et al.* [44] used microwave irradiation to enhance production of biodiesel in a batch reactor. They made biodiesel with a quantitative conversion obtained after heating vegetable oil, methanol (1:6 molar ratio) and potassium hydroxide (1wt%) to 50^{o}C in a microwave apparatus called MARS and maintaining this temperature for one minute. Finally, they [42] achieved continuous-flow preparation of biodiesel in the apparatus. The apparatus could produce approximately 6.1 L of biodiesel per minute with attainment of 99% conversion. Rudimentary energy consumption studies showed that the continuous-flow preparation of biodiesel using microwave heating proved to be more energy efficient than the conventional synthesis of biodiesel in large tank reactors. Leadbeater *et al.* [45] also used this apparatus to make biodiesel from vegetable oils and 1-butanol at flow rates up to 2.3L/min with sulfuric acid or potassium hydroxide as catalyst. Azcan *et al.* [46] reported that reaction times of transesterification of cottonseed oil with methanol by microwave irradiation were reduced to 7 min while conventional heating typically required reaction times of 30 min to obtain similar conversion at 60^{o}C. In experiments to study microwave assisted transesterification of rapeseed oil in the presence of 1.0% KOH, 93.7% of biodiesel yield and 97.8% of biodiesel purity were obtained at 50 ^{o}C using a 5 min reaction time [47].

With the exception of the microwave reactor all the above novel reactors intensify the biodiesel production process by improving the mixing of oil and methanol. In addition to the geometric configuration of mixers the mixing intensity of static mixers depends on the flow rate of the reactants (or superficial velocity). The mean droplet size was 63 μ m in a static mixer when the superficial velocity was 1.3m/s [48]. In the micro-channel reactor, the droplet

size of emulsion decreases and the specific interfacial area increases and hence reaction rate is enhanced greatly compare to the batch stirred reactors. Mean droplet sizes of down to 1.93 μm were reported in a zigzag micro-channel reactor at a residence time of 28 s, approximately one third that observed in a batch stirred reactor at the residence time of 1 h [26]. The degree of mixing is also dependent on the oscillatory motion or the oscillatory frequency and is not related to the bulk flow. The oscillatory Reynolds number of typically 700 is required to achieve good mixing [27]. Cavitational reactors utilizing ultrasonic mixing produced the minimum droplet size of about 140 nm, which is three times smaller than the droplets obtained with impeller at 1,000 rpm at the same input energies [49]. In spinning tube reactors, high mixing intensity is achieved through the high shear forces created in the narrow gap between the stator and the rapidly spinning rotor. The droplet sizes from cavitational reactors and spinning tube reactor are relatively smaller than other reactors.

2.3.2 Reaction/Separation Coupled Technologies

- **Membrane Reactors**

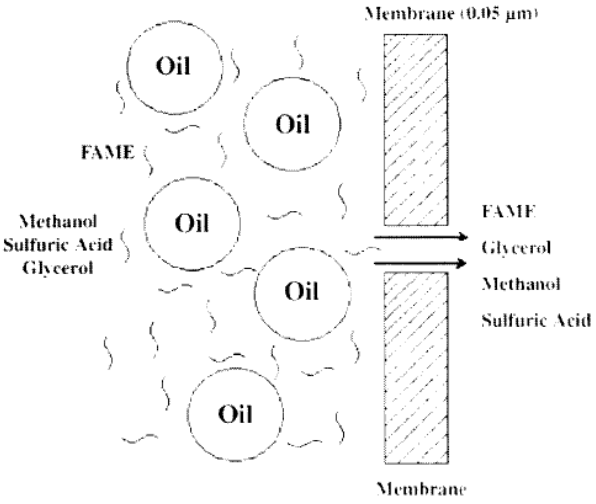

Figure 2.18 Schematic of biodiesel production in a membrane reactor [50]

Membrane reactors integrate reaction and membrane-based separation into a single process. They can increase the conversion of equilibrium-limited reactions by removing some products from the reactants stream via membranes. Dube *et al.* [50] exploited the possibility of biodiesel production from canola oil and methanol using a two-phase tubular membrane reactor as shown in Figure 2.18. The pore size of the carbon membrane used in the reactor was 0.05μm. The inner and outer diameters were 6 and 8 mm, respectively. Its length was 1200mm giving 0.022m^2 surface area. The transesterification of canola oil was performed via both acid- or base-catalysis in the 300 ml membrane reactor in semi-batch mode at 60°C, 65°C and 70°C and at different catalyst concentrations and feed flow rates. At high flow rate of methanol/acid catalyst, they obtained 65% conversion. When base was used as catalyst, conversions of greater than 95% were attained at different flow rates. They found that the microporous carbon membrane selectively permeates FAAE, methanol and glycerol while excluding bound glycerides (TG, DG, MG) from passing through. Hence, there are almost no bound glycerides in the permeate stream thus yielding high purity biodiesel. The reactor was also used to handle feedstock with high FFA content because the membrane retained soap from the side reaction and also retained other non-reacting components. Cao *et al.* [51] investigated the effects of the pore size of the membrane on the performance of a semi-continuous reactor. The analysis results show that no oil was found in the permeate stream and all permeate samples obtained were biodiesel of high purity at 65°C. It also indicated that the oil droplets in the membrane reactor were of greater size than the pore sizes tested. The kinetics of canola oil transesterification in a membrane reactor was also reported [52]. The study showed that the membrane reactor could enhance reaction rate by the

excellent mixing in the membrane reactor loop and the continuous removal of product from the reaction medium.

- **Reactive Distillation**

Reactive distillation (RD) is a technique which combines chemical reactions and product separations in one unit. Currently reactive distillation has attracted more and more attention and been used widely [53-56] due to its many advantages over conventional sequential processes, such as a fixed-bed-reactor followed by a distillation column. One of the most important advantages of reactive distillation is that conversion limitation is avoided by continuous in-situ product removal for equilibrium-controlled reactions. Integration of reaction and separation reduces capital investment and operating costs.

For reversible transesterification reaction of vegetable oils with alcohol, usually an excess amount of alcohol (6:1 or higher alcohol: oil molar ratio) is used to drive the equilibrium to the product side in order to obtain high conversion rates and high final equilibrium conversion. Since recovery of excess alcohol from the esters and glycerol streams involves additional operating cost, application of reactive distillation to biodiesel production may lead to a more efficient process. He *et al.* [57, 58] reported a novel reactor system using RD for biodiesel production from canola oil and methanol using KOH as catalyst. In this system, reaction at methanol: oil molar ratio of 4:1 yielded 95% conversion rate in about 3 min at 65^{o}C column temperature. The experimental conditions of a continuous-flow reactive distillation reactor were optimized for biodiesel production [59, 60]. The upward-flowing methanol vapor served as an agitator in the reactant mixture, providing uniform mixing while it was bubbling through the liquid phase on each plate. This process has several advantages over conventional biodiesel production processes.

(1) short reaction time and high unit productivity, (2) no excess alcohol requirement, (3) lower capital costs due to the small size of RD and no need for additional separation units. Figure 2.19 shows the FAME production process based on reactive distillation. Williams [62] patented a process for low-sulfur, low-glycerin biodiesel fuel by reactive distillation from feedstocks containing fatty acids, glycerated fatty acids and glycerin.

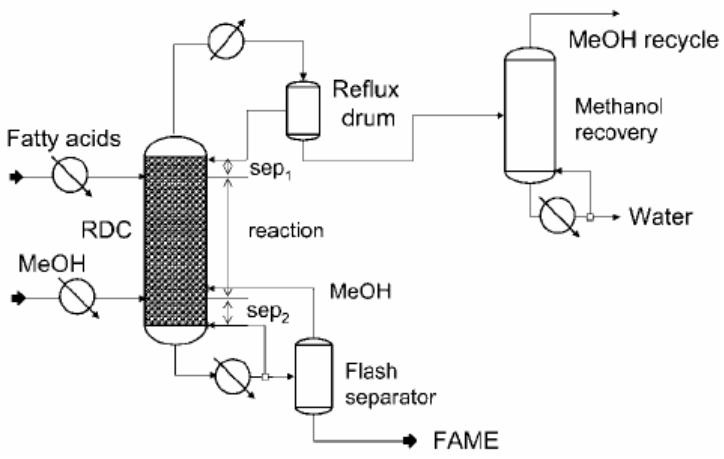

Figure 2.19 FAMEs production by esterfication with methanol in a reactive distillation column [61]

- **Centrifugal contactors**

The centrifugal contactor is another process intensification technology because it integrates reaction and centrifugal separation into a unit. It consists of a mixing zone and a separating zone as shown in Figure 2.20. As the rotor in the contactor is rapidly rotating within a stationary cylinder, it can achieve intense mixing and good mass transfer by high shear stress and quick phase separation by high centrifugal force simultaneously. However, the residence time in a conventional centrifugal contactor is as low as about 10 seconds and cannot allow reaction to reach equilibrium. The researchers [64] at Oak Ridge National Laboratory modified the design of a centrifugal contactor and achieved the control of residence time in mixing zone. They used the updated centrifugal contactor to continuously

produce biodiesel via base-catalyzed production. Figure 2.21 presents the experimental setup for biodiesel production using the modified centrifugal contactor. At 60^{o}C more than 99% conversion was achieved after about 1 minute using a volumetric phase ratio of 5:1 oil to methoxide and potassium hydroxide as catalyst when rotor was spinning in 3600 rpm. Good product separation was realized after 3 minutes. The technology has been commercialized with Nu- Energie, LLC [65].

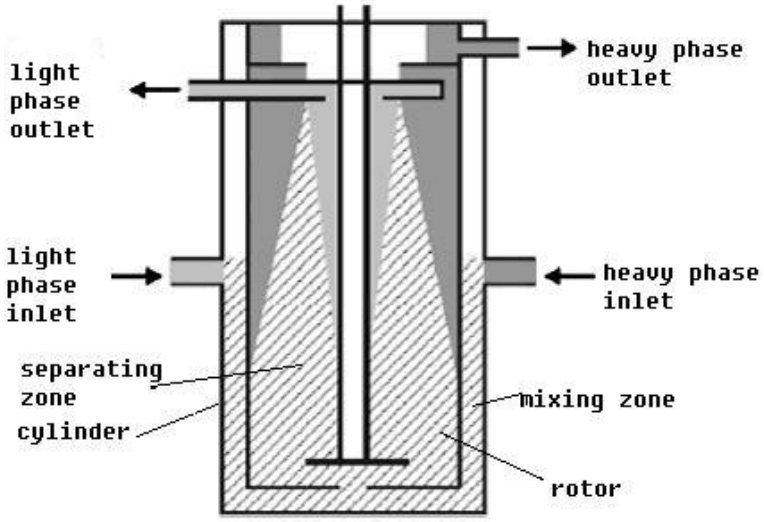

Figure 2.20 Schematic of a centrifugal contactor [63]

Ktaai *et al.* [63] tested the performance of a centrifugal contact separator for the continuous production of biodiesel from sunflower oil. At an elevated temperature of 60^{o}C, a yield of 96% of FAME was achieved after about 40 minutes using a 6:1 molar ratio of methanol to oil and 1% NaOMe as catalyst at 30Hz(1800 rpm). The study showed that the flow rate of the two phases affected the conversion due to the change of residence time.

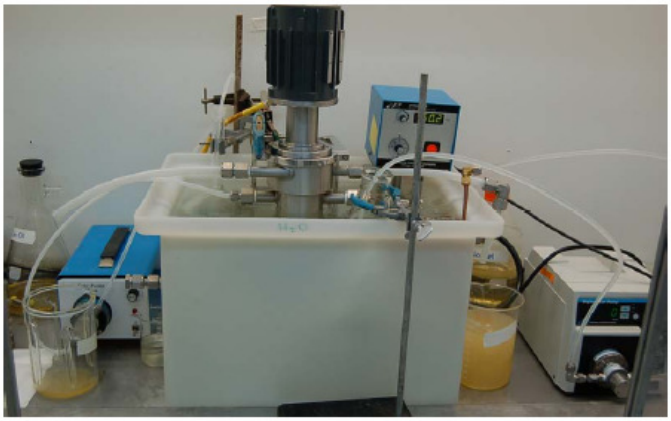

Figure 2.21 Experimental setup for biodiesel synthesis using a centrifugal contactor [64]

Biodiesel production can be enhanced by process intensification technologies. Each technology has the potential to improve production efficiency and thus reduce operating cost of the process. Table 2.1 summarizes the advantages of these technologies used in continuous biodiesel production over traditional stirred tank reactors. A rudimentary assessment of reaction time, energy efficiency, operating/capital cost, the difficulty of temperature control, and current status is presented in the table. Process intensification technologies have significant potential for enhancement of biodiesel production. Enhancement in transport processes and higher reaction rates provide the scope for continuous production. Hence higher conversion yields are possible, under milder conditions and involving reduced molar ratios of methanol to oil, lower reaction temperature and catalyst concentration than conventional stirred reactors. Some process intensification technologies offer the flexibility to process a variety of feedstocks. Compared to conventional tank systems, these technologies are proved more energy efficient because of enhanced heat transfer. Their small "footprint" allows them to be scaled up easily and reduces the capital and operating cost and thus increases profit.

Table 2.1 Comparison of process intensification technologies for continuous biodiesel production with conventional stirred tank reactors

	Residence time	Energy efficiency (g/J)	Operating and capital cost	Temperature control	Current status
Static mixer	~30 min	14.9~384[48]	Low	Good	Lab scale
Microchannel reactor	28s~several minutes	0.018 [26]	Low	Good	Lab scale
Oscillatory flow reactor	30 min	N/A	Low	Good	Pilot plant
Cavitational reactor	Microseconds~ several seconds	1×10^{-4} ~ 2×10^{-4} (hydrodynamic cavitation), 5×10^{-6} ~ 2×10^{-5} (acoustic cavitation)	Low	Good	Commercial scale
Spinning tube in tube reactor	< 1 min	N/A	Low	Good	Commercial scale
Microwave reactor	Several minutes	~0.038L/kJ [42]	Low	Good	Lab scale
Membrane reactor	1~3 hr	N/A	Lower	Easy	Pilot plant
Reactive distillation	Several minutes	~1.6×10^{-6}[61]	Lower	Easy	Pilot plant
Centrifugal contactor	~1 min	N/A	Lower	Easy	Commercial scale

2.4 Summary

In this chapter, the worldwide biodiesel production and installed capacity was investigated and discussed. Data show that most biodiesel is produced by the Europe and the United States. The increase of production capacity is very fast in the recent years.

Biodiesel is mainly synthesized using the alkali-catalyzed transesterification reaction. This reaction has been fully reviewed with respect to its mechanism, kinetics and phase behaviors. To reduce the mass transfer limitation related to transesterification, alternative process intensification technologies were provided to obtain efficient mixing, increase interfacial contact between two phases and improve reaction rate. These technologies include the novel reactors and reaction/separation coupled technologies, which can improve production efficiency and reduce cost by enhancing process mass and heat transfer, in situ production separation. At the same time, these methods provide some insights to the development of new process intensification technologies for biodiesel production.

2.5 References

1. T. Krawczyk, Biodiesel- Alternative fuel makes inroads but hurdles remain, INFORM 7 (1996) 801-829.
2. http://www.serconline.org/biodiesel/faq.html
3. http://www.emerging-markets.com/biodiesel/
4. http://www.ebb-eu.org/stats.php#
5. http://www.biodiesel.org/resources/faqs/
6. http://www.biodiesel.org/pdf_files/fuelfactsheets/Production_Capacity.pdf

7. B. Freedman, R.O. Butterfield, E.H. Pryde, Transesterification kinetics of soybean oil, JAOCS 63 (1986) 1375-1380.
8. B. Freedman, E.H. Pryde, T.L. Mounts, Variables affecting the yields of fatty esters from transesterified vegetable oils, JAOCS 61 (1984) 1638-1643.
9. Algal oil yields, http://www.oilgae.com/algae/oil/yield/yield.html
10. K. Addison, Oil yields and characteristics, Journey to Forever, (2008). http://journeytoforever.org/biodiesel_yield.html
11. E.W. Eckey, Esterification and interesterification, JAOCS 33 (1956) 575-579.
12. R. Sridharan, I.M. Mathai, Transesterification reactions, J. Sci. Ind. Res. 33 (1974) 178-187.
13. D. Darnoko, M. Cheryan, Kinetics of palm oil transesterification in a batch reactor, J. of the American Oil Chemists' Society, 77 (2000) 1263-1267.
14. H. Noureddini and D. Zhu, Kinetics of transesterification of soybean oil, J. of the American Oil Chemists' Society, 74 (1997) 1457-1463.
15. W. Zhou and D.G.B Bookcock, Phase behavior of the base-catalyzed transesterification of soybean oil, JAOCS, 83 (2006) 1041-1045.
16. W. Zhou and D.G.B Bookcock, Phase distributions of alcohol, glycerol, and catalyst in the transesterification of soybean oil, JAOCS, 83 (2006) 1047-1052.
17. H.J. Wright, J.B. Segur, H.V. Clark, S.K. Coburn, E.E. Langdon, R.N. DuPuis, A report on ester interchange, Oil and Soap 21 (1944) 145-148.
18. G. Jon, Biodiesel processing and production. Fuel processing technology 86 (2005) 1097-1107.

19. H. Noureddini, D. Harkey, V. Medikonduru, A continuous process for the conversion of vegetable oils into methyl esters of fatty acids, J. Am. Oil Chem. Soc. 75 (1998) 1755-1783.
20. C.L. Peterson, J.L. Cook, J.C. Thompson, J.S. Taberski, Continuous flow biodiesel production, Appl. Eng. Agric. 18 (2002) 5-11.
21. J.C. Thompson, B.B. He, Biodiesel production using static mixers, Trans. ASABE 50 (2007) 161-165.
22. M.B. Boucher, C. Weed, N.E. Leadbeater, B.A. Wilhite, J.D. Stuart, R.S. Parnas, Pilot scale two-phase continuous flow biodiesel production via novel laminar flow reactor-separator, Energy & Fuels 23 (2009) 2750-2756.
23. J. Kobayashi, Y. Mori, S. Kobayashi, Multiphase organic synthesis in microchannel reactors, Chem. Asian J. 1 (2006) 22-35.
24. N. Canter, Making biodiesel in a microreactor, Tribol. Lubr. Technol. 62 (2006) 15-17.
25. J. Sun, J. Ju, L. Ji, L. Zhang, N. Xu, Synthesis of biodiesel in capillary microreactors, Ind. Eng. Chem. Res. 47 (2008) 1398-1403.
26. Z. Wen, X. Yu, S.-T. Tu, J. Yan, E. Dahlquist, Intensification of biodiesel synthesis using zigzag micro-channel reactors, Bioresour. Technol. 100 (2009) 3054-3060.
27. A.P. Harvey, M.R. Mackley, T. Seliger, Process intensification of biodiesel production using a continuous oscillatory flow reactor, J. Chem. Technol. Biotechnol. 78 (2003) 338-341.
28. http://www.ceb.cam.ac.uk/pages/biofuels.html.

29. T.G. Leighton, The Acoustic Bubble, Academic Press, London, UK, 1994.

30. http://cav.safl.umn.edu/images/gallery/safl-02-supercav.jpg.

31. F.R. Young, Cavitation, McGraw Hill, London, UK, 1989.

32. J.L. Luche, Synthetic Organic Chemistry, Plenum Press, New York, USA, 1999.

33. M.A. Kelkar, P.R. Gogate, A.B. Pandit, Cavitation as a novel tool for process intensification of biodiesel synthesis, in: Proceedings of the 6th International Symposium on Catalysis in Multiphase Reactors, Pune, India, 2007.

34. P.R. Gogate, A.B. Pandit, Hydrodynamic cavitation: a state of the art review, Rev. Chem. Eng. 17 (2001) 1-85.

35. P.R. Gogate, A.B. Pandit, Engineering design methods for cavitation reactors. II. Hydrodynamic cavitation, AIChE J. 46 (2000) 1641-1649.

36. O.V. Kozyuk, Apparatus and method for producing biodiesel from fatty acid feedstock, US 2009/0043118 A1.

37. D.G. Mancosky, D.A. Armstead, T. McGurk, G. Hopkins, K. Hudson, The use of a controlled cavitation reactor for bio-diesel production, in: Proceedings of the AIChE Spring Meeting, Houston, USA, 2007.

38. http://www.hydrodynamics.com/product pics2.htm.

39. http://www.rccostello.com/STT.html.

40. http://www.kreido.com/downloads/ps stt tech.pdf.

41. H. Lodhar, R.J.J. Jachuck, Intensified biodiesel reaction using continuous rotating tube reactor technology, in: Proceedings of the AIChE Annual Meeting, Salt Lake City, USA, 2007.

42. T.M. Barnard, N.E. Leadbeater, M.B. Boucher, L.M. Stencel, B.A. Wilhite, Continuous-flow preparation of biodiesel using microwave heating, Energy & Fuels 21 (2007) 1777-1781.

43. A. Breccia, B. Esposito, G.B. Fratadocchi, A. Fini, Reaction between methanol and commercial seed oils under microwave irradiation, J. Microwave Power Electromagn. Energy 34 (1999) 3-8.

44. N.E. Leadbeater, L.M. Stencel, Fast, easy preparation of biodiesel using microwave heating, Energy & Fuels 20 (2006) 2281-2283.

45. N.E. Leadbeater, T.M. Barnard, L.M. Stencel, Batch and continuous-flow preparation of biodiesel derived from butanol and facilitated by microwave heating, Energy & Fuels 22 (2008) 2005-2008.

46. N. Azcan, A. Danisman, Alkali catalyzed transesterification of cottonseed oil by microwave irradiation, Fuel 86 (2007) 2639-2644.

47. N. Azcan, A. Danisman, Microwave assisted transesterification of rapeseed oil, Fuel 87 (2008) 1781-1788.

48. D. Frascari, M. Zuccaro, A. Paglianti, A pilot-scale study of alkali-catalyzed sunflower oil transesterification with static mixing and with mechanical agitation, Energy & Fuels 22 (2008) 1493-1501.

49. P. Wu, Y. Yang, J.A. Colucci, E.A. Grulke, Effect of ultrasonication on droplet size in biodiesel mixtures, J. Am. Oil Chem. Soc. 84 (2007) 877-884.

50. M.A. Dube, A.Y. Tremblay, J. Liu, Biodiesel production using a membrane reactor, Bioresour. Technol. 98 (2007) 639-647.

51. P. Cao, A.Y. Tremblay, M.A. Dube, K. Morse, Effect of membrane pore size on the performance of a membrane reactor for biodiesel production, Ind. Eng. Chem. Res. 46 (2007) 52-58.

52. P. Cao, A.Y. Tremblay, M.A. Dube, Kinetics of canola oil transesterification in a membrane reactor, Ind. Eng. Chem. Res. 48 (2009) 2533-2541.

53. G.J. Harmsen, Reactive distillation: the front-runner of industrial process intensification: a full review of commercial applications, research, scale-up, design and operation, Chem. Eng. Process. 46 (2007) 774-780.

54. F. Omota, A.C. Dimian, A. Bliek, Fatty acid esterification by reactive distillation. Part 1. Equilibrium-based design, Chem. Eng. Sci. 58 (2003) 3159-3174.

55. F. Omota, A.C. Dimian, A. Bliek, Fatty acid esterification by reactive distillation. Part 2. Kinetics-based design for sulphated zirconia catalysts, Chem. Eng. Sci. 58 (2003) 3175-3185.

56. L.G. Matallana, L.F. Gutiérrez, C.A. Cardona, Biodiesel production by reactive distillation, in: Empromer 2005-2nd Mercosur Congress on Chemical Engineering and 4th Mercosur Congress on Process Systems Engineering, Agosto, 2005.

57. B.B. He, A.P. Singh, J.C. Thompson, A novel continuous-flow reactor using reactive distillation for biodiesel production, Trans. ASAE 49 (2006) 107-112.

58. A.P. Singh, B.B. He, J.C. Thompson, A continuous-flow reactor using reactive distillation for biodiesel production from seed oils, in: Proceedings of the ASAE/CSAE Annual International Meeting, Ottawa, Canada, 2004.

59. B.B. He, A.P. Singh, J.C. Thompson, Experimental optimization of a continuous flow reactive distillation reactor for biodiesel production, Trans. ASAE 48 (2005) 2237-2243.

60. A.P. Singh, B.B. He, J.C. Thompson, Experimental optimization of a continuous-flow reactive distillation reactor for biodiesel production via transesterification, in: Proceedings of the ASAE Annual International Meeting, Tampa, Florida, 2005.

61. A.A. Kiss, A.C. Dimian, G. Rothenberg, Biodiesel by catalytic reactive distillation powered by metal oxides, Energy & Fuels 22 (2008) 598-604.

62. M. William Douglas, Production of biodiesel fuels which are low in glycerin and sulfur, WO patent, 2008/112881 A1, 2008; US patent, 2008/0223752 A1, 2008.

63. G.N. Kraai, F. van Zwol, B. Schuur, H.J. Heeres, J.G. de Vries, Two-phase (Bio) catalytic reactions in a table-top centrifugal contact separator, Angew. Chem. Int. Ed. 47 (2008) 3905-3908.

64. J. McFarlane, J.F. Birdwell Jr., C. Tsouris, H.L. Jennings, Process intensification in continuous base-catalyzed biodiesel production, in: Proceedings of the AIChE Annual Meeting, 2008.

65. http://www.nu-industries.com/our-technology.php.

Chapter 3 Interfacial Turbulence and its Visualization of Liquid-Liquid Systems under the Influence of Electrostatic Fields

3.1 Introduction

3.1.1 Interfacial Turbulence in Liquid-Liquid Systems

Interfacial turbulence is a very important interfacial phenomenon in mass transfer processes. It has been widely known for over a century since spontaneous interfacial turbulence was first observed by Weber [1] in 1854 and described by Thomson in 1855 [2]. Interfacial turbulence accompanying the mass transfer of a solute across a flat interface was first reported in 1888 [3], but the first investigation of this phenomenon was undertaken by Lewis and Pratt [4] in 1953. They found some unusual fluid disturbances at the surface of a droplet when measuring the interfacial tension between two liquids by the drop weight method. Since then, interfacial turbulence has been observed and studied in gas-liquid [5, 6] and in liquid-liquid systems [4, 7]. The phenomenon can be induced by the formation of local interfacial tension gradients and/or the presence of unstable density gradients. Interfacial tension gradient driven convection is known as Marangoni convection named by Carlo Marangoni [8, 9]. Marangoni convection provides an additional component to the interfacial flux, and the interfacial flows modify the hydrodynamic behavior of the fluid layers near to the interface thus affecting drop coalescence, jet break-up and drop drag coefficients. Only Marangoni convection in liquid-liquid systems will be discussed here.

- **Mechanisms of Marangoni Convection**

Marangoni convection is driven by interfacial tension gradients. Interfacial tension itself is a function of solute concentration C at the interface, interfacial temperature θ and the

surface density σ of electric charges. Sawistowski [10] applied Maxwell's relaxation law to interfacial conditions by regarding interfacial tension as a two-dimensional stress tensor, and derived the possible conditions of appearance of Marangoni convection in Equation 1.

$$\frac{\partial \gamma_{yy}}{\partial y} = \frac{\partial \gamma_{\infty}}{\partial C}\frac{\partial C}{\partial y} + \frac{\partial \gamma_{\infty}}{\partial \theta}\frac{\partial \theta}{\partial y} + \frac{\partial \gamma_{\infty}}{\partial \sigma}\frac{\partial \sigma}{\partial y} + \mu_c \frac{\partial^2 \upsilon}{\partial y^2} - \tau_c \frac{\partial^2 (\gamma_{yy} - \gamma_{\infty})}{\partial y \partial t} \qquad (1)$$

where γ_{yy} is the normal component of the dynamic stress tensor or dynamic interfacial tension, γ_{∞} is the static interfacial tension, μ_c is the compressional surface viscosity, τ_c is the corresponding surface modulus, υ is the y-component of the velocity vector and t denotes time. From Equation 1, the Marangoni effect can therefore result from the appearance in the interface of a gradient of concentration, temperature or surface density of electric charges, as a result of compression or dilation of a surface film (dynamic effect) and owing to the non-Newtonian behavior of the surface film which results in the appearance of a time delay between stress and strain. If the interface is Newtonian and dynamic effects of compression and dilation can be neglected, interfacial tension gradients may be created by local changes of solute concentration, temperature and interfacial electrical potential in liquid-liquid systems. The interfacial solute concentration and temperature can be changed due to mass transfer from the bulk into the interface and the heat of solution.

According to its origin and relative depth of penetration into the liquid bulk phases, interfacial convection can be classified into (i) Marangoni instabilities; (ii) Marangoni disturbances and (iii) thin-film phenomena [11]. In the first two cases the depth of penetration of the interfacial convection into the two phases is small with respect to the thickness of the phases. The difference between Marangoni instabilities and Marangoni disturbances is the magnitude of the mass transfer driving force required to produce

interfacial perturbations. In very thin films such as those trapped between drops before coalescence, the depth of the interfacial flow caused by a local change in interfacial tension is large enough to change the thickness of the film substantially. Both Marangoni instabilities and Marangoni disturbances are likely to increase the interfacial flux by introducing a convective component into the mass transfer mechanism, while thin-film phenomena may affect contactor performance by changing the specific interfacial area.

The onset of interfacial turbulence in a system depends on the local variations of its interfacial tension. However, its development into sustained interfacial convection requires additional conditions [12]. Two physical properties play an important role in interfacial convection: solute diffusivity and kinematic viscosity. Rather than their absolute value, it is their value for the two phases that affects the behavior of the system. Unlike a plane interface, for a spherical one there are two critical values of the ratio of the diffusion coefficients in phases [13]. They restrict the interval within which interfacial turbulence may occur if mass transfer goes in one direction only and out of which it is possible for the interfacial turbulence to appear regardless of the direction of mass transfer. The intensity of interfacial turbulence mainly depends on the magnitude of the interfacial tension gradient and the relative rate of transfer of mass and momentum in the two phases. Surfactants can affect the intensity of interfacial turbulence by reducing the interfacial tension and changing the structure of the interface [14].

- **Stability Criteria**

Interfacial turbulence is a very complicated phenomenon. The stability of the interface depends on the response of the systems to interfacial flows. If the interfacial instability sustains or grows in time the system is unstable, otherwise it is stable. In order to describe the

phenomena quantitatively, Sternling and Scriven [15] applied a linearized stability analysis to ternary systems and proposed the stability criteria of ordered Marangoni instabilities in the first time. The analysis shows the occurrence of instabilities depends on the interplay between concentration dependence of interfacial tension, solute diffusivities and viscosities of both phases. This stability criterion has been tested experimentally by many authors and gives reasonable results in many cases [16-21]. However, there are still some experimental results, which cannot be explained by Sternling and Scriven's theory. Afterwards, some more general models extended Sternling and Scriven analysis.

Ortiz and Sawistowski [22] conducted a stability analysis of binary systems based on the mechanism of thermally induced Marangoni instabilities and developed stability criteria. If the system is binary (one of the phases is also the solute) and the interfacial equilibrium is assumed to be attained instantaneously, under isothermal conditions the phase rule precludes changes in interfacial concentrations and consequently the occurrence of interfacial tension gradients. Binary systems should therefore be Marangoni stable. However, interfacial turbulence has been observed in these systems [23]. It was explained in terms of either local variations in interfacial tension due to disturbances to the temperature gradients caused by heats of solution or by dynamic changes of interfacial tension.

Hampe [24] described the interface as a Bingham fluid and proposed a criterion for the yield shear stress of the interface. No Marangoni effect can be observed if the interface is rigid. Modigell [25] proposed a simple stability criterion in addition to the stability criteria of Sternling and Scriven describing whether interfacial instabilities will occur or not. His proposal was that a critical gradient of interfacial tension has to be reached before instabilities will appear in the system. But Modigell did not succeed in finding a theoretical

interpretation of the observed disordered interfacial instabilities such as eruptions or spontaneous emulsification.

Wolf and Stichlmair [26] investigated the stability behavior of different liquid-liquid systems for drops and flat interfaces, and they further noted that the onset of interfacial stabilities is affected not only by the direction of mass transfer and the concentration difference between two phases but also by the velocity near the interface and the relative direction of flow of the phases. The criteria of Sternling and Scriven which predict for quiescent bulk phases instabilities for mass transfer into the organic phase, are not able to predict reliably the occurrence of interfacial turbulence for flowing bulk phases.

Schott and Pfenning [27] developed a stability criterion allowing the prediction of the onset of disordered convection using Monte Carlo simulations. They presented that under certain conditions mass transfer across interfaces induces the formation of nano-droplets in the close vicinity of the interface. The different combinations of the nano-droplet behavior due to attractive or repulsive long-range forces together with the characteristics of coalescence may lead to different macroscopic interfacial instabilities such as spontaneous emulsification or eruptions.

There are some modes developed in the case of surfactants existing in liquid-liquid systems. Nakache *et al.* [28, 29] proposed a semi-empirical stability criteria for "surfactant" transfer across a liquid-liquid interface, which attempts to characterize the system by a ratio of convective flux to diffusive flux at the interface. Slavtchev *et al.* [30] developed a linear stability theory to predict the onset of Marangoni convection in liquid-liquid systems with added surface-active solutes. They proposed a Marangoni coefficient as an empirical parameter and its application to some binary systems has been shown to be very successful.

They found that the ionic surfactants present in the system increased Marangoni convection and enhanced initial mass transfer fluxes. However, the addition of non-ionic surfactants into the system suppressed the interfacial turbulence and reduced the mass transfer fluxes [31, 32]. It is very difficult to predict accurately interfacial stability theoretically, but the models will be improved greatly with in-depth understanding of interfacial convection and the use of simulation techniques.

- **Interfacial Turbulence Induced by Electric Fields**

Equation 1 tells us that local variations in droplet surface charge density will lead to local variations in the effective interfacial tension and thus result in Marangoni convection and increased mass transfer rate when the pendant droplet is electrically charged [33]. Austin *et al.* [34] firstly investigated the phenomena by applying an electric field across a plane interface of four partially miscible binary systems. At low voltages interfacial turbulence was initiated at the interface and limited in a region close to the interface. As the voltage was increased, turbulence propagated into the continuous phase. The confinement of the effect to the organic phase may be connected with the movement of charge within the phase. Iyer and Sawistowski [35] found that turbulence originated in the bulk of toluene phase for the system of toluene/formic acid when an electric field was applied. They also investigated the effect of polarity of the lower electrode in binary systems on turbulence. For the n-butanol/water system, turbulence first appeared in the bulk when the polarity is negative, but it was initiated at the interface when polarity is positive. Additionally, there is no general rule for the effect of polarity on intensity of turbulence. They have not discussed the structure or forms of the electrically driven interfacial turbulence, and have not investigated the phenomena for a pendant droplet under an applied electric field.

Gneist and Bart [36] investigated the influence of DC and high–frequency AC fields on mass transfer from aqueous pendant and moving droplets into a continuous organic phase. The results show that AC charge inhibits Marangoni effects whereas DC voltage enhances or initiates Marangoni phenomena. The differences could be accredited to ion-drag phenomena under DC voltage inside the organic phase. The ion-drag phenomena are caused when ions generated in a dielectric liquid (organic phase) by an electric field move toward an electrode under the Coulomb's force action, dragging liquid molecules and thus causing movement of bulk liquid. Hence, only DC electric fields were used in my project.

3.1.2 Optical Techniques for Visualization of Interfacial Turbulence

Interfacial convection or Marangoni convection in liquid-liquid systems has been observed in droplets and flat interfaces both visually and photographically whether or not it was driven by electric fields [7, 10, 18, 34-36]. It may appear in ordered or disordered structures as shown in Table 3.1. Stationary and oscillatory convective cells belong to the former and eruptions and interfacial turbulence to the latter.

Table 3.1 Classification of interfacial convection [27]

Ordered convection	Disordered convection
Roll cells	Eruptions
Oscillations	Turbulent movements at interface
Ripples at interface	Spontaneous emulsification

Some optical techniques have been applied to visualize the structure of interfacial convection. These methods include the use of Schlieren optical techniques [16, 20, 21, 27，36], laser photochromic dye tracer technique [37], holographic interferometry [26, 38, 39] and microinterferometric and Mach-Zender interferometric methods [40]. Of these methods,

the Schlieren technique is a most common and simple optical technique used to study interfacial flow qualitatively. Its principle is that the refractive index gradient inside the test area blends light rays at the knife edge and forms a different illumination of the fluid field [41]. A simple lens-type Schlieren System is shown in Figure 3.1. At its simplest, a parallel beam of light passes through the test area and is focused onto a knife edge. Any change in air density causes part of the beam to be refracted and to fall above or below the knife edge. This makes that part of the image to appear brighter or darker than the background. Modern systems may use filters in place of the knife edge to make a colored image. Another arrangement is a z-type mirror-based schlieren system. Usually two spherical, parabolic and off-axis concave mirrors are used in this system. The advantage of this arrangement is free of coma and chromatic aberration [41], but it needs more space and is more difficult to align.

Spontaneous interfacial cellular convection accompanying the mass transfer of acetic acid from ethylene glycerol with ethyl acetate was investigated photographically with a Schlieren technique by Orell and Weatwater[20]. The flat liquid-liquid interface exhibited a dominant pattern of stationary and propagating polygonal cells, accompanied by stripes, cell cluster boundaries, and confined or unconfined ripples. Bakker *et al.* [21] continued this study for the ethylene glycol-acetic acid-ethyl acetate, water-acetic acid-isobutyl alcohol, and water acetic acid-ethyl acetate liquid-liquid extraction systems. They obtained optical results similar to those of Orell and Westwater. Schott and Pfennig [27] used Schlieren optics to observe eruption and turbulent movement at a single liquid drop and at a planar interface with a system methyl-isobutyl-ketone(M1BK) + water + acetic acid.

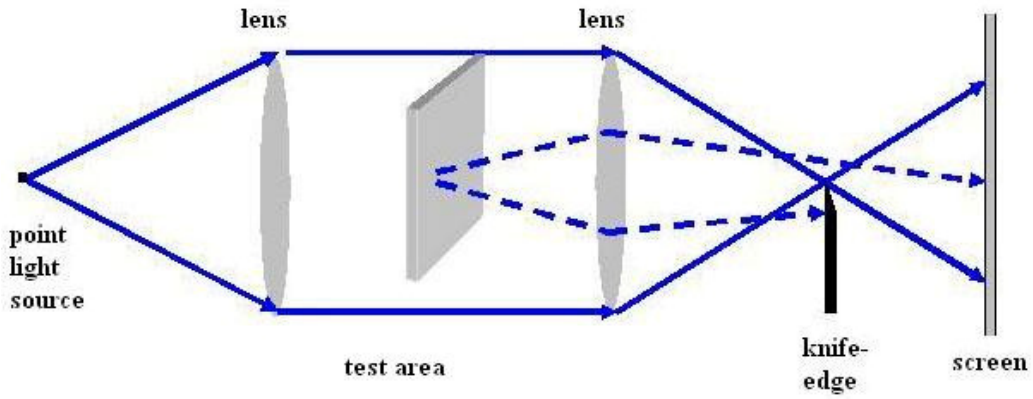

Figure 3.1 Diagram of a simple lens-type schlieren system with a point light source [41]

Holographic interferometry (HI) is another method more widely used in the study of interfacial turbulence. It is based on the physical dependency of refractive index on the composition of a solution. The holographic interferogram, which records the change in the index of refraction, can be used to determine changes in the concentration profile. Hence, in addition to providing a qualitative visualization of the macroscopic flow field, holographic interferometry can determine the influence on concentration profiles [26, 39]. The optical method is more complicated and expensive than others although it can give more information at the interface. In my work a lens-type Schlieren optical technique was selected for visualizing interfacial turbulence in the presence of electric fields because of its relatively low cost and high sensitivity.

Although Marangoni convection in the electric fields has been investigated, there is still something needed to clarify and verify. These problems include where it originates, the form of interfacial flow, and the effect of magnitude of applied potentials and the solute concentration of aqueous phases. Moreover, the time dependent nature of interfacial turbulence without an electric field has been reported [42-44], but few studies were carried out on the electrostatic field driven interfacial turbulence. In addition, no literature has been

reported on the interfacial phenomena study of the 1-decanol-ethanol-water system. Therefore, the first aim was to fabricate a Schlieren optical system for visualization of interfacial turbulence in the 1-decanol-ethanol-water ternary system. Pendant drops and plane interfaces were used as two experimental methods. The second aim is to record the interfacial turbulence with time occurring under different electrical potentials and with various ethanol concentrations in the aqueous phase for each method. Finally, the mechanism, stability of interfacial turbulence, and time-dependent nature were discussed, and the effect of electric fields and ethanol concentrations in the aqueous phase were also investigated qualitatively.

3.2 Experimental

3.2.1 Test System

Deionized water and 1-decanol (Sigma-Aldrich, USA) were used as the solvents of the aqueous phase and the continuous phase in our experiment. Deionized water was pre-saturated with 1-decanol in order to avoid the effect of mass transfer between them on interfacial turbulence. Ethanol (Sigma-Aldrich, USA) was the solute of the aqueous phase. Four aqueous solutions with different concentrations were prepared at 0.5wt%, 1.0wt%, 5wt% and 10wt% ethanol, respectively before experiment. Some physical properties of the liquids are listed in Table 3.2.

Table 3.2 Physical properties of pure components at 25° C [49]

Components	Density, $kg.m^{-3}$	Viscosity, mPa.s	Surface tension, mN/m	Diffusivity of ethanol, m^2/s
Water	998	0.95	71.97	1.28×10^{-9}
1-decanol	830	11.79	29.80	-
Ethanol	789	1.074	22.27 (20° C)	-

3.2.2 Schlieren Optical System

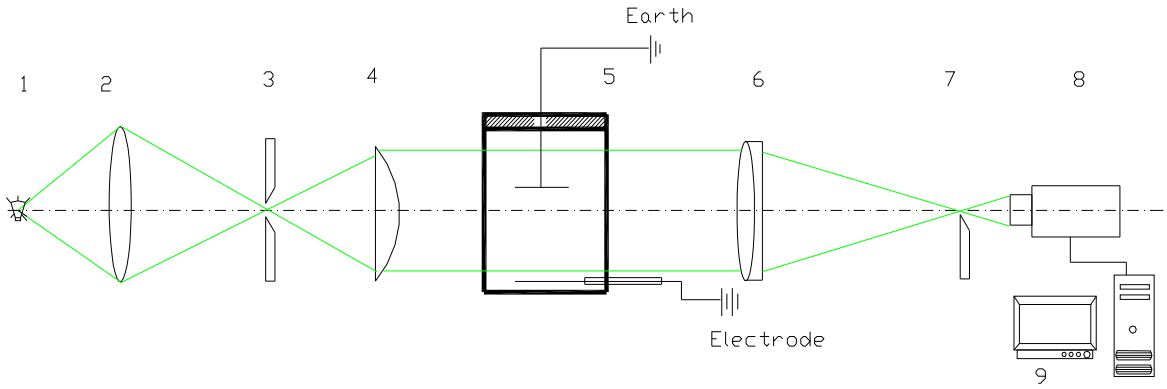

1-Light source; 2-condenser; 3-slit; 4-planoconvex lens; 5- Schlieren cell; 6-achromat; 7-knife edge; 8-CCD camera; 9- computer

Figure 3.2 Schematic diagram of Schlieren optical technique for visualization of electric field driven interfacial turbulence

Figure 3.2 shows the schematic diagram of experimental setup of an optical Schlieren system for visualization of Marangoni phenomena. The experimental setup consists of an optical Schlieren system and a Schlieren cell. The Schlieren optics consists of a light source, a condenser, a slit, two lenses, a knife edge, a CCD camera and a computer. These components are sitting on a 2m long aluminum triangular optical rail (Earling Catalog, Inc., USA) through the post holders (Earling Catalog, Inc., USA) mounting on the carriers (Earling Catalog, Inc., USA). The horizontal positions of the optical components can be adjusted by sliding the carriers back and forward on the rail. A dovetail stage provides more precise positions for the knife edge. The light from an automotive headlamp (CEC Industries Ltd., Korea) is focused with a condenser with Ø50mm (Edmund Industrial Optics, USA) on a rectangular aperture (Earling Catalog, Inc., USA) to obtain the uniform light source which forms a parallel light beam by a 50mm×500mm planoconvex lens (Edmund Industrial Optics, USA). The parallel light beam passes through the schlieren cell and is then focused on a

knife edge (razor blade) by a 75mm×200mm achromat lens (Edmund Industrial Optics, USA) and recorded with a CCD camera (The Imaging Source, USA). The Schlieren photograph can be viewed on a computer connected with CCD camera through a firewire cable. The Schlieren optical system is shown in Figure 3.3.

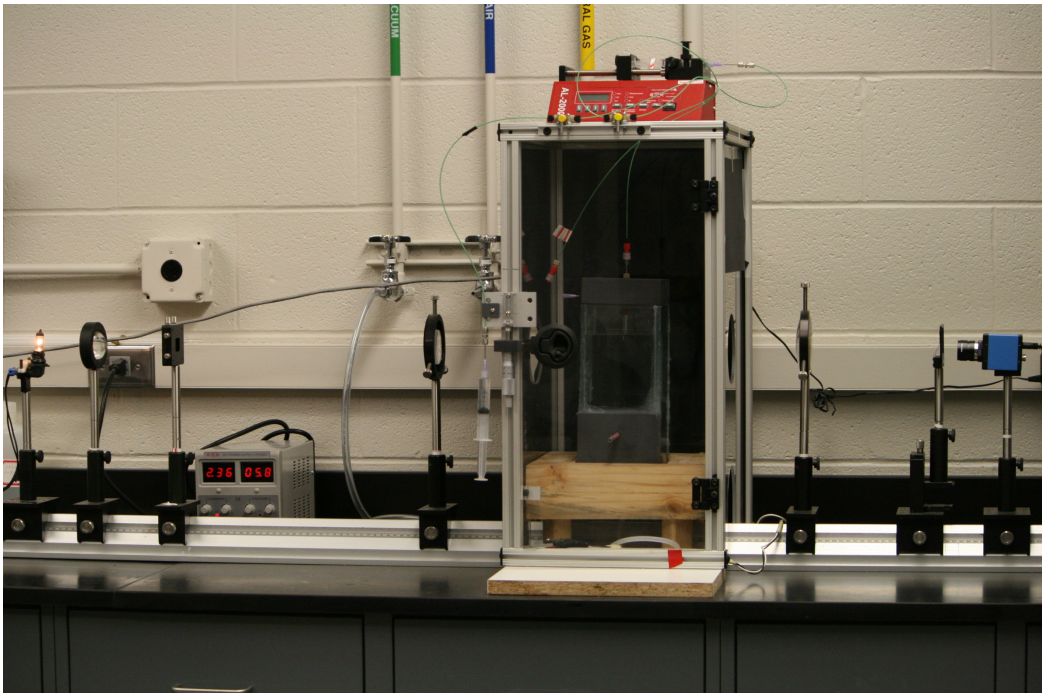

Figure 3.3 Schlieren optical system for visualization of electrostatically driven interfacial turbulence

3.2.3 Schlieren Cells

Different types of Schlieren cells have been used to investigate interfacial turbulence in liquid-liquid systems. Of them, pendant droplets [18, 36, 37] and plane interfaces [32, 34, 35] are the most widely used methods. Usually pendant droplets are easily formed at the tip of a nozzle through the injection of dispersed phases by a pump or syringe. Wolf and Stichlmair [26] designed a measuring cell used to investigate the effect of Marangoni instabilities on the mass transfer at a pendant droplet, which was injected into the continuous phase by a syringe, and fixed between the two glasses of the measuring cell. Its advantage is that it is free of

density instabilities because the cell was located in horizontal position. Gneist and Bart [36] used a stainless steel capillary to produce pendant droplets for the visualization of interfacial turbulence in the presence of electrostatic fields. It is necessary to use conductive stainless steel tube or needle in order to obtain electrically charged droplets. Additionally, the nozzle must be modified to obtain samples from the pendant droplet to examine mass transfer between the droplet and its surrounding continuous phases. Sawistowski *et al.* [45-47] designed a double-orifice nozzle. The drop was formed though the annulus of the nozzle by the action of one pump and withdrawn through the central tube of the nozzle by the second pump before it reached a critical size. Burkhart *et al.* [21] figured out similar experimental equipment, which consisted of a Teflon nozzle with an annulus to study the effect of different amounts of internal circulation on mass transfer rates in liquid drops. The dispersed phase entered through the center of the nozzle. The annulus was used for withdrawal of the dispersed phases from the drop at the same rate of introduction in order to maintain the constant volume of the drop over an extended period time. A quasi-steady state droplet technique was used to study the time-dependent behavior of mass transfer rate [42-44]. The technique involves the formation of a suspended, aqueous pendant hemispherical droplet from a concentric nozzle in an organic continuous phase contained in a column.

Based on these reviews, a concentric nozzle was designed to visualize interfacial turbulence as well as to measure mass transfer from the pendant droplet as shown in Figure 3.4. The concentric nozzle consists of a glass tubing (6mm OD and 4mm ID) and a stainless steel needle (22 gauge needle), which are fixed in the center of a PVC lid by screws. The dispersed phase can be introduced via an inlet at the side of PVC lid, then passes through the annulus between needle and glass tubing. When a semispherical droplet is formed at the tip

of nozzle, the dispersed phase in the droplet is withdrawn back through the stainless steel needle at the same rate to keep the drop size constant or the injection is just stopped. In this experiment, the second method was used. The PVC lid sits on a cubical glass column which is filled with continuous phase. The glass column has the dimensions of 26cm(height)× 10cm(width)× 10cm(length). There is a plane grounded electrode (3.25mm OD) at the bottom of the column, and the distance is 13.8cm between the earth and the tip of the needle.

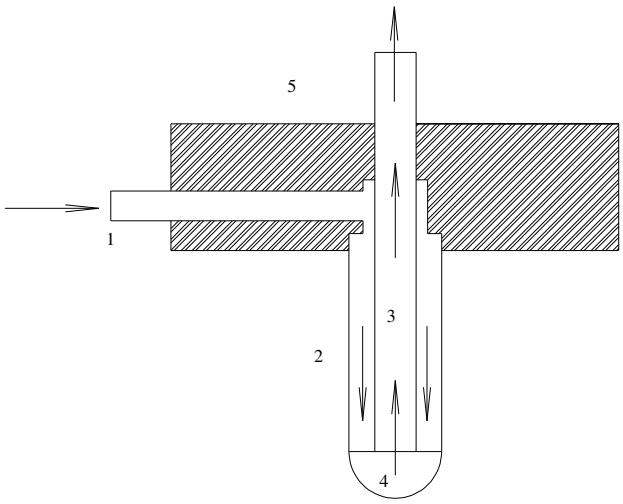

1-Inlet of dispersed phase; 2- glass tube; 3-stainless steel needle; 4-liquid droplet; 5- PVC lid

Figure 3.4 Structural diagram of the concentric nozzle

Compared to pendant droplets, the interfacial area of the plane interface is well defined because it is confirmed within the boundary of the cell. However, it is more difficult to form a hydrodynamically quiescent plane interface without causing any hydrodynamic disturbance and mixing when the light phase is added. Some measurements have been provided to solve this problem. Berg and Morig [48] used a vertical cell consisting of a pair of glass plates to observe interfacial turbulence. The cell was held apart by a polypropylene spacer which includes a step. Before the start of the experiment, the heavy phase was first injected into the cell up to the level of the step. Then the lighter phase was injected by a syringe directed onto

the step so that it could spread out from the step onto the surface of the lower phase. The aim of the step was used to overcome the dispersion of the light phase into the heavy phase, but it was still difficult to obtain a motionless interface. Orell and Westwater [20] used a plunger made of a cork diaphragm to separate the test cell into two halves and seal the liquid interface of a heavy phase. A light phase was poured next on top of the diaphragm. The plunger was pulled straight up and out of the cell at an extremely slow rate to permit the formation of a calm, unperturbed interface. Bakker *et al.* [21] built a container in order to study the behavior of a flat interface using the Schlieren method. The container was composed of two compartments separated by a thin horizontal steel slide. The heavy phase was introduced into the container first. Then the lighter phase was added after the slide was closed and any liquid remaining on top of the slide was removed. The slide could be removed smoothly to allow a formation of an undisturbed interface. This arrangement appeared more promising than those reviewed above because of the high degree of control of interface and simplicity of operation. In view of these, it was modified and used in our experimental setup as shown in Figure 3.5. The plane interface cell (75mm×25mm×100mm) was of rectangular cross section, fabricated from two pieces of big plane section glass to facilitate visualization of the interfacial phenomena, and two pieces of small plane acrylic plexiglass. Two plane stainless steel gauze electrodes (15mm×40mm) were located at the 20mm far from the lower and upper ends of the cell, allowing the imposition of a DC electrical field of either positive or negative polarity across the liquid-liquid interface. The cell was divided into the upper and lower sections for two phases by a removable rectangular flat plate of acrylic plexiglass. This was located through a narrow aperture in one of the vertical plexiglass walls of the cell. The plane sheet could be gently removed by sliding it out through the aperture, with minimal

hydrodynamic disturbance of the liquids in the cell. The slide was sealed using a rubber sheet fixed by screws. The application of rubber material improved the smoothness of operation significantly during removal of the slide. This arrangement was necessary in order to allow the charging of the cell with the two liquid phases without significant contact prior to the start of the experiment.

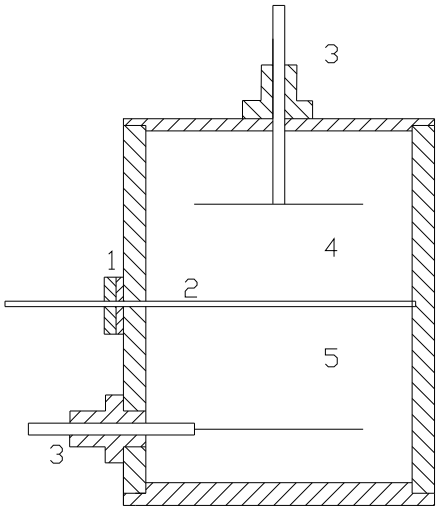

1-Rubber sheet; 2- slide; 3-plane electrode; 4-light phase; 5- heavy phase

Figure 3.5 Structural diagram of the plane interface cell

3.2.4 Experimental Procedures

The setup, alignment and adjustment of the Schlieren system were not very difficult. The procedures of how to achieve them were discussed in detail by Settles [41] and are not described here. Before the experiment, all glassware was cleaned using cleaning solution (Fisher Scientific, USA), and then rinsed using deionized water completely. For the pendant droplet case, about 3 liters of 1-decanol was added slowly into the Schlieren cell. Then the concentric nozzle was inserted and the tip of the nozzle was immersed into the organic phase in the Schlieren cell. After the organic phase was quiescent, the aqueous phase was injected gently through the inlet located at a side of the PVC lid using a syringe by hand. Once a

hemispherical droplet was obtained, the injection was stopped, and the high voltage unit was started. Simultaneously, the recording of Schlieren images was begun at the interval of 10 seconds. For the plane interface case, about 90 ml of aqueous phase was added gently into the Schlieren cell to allow the liquid level to reach the bottom surface of the slide. The slide was pushed to close the lower section of the cell, and any liquid remaining on the top of the slide was removed using tissue paper. Then the aqueous phase was injected gently into the upper section of the cell. After both phases were quiescent hydrodynamically, the slide was pulled back smoothly to allow a formation of an undisturbed interface. Following the application of the electric field, the recording of Schlieren images was started at the interval of 10 seconds.

3.3 Results and Discussion

3.3.1 Pendant Droplets

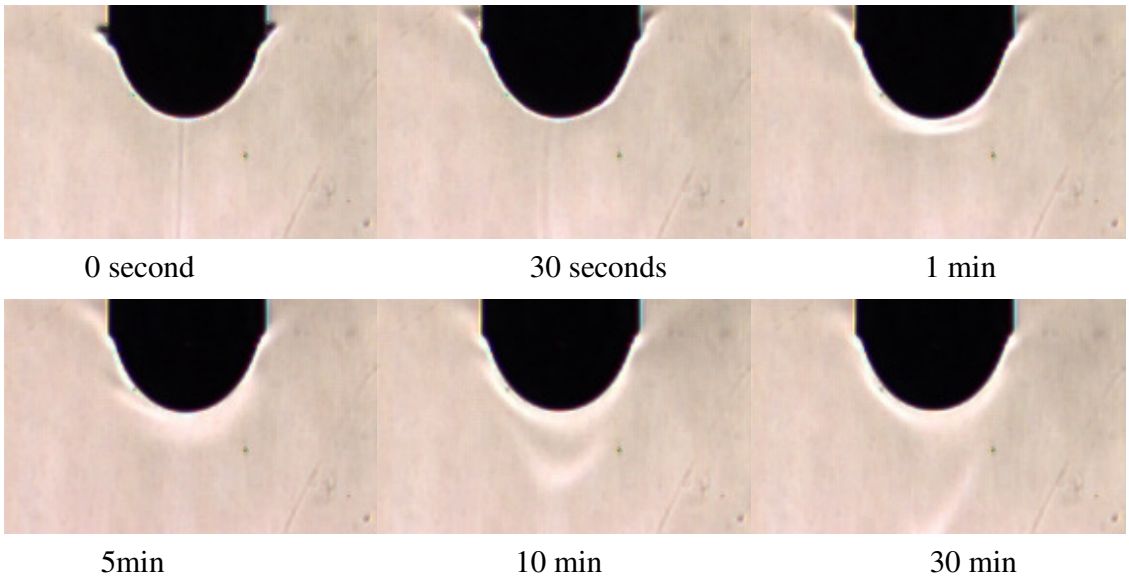

Figure 3.6 Diffusional transfer of ethanol from a pendant aqueous droplet (1wt%) into a solute-free 1-decanol phase

Firstly the interfacial phenomena of a pendant aqueous droplet with three different ethanol concentrations immersed into 1-decanol phase were investigated in the absence of electric fields. When the concentration of ethanol in the aqueous droplet was 1 wt%, no interfacial convection was observed as shown in Figure 3.6 where there are only diffusional layers evident even after 30 min. When the ethanol concentration in the aqueous droplets was increased to 5 wt% or higher 10 wt%, interfacial convection occurred around the drop surfaces in the form of ripples, which could swing and disappeared finally after 30 min. The Schlieren photographs are shown in Figure 3.7 and Figure 3.8, respectively. The onset of interfacial convection may be related to the concentration of ethanol in the aqueous phase or to the mass transfer driving force. Higher ethanol concentrations could further lower the interfacial tension to some critical value which initiated interfacial convection. In addition interfacial turbulence died down in time, which shows the ethanol-water-1-decanol system is stable.

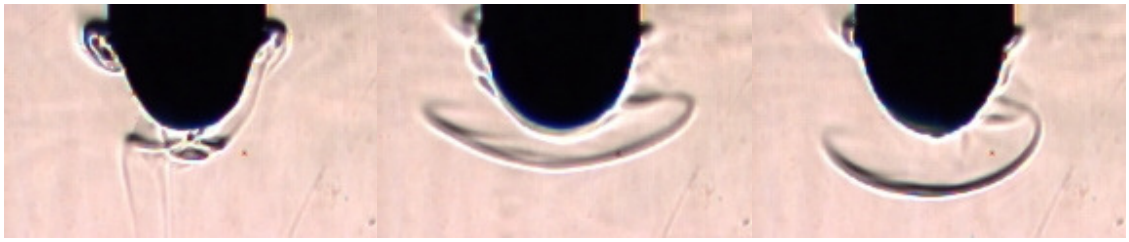

0 second 30 seconds 1 min

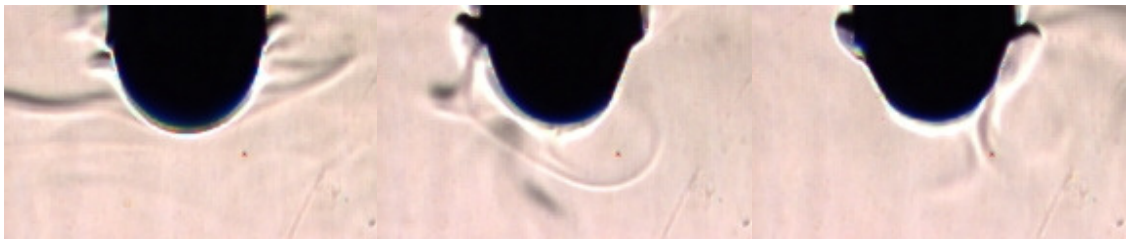

5min 10 min 30 min

Figure 3.7 Interfacial turbulence in the transfer of ethanol from a pendant aqueous droplet (5wt%) into a solute-free 1-decanol phase

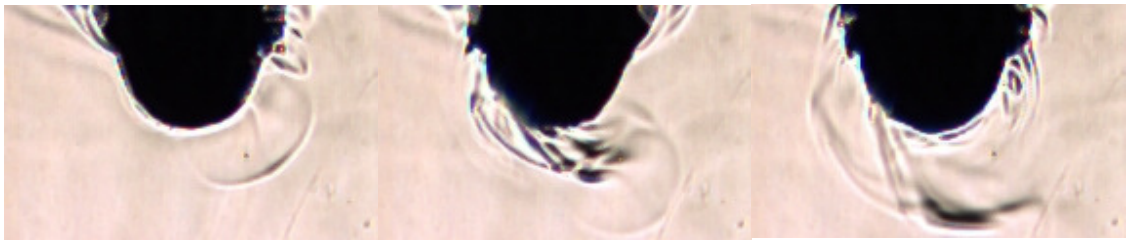

0 second 30 seconds 1 min

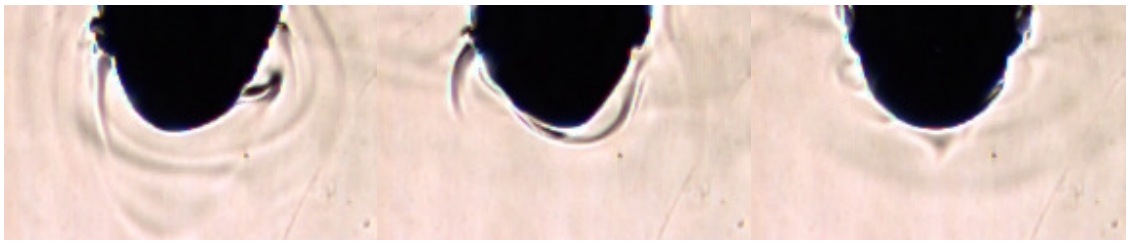

5min 10 min 30 min

Figure 3.8 Interfacial turbulence in the transfer of ethanol from a pendant aqueous droplet (10wt%) into a solute-free 1-decanol phase

When a 1kV (nominal) DC electrostatic field was applied, interfacial turbulence was promoted immediately in the form of eruption patterns which were observed at all concentrations as presented in Figure 3.9, Figure 3.10 and Figure 3.11. In the same way, the ethanol concentration in the aqueous droplets appeared to have a positive effect on the intensity of the interfacial turbulence. Figure 3.12 shows that the observed relationship between interfacial turbulence and the strength of applied electric field. With the increasing applied potential, the induced interfacial turbulence becomes stronger. It could be also observed from these photographs that interfacial convection or turbulence shows an apparent time-dependent nature whether the electrostatic field was applied or not. They were reported previously in some literatures [36, 42-44]. At 0kV, interfacial convection declined with time and stops until 30 min. After that, only a diffusional layer remained. However, in the

presence of electric fields interfacial mass transfer was faster and no diffusional layer appeared after 30 min.

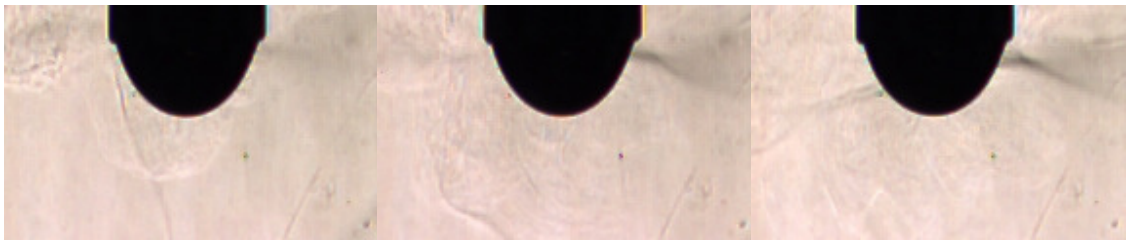

0 second 30 seconds 1 min

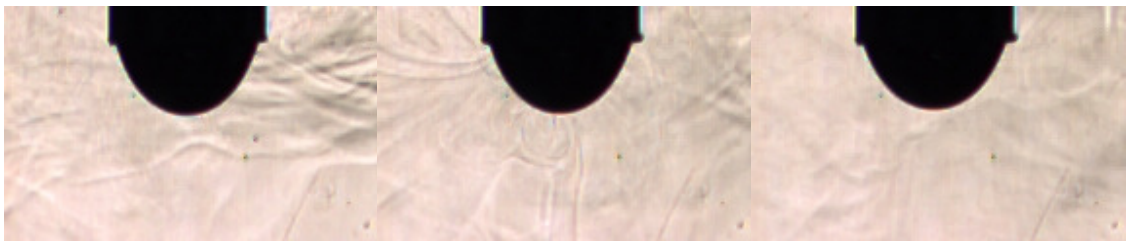

5min 10 min 30 min

Figure 3.9 Interfacial turbulence in the transfer of ethanol from a pendant aqueous droplet (1wt%) into a solute-free 1-decanol phase on 1kV DC electric field

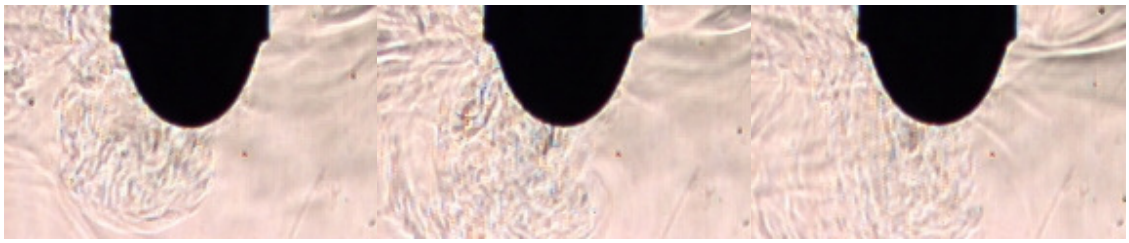

0 second 30 seconds 1 min

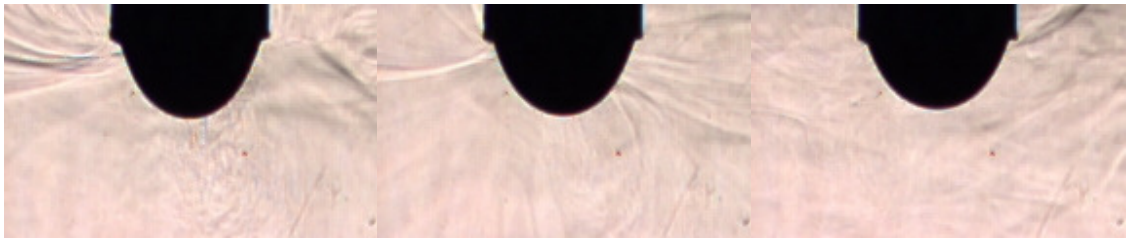

5min 10 min 30 min

Figure 3.10 Interfacial turbulence in the transfer of ethanol from a pendant aqueous droplet (5wt%) into a solute-free 1-decanol phase on 1kV DC electric field

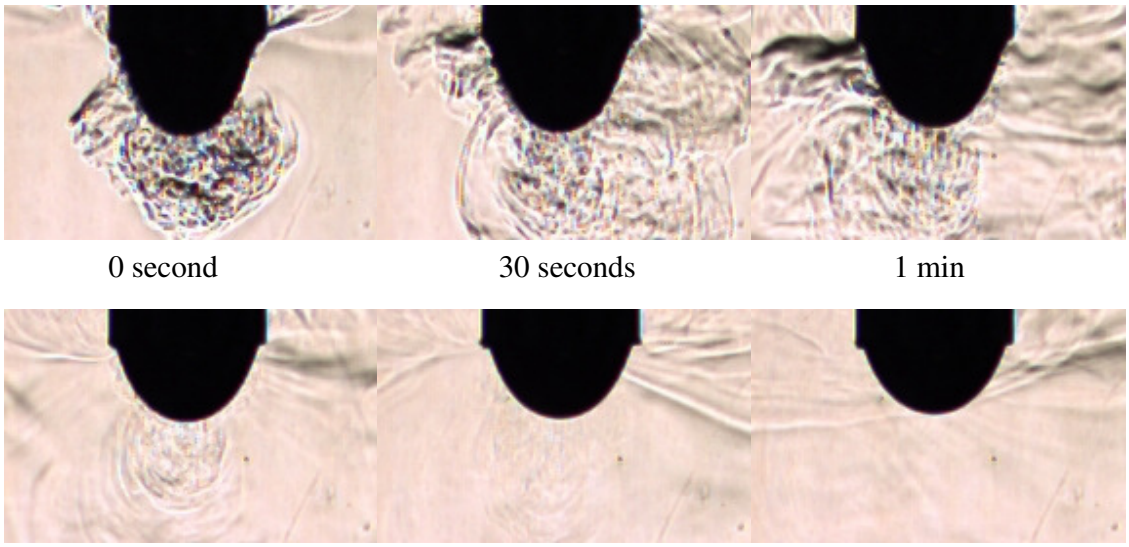

Figure 3.11 Interfacial turbulence in the transfer of ethanol from a pendant aqueous droplet (10wt%) into a solute-free 1-decanol phase on 1kV DC electric field

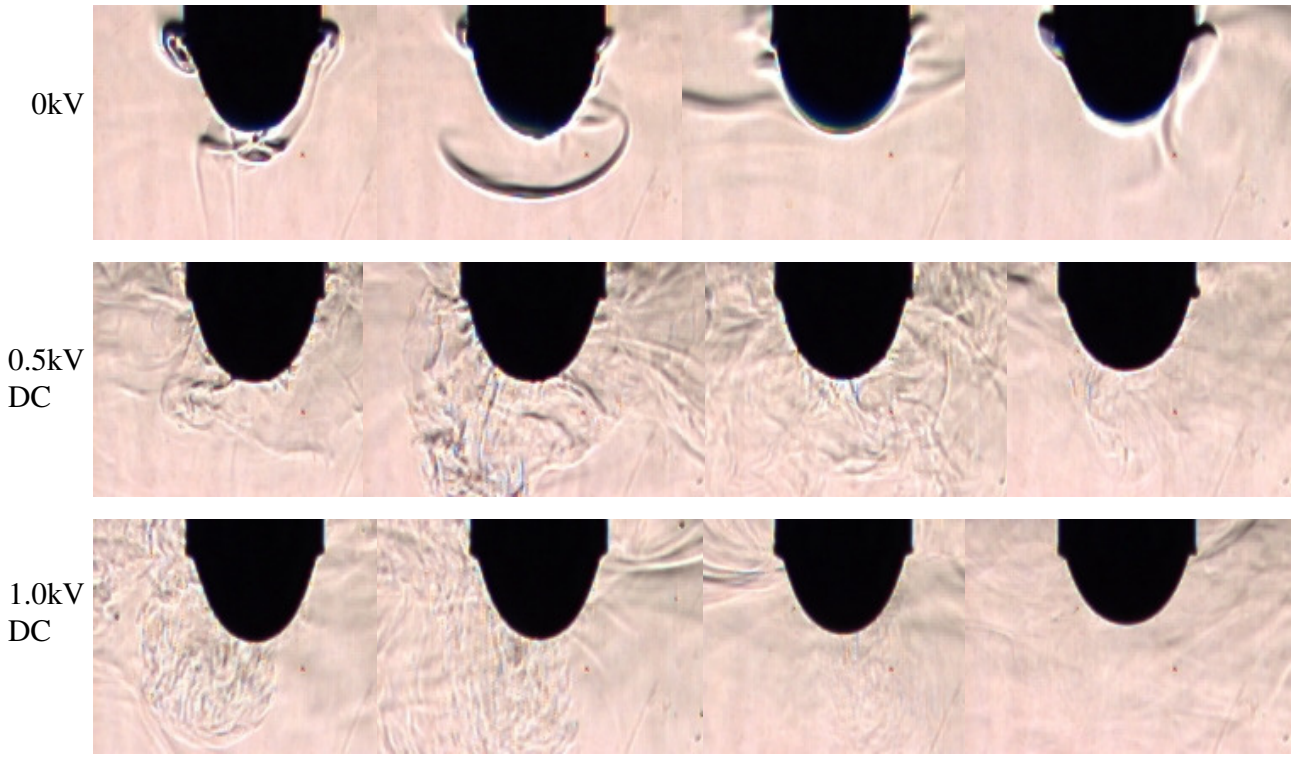

Figure 3.12 Effect of applied potential on interfacial convection in the transfer of ethanol from a pendant aqueous droplet (5 wt%) into a solute-free 1-decanol phase

3.3.2 Plane Interfaces

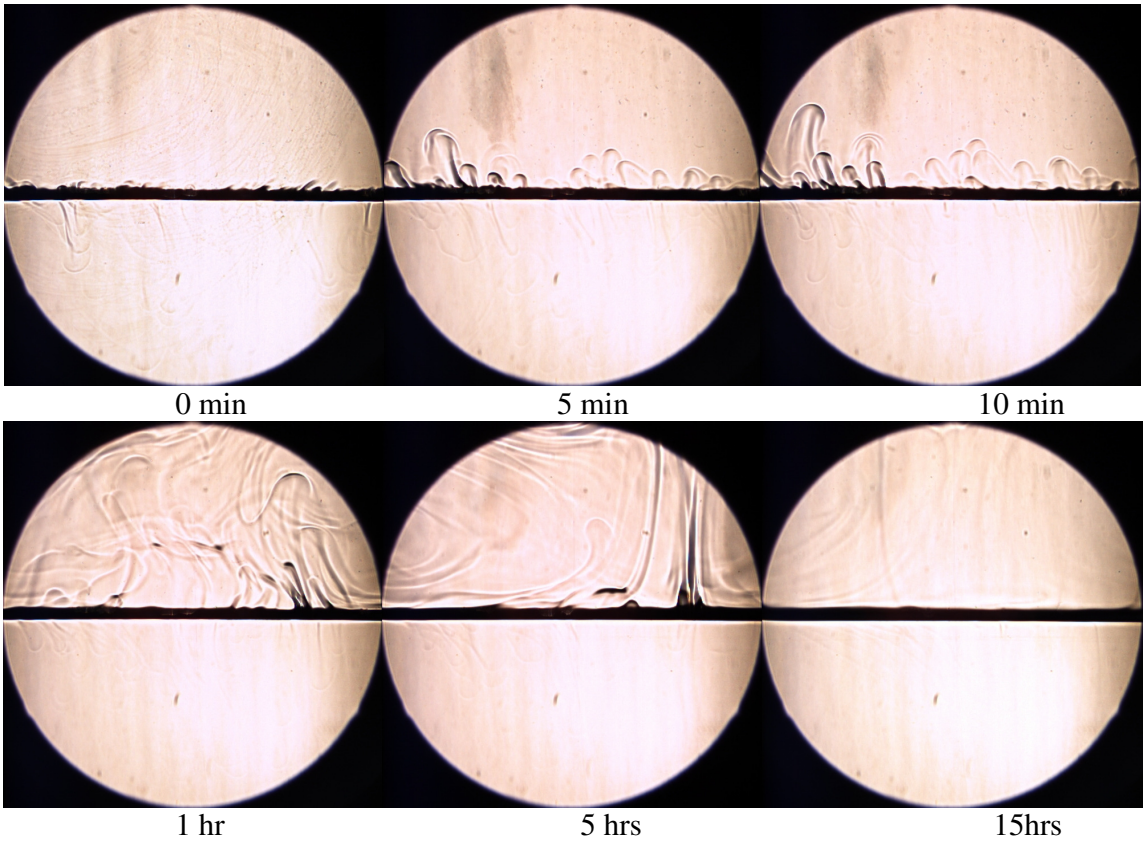

Figure 3.13 Development of interfacial convection in the transfer of EtOH in the aqueous phase (5wt%) across the plane interface into a solute-free 1-decanol phase

Further to the study of the pendant drops, interfacial phenomena at a plane interface between aqueous ethanol and 1-decanol were also visualized and recorded using the Schlieren optical technique. At 5wt% of ethanol in aqueous phase, interfacial convection was observed in Figure 3.13 as occurred in pendant droplets. Initially, it originated at the interface and propagated into two phases. However, the convection in the organic phase is apparently stronger than that in the aqueous phase. Gradually it occupied the whole organic phase. The development could lead to agitation in the organic phase. Finally the intensity of interfacial turbulence became weak and disappeared. When a 1kV electric field was added, more intensive turbulence than that in the absence of electric field was evident as observed in

Figure 3.14. When the concentration of ethanol in the aqueous phase was as low as 0.5 wt%, interfacial turbulence was also promoted as shown in Figure 3.15, but the structure of convection appeared to become finer. Interfacial turbulence exhibited time-dependence as was also observed in the case of the pendant droplet studies. However, the turbulence observed at the plane interface persisted for a longer time possibly because of larger interfacial areas.

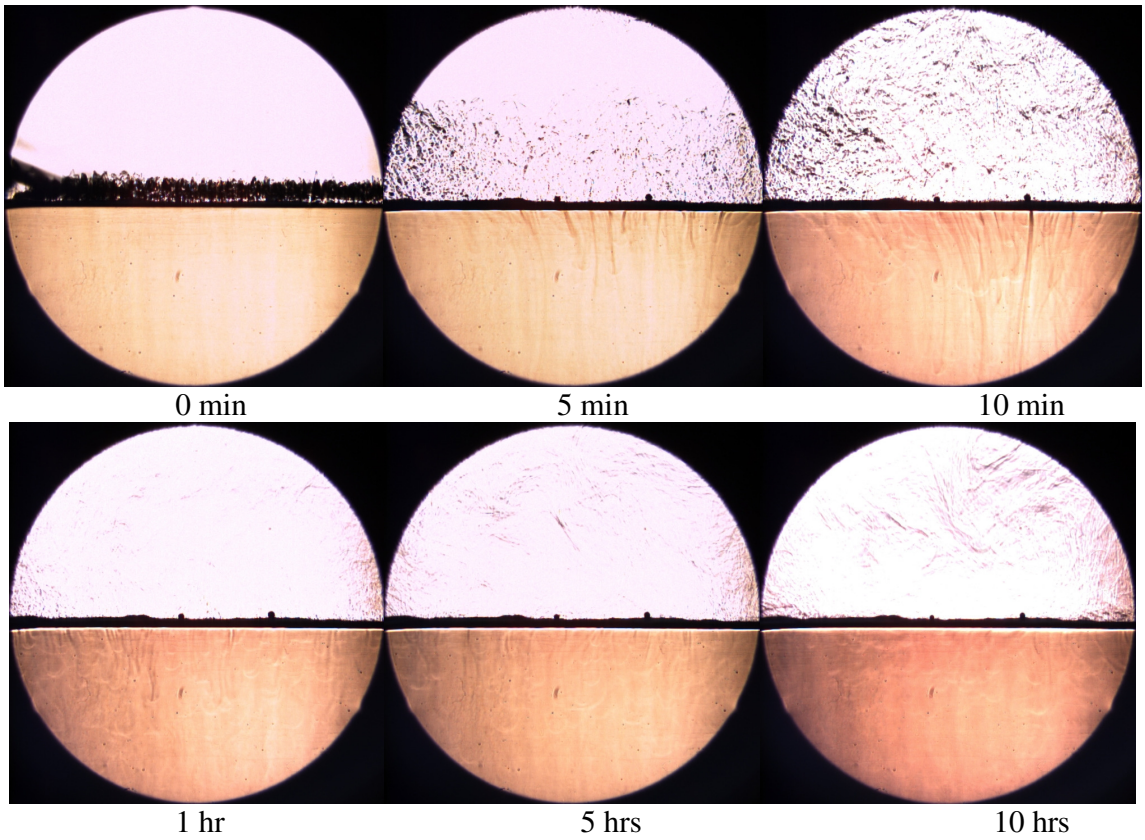

Figure 3.14 Development of interfacial convection in the transfer of EtOH in the aqueous phase (5wt%) across the plane interface into a solute-free 1-decanol phase on 1kV DC electric field

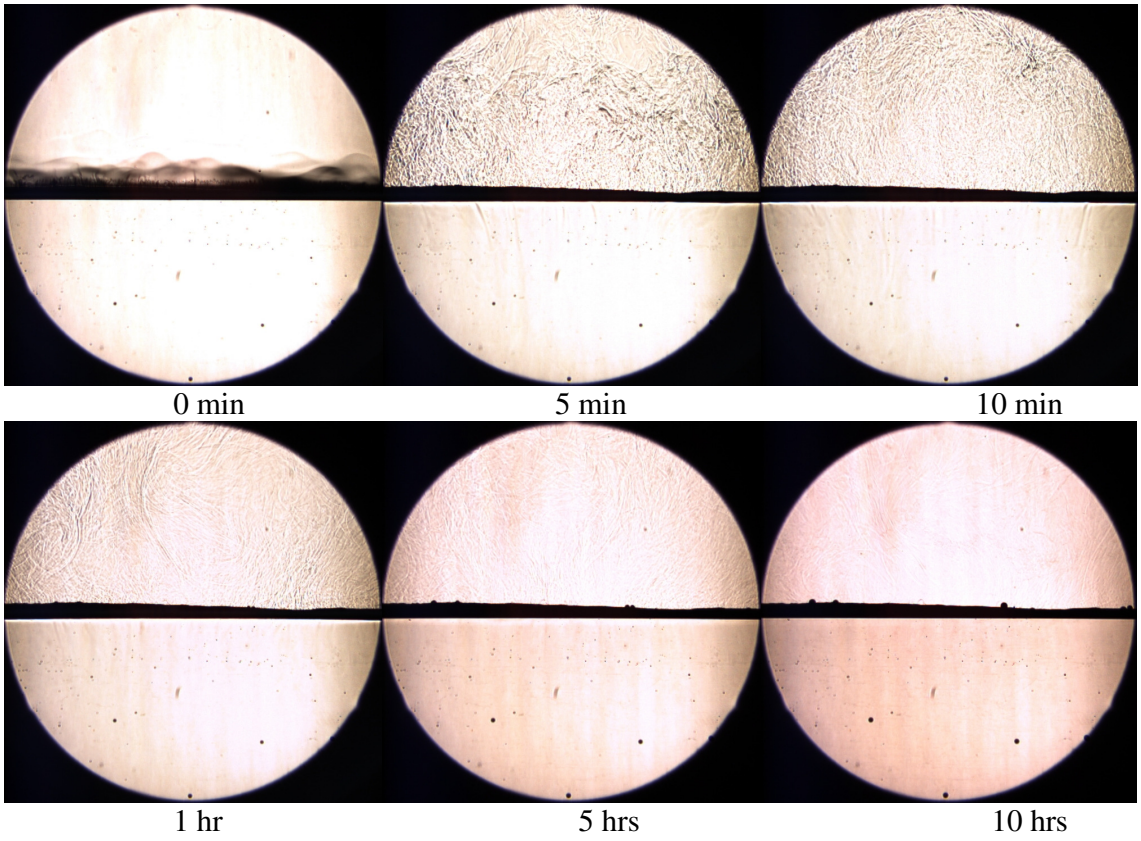

Figure 3.15 Development of interfacial convection in the transfer of EtOH in the aqueous phase (0.5wt%) across the plane interface into a solute-free 1-decanol phase on 1kV DC electric field

3.4 Conclusions

The Schlieren optical technique was successfully developed and an experimental setup was built for the visualization of interfacial phenomena in the ethanol-water-1-decanol system. Two Schlieren cells were designed and fabricated, and were successfully used for the interrogation of interfacial disturbances in pendant droplets and at plane interfaces. It was proved experimentally that a hydrodynamically quiescent plane interface could be obtained through simple operation and the design was feasible. The setup will provide a useful tool to study electrically driven interfacial turbulence under all kind of conditions in the future.

At the lower concentrations of ethanol in aqueous phases, no interfacial convection was observed in the absence of electric fields. A higher concentration of ethanol was required to initiate interfacial convection, which occurred only when a critical value of interfacial tension was reached. It further confirms the stability criterion proposed by Modigell [25]. The intensity of the interfacial convection is weak. However, electric fields are able to induce interfacial turbulence in the ethanol-water-1-decanol system easily even when the concentration of ethanol is low. This also denotes that the onset of interfacial turbulence is affected no only by the local changes of interfacial concentration and temperature but also by the gradient of surface charge density. The intensity of interfacial turbulence is affected by the applied potential, becoming intense with increasing potentials. It was shown that interfacial mass transfer can be enhanced by electrostatic fields.

For the ethanol-water-1-decanol system, interfacial convection originated at the interface and spread into the 1-decanol phase for both pendant droplets and plane interfaces. Some weak interfacial convection was also observed in the aqueous phase for the plane interfaces. The interfacial convection clearly exhibited time-dependency with evidence of attainment of interfacial equilibrium after some finite time.

Interfacial turbulence is a complicated phenomenon especially when electric fields are applied. The stability criteria of Sternling and Scriven predict interfacial instabilities for mass transfer only in the presence of a concentration gradient. They are not able to predict the occurrence of electrically induced interfacial turbulence. To obtain the effect of electric fields on the onset of interfacial turbulence, the third term on the right hand side of Equation 1 becomes very important and it should be considered during stability analysis. The experimental results may provide some insight of this kind of effect and some evidence for

the predicted results from stability analysis. However, the current effort is not enough to understand its effect on mass transfer completely. There is a lot of more work needed to do. These tasks may include the examination of charge density distribution at interfaces during the development of interfacial turbulence, the investigation of interfacial turbulence in the presence of pulsed DC and for some liquid-liquid systems with different viscosities and interfacial tensions, the study of the influence of the direction of mass transfer and surface active agents. In our work, interfacial turbulence was observed when the two phases were quiescent. Hence, another possible task is to explore the interfacial turbulence when the both phases are flowing under controlled conditions including the relative direction and velocity near the interface of flow the two phases. This will be further used to verify the results obtained by Wolf and Stichlmair [26].

3.5 References

1. E.H. Weber, Mikroskopische Beobachtungen sehr gesätzmässiger Bewegungen, welche die Bildung von Niederschlägen harziger Körper aus Weingeist begleiten, Ber. Verh. König. Sächs. Ges. Wiss., Math.-Physische Cl., (1854) 57-68.
2. J. Thomson, On certain curious motions observable at the surfaces of wine and other alcoholic liquors, Philos. Mag., 10(1855) 330-333.
3. G. Quincke, Ueber periodische Ausbreitung von Flüssigkeitsoberflächen und dadurch hervorgerufene Bewegungsercheinungen, Annalen der Physik u. Chemie., 35(1888) 593.
4. J.B. Lewis and H.R.C. Pratt, Oscillating droplets, Nature, 171(1953) 1155.
5. C. Ramshaw and J. D Thornton, Droplet circulation and interfacial disturbances in gas-liquid systems, Nature, 184(1959) 719.

6. P.V. Danckwerts and A. Tavares da Silva, Surface instability during the absorption of CO2 by monoethanolamine solutions, Chem. Eng. Sci., 22(1967) 1513-1514.
7. H. Sawistowski, Interfacial phenomena. Recent advances in liquid-liquid extraction, Pergamon press, Oxford, (1971) 293-366.
8. C. Marangoni, Sull'e Expansione dells Goccie di un Liquido Galleggiante sulla Superfice di altro Liquido, Fusi, Pavia, 1865.
9. C. Marangoni, Über die Ausbreitung der Tropfen einer Flüssigkeit auf der Oberfläche einer anderen, Ann. Phys. (Leipzig), 143 (1871) 337-354.
10. H. Sawistowski, Surface-tension-induced interfacial convection and its effect on rates of mass transfer, Chemie-Ing.-Techn., 45 (1973) 1093-1140.
11. H. Sawistowski, Interfacial convection, Ber. Bunsenges. Phys. Chem., 85 (1981) 905-909.
12. J.D. Thornton, Science and practice of liquid –liquid extraction, Volume 1, Phase equilibria; mass transfer and interfacial phenomena; extractor hydrodynamics, selection and design, Clarendon Press, Oxford, (1992).
13. A.A. Golovin, The onset of the interracial instability of drops during extraction, I. Chem. E. Symp. Ser., 119 (1990) 327.
14. M.A. Mendes-Tatsis, D. Agble, The effect of surfactants on Marangoni convection in the isobutanol/water system, J. Non-Equilib. Thermodyn., 25 (2000) 239-249.
15. C.V. Sternling and L.E. Scriven, Interfacial turbulence hydrodynamic instability and the Marangoni effect, AIChE J., 5 (1959) 514-523.
16. H. Linde and E. Schwarz, Untersuchungen zur Charakteristick der freien Grenzflächenkonvektion beim Stoffübergang an fluiden Grenzflächen, Mber. Dtsch. Akad. Wiss Berlin, 3(1961) 554.

17. H. Linde and E. Schwarz, Über großräumige Rollzellen der freien Grenzflächenkonvektion, Mber. Dtsch. Akad. Wiss Berlin, 7(1964) 330.
18. H. Linde and B. Shert, Schlierenoptischer Nachweis der Marangoni-Instabilität bei der Tropfenbildung, Mber. Dtsch. Akad. Wiss Berlin, 7(1965) 341-348.
19. A. Orell and J. W. Westwater, Natural convection cells accompanying liquid-liquid extraction, Chem. Eng. Sci., 16 (1961) 127.
20. A. Orell and J. W. Westwater, Spontaneous interfacial cellular convection accompanying mass transfer: ethylene glycol-acetic acid-ethyl acetate, AIChE J., 8 (1962) 350-356.
21. C.A. Bakker, B. van Buytenen and W.J. Beek, Interfacial phenomena and mass transfer, Chem. Eng. Sci., 21 (1966) 1039-1046.
22. E.S. Perez De Ortiz and H. Sawistowski, Interfacial stability of binary liquid-liquid systems-I. Stability analysis, Chem. Eng. Sci., 28(1973a), 2051.
23. E.S. Perez De Ortiz and H. Sawistowski, Interfacial stability of binary liquid-liquid systems-II. Stability behaviour of selected systems, Chem. Eng. Sci., 28(1973b), 2063.
24. M.J. Hampe, Zur Theormodynamik der transportprozesse in Grenzflächensystemen, Dissertation, TU München, (1980).
25. M. Dodigell, Untersuchung der Stoffübertragung zwischen zwei Flussigkeiten unter Berüksichtigung von Gernzflächenphänomener, Dissertation, RWTH Aachen, (1981).
26. S. Wolf and J. Stichlmair, The influence of the Marangoni-effect on mass transfer, ISEC, Melbourne, Australia, (1996) 51-56.
27. R. Schott and A. Pfennig, Modelling of mass-transfer induced instabilities at liquid-liquid interfaces based on molecular simulations, Molecular Physics, 102 (2004) 331-339.

28. E. Nakache, M. Duperyrat, M. Vignes-Adler, Experimental and theoretical study of an interfacial instability at some oil-water interfaces involving a surface-active agent: I. Physicochemcial description and outlines for a theoretical approach, J. Coll. Int. Sci., 94 (1983) 120.
29. E. Nakache, S. Raharimalala, M. Vignes-Adler, Marangoni effect in liquid-liquid extraction with surface active agent, phase-interface phenomena in multiphase flow, Hemisphere Publications Corporation, London, (1991) 573.
30. S. Slavtchev, M. Hennenberg, J.-C. Legros, G. lebon, Staionary solutal Marangoni instability in a two-layer system, J. Coll. Int. Sci., 203 (1998) 354.
31. D. Agble and M.A. Mendes-Tatsis, The prediction of Marangoni convection in binary liquid-liquid systems with added surfactants, Int. J. Heat Mass Transfer, 44(2001) 1439-1449.
32. M.A. Mendes-Tatsis and D. Agble, The effect of surfactants on Marangoni convection in the isobutanol/water system, J. Non-Equilib. Thermodyn., 25 (2000) 239-249.
33. G. Stewart and T.D. Thornton, Charge and velocity characteristics of electrically charged droplets. Part I. Theoretical considerations, Int. Chem. Engng. Symp. Ser., 26(1967a) 29-36.
34. L.J. Austin, L. Bancyk, and H. Sawistowski, Effect of electric field on mass transfer across a plane interface, Chem. Eng. Sci., 26 (1971) 2120-2121.
35. P.V.R. Iyer and H. Sawistowski, Effect of electric field on mass transfer across a plane interface, Proceedings of the international solvent extraction conference, Lyon, (1974) 1029-1046.

36. G. Gneist, H.-J. Bart, Influence of high-frequency AC fields on mass transfer in solvent extraction, J. of Electrostatics, 59 (2003) 73-86.

37. J.D. Thornton, T.J. Anderson, K.H. Javed and S.K. Achwal, Surface phenomena and mass transfer interactions in liquid-liquid systems, Part 1: Droplet formation at a nozzle, AIChE J., 31(1985) 1069-1076.

38. M. Pertler, M. Häberl, W. Rommel and E. Blass, Mass transfer across liquid-phase boundaries, Chem. Eng. Proc., 34 (1995) 269-277.

39. A. Guzun-Stoica, M. Kurzeluk, and O. Floarea, Experimental study of Marangoni effect in a liquid-liquid system, Chem., Eng. Sci., 55 (2000) 3813-3816.

40. Y. Nakaike, Y. Tadenumma, T. Sato and K. Fujinawa, An optical study of interfacial turbulence in a liquid-liquid system, 14 (1971) 1951-1961.

41. G.S. Settles, Schlieren and shadowgraph techniques, visualizing phenomena in transparent media, Springer-Verlag, Berlin Heidelberg, New York, (2001).

42. K.H. Javed and J.D. Thornton, Time dependent mass transfer rates in a liquid-liquid system exhibiting interfacial turbulence, I. Chem. E. Symposium Series, 88 (1984) 203-216.

43. D. Rogers, P.J. Thompson, J.D. Thornton, The time dependence of the mass transfer of uranyl nitrate between nitric acid and tri-butyl phosphate, I. Chem. E. Symposium Series, 103 (1987) 15-27.

44. K.H. Javed, J.D. Thornton, T.J. Anderson, Surface phenomena and mass transfer interactions in liquid-liquid systems: Part 2, AIChE J., 35(1989) 1125-11136.

45. H. Sawistowski, G.E. Goltz, The effect of interface phenomena on mass-transfer rates in liquid-liquid extraction, Trans. Instn Chem. Engrs, 41 (1963) 174-181.

46. H. Sawistowski, B.R. James, Einfluß von Oberflächenerscheinungen auf die Stoffdurchgangszahlen bei der Flüssig-Flüssig-Extraktion, Chemie-Ingr-Tech., 35 (1963) 175-179.

47. H. Sawistowski, B.R. James, III. Internationale Vortragstagung über Grenzflächemaktive Stoffe, Abh. Dt. Akad. Wiss. Berlin Nr. 6b, (1966) 757.

48. J.C. Berg and C.R. Morig, Density effects in interfacial convection, Chem. Eng. Sci., 24 (1969) 937-946.

49. G.J. Laughland, M.K. Millar, and L.R. Weatherley, L. R., Electrostatically enhanced recovery of ethanol from fermentation liquor by solvent extraction, IChemE symposium series no. 103, EFCE publication series no. 347 (1987) 263-278.

Chapter 4 Mass Transfer across Liquid-Liquid Interfaces under Electric Fields

4.1 Introduction

As discussed in Chapter 3, spontaneous Marangoni convection or interfacial turbulence can be induced at or near liquid-liquid interfaces either because of a solute concentration gradient or on account of the presence of applied electrostatic fields. Enhanced liquid-liquid mass transfer due to interfacial turbulence has been reported widely in experiment and theory [1-13, 16]. Austin *et al.* [14] investigated the effect of electric field induced interfacial turbulence on mass transfer across a plane interface. Approximately a tenfold increase of the mass transfer coefficient was found in four partially miscible binary systems in a small countercurrent, laminar flow horizontal contactor by the application of a 2 kV electric field. However, mass transfer coefficients were increased only by a factor of 3 in ternary systems [15]. Glitzenstein *et al.* [17] studied the electrically enhanced mass transfer of acetic acid from kerosene in to water across a plane interface. At a nominal electric field of 357kV/m, the coefficient of mass transfer through the bulk of the kerosene phase was increased to twice the value with no electric field applied. It was further noted that this enhancement mainly resulted from electrically driven bulk motion rather than interfacial turbulence. The motion rate increased with increasing the voltage and its direction was independent of polarity. After investigating the mass transfer of benzoic acid from water dispersed into mineral oil with high viscosity, He *et al.* [18] denoted that the enhancement of mass transfer efficiency mainly resulted from increased specific interfacial area and accelerated drop velocity due to electric

fields. Gneist and Bart [19] investigated the influence of high-frequency AC fields on mass transfer from aqueous pendant droplets and, separately from moving droplets into a continuous organic phase. The results show that AC fields inhibit Marangoni effects whereas DC fields enhance or initiate Marangoni phenomena. The differences could be attributed to ion-drag phenomena under a DC field inside the organic phase. The measurement of mass transfer from falling single droplets showed no mass transfer enhancement under applied electric fields at constant droplet size. Several possible reasons can be put forward. Firstly, it is possible that electric field effects decline as the droplet detaches from the nozzle. Secondly, the droplet oscillation as well as circulation may be inhibited when the viscosity of the continuous phase is high. It further verified the conclusion of He *et al.* that the intensification is mainly due to increased interfacial area rather than interfacial turbulence. These literatures told us that effect of electric fields on mass transfer in liquid-liquid systems is relatively complex.

A variety of different test apparatus were developed to examine the influence of interfacial convection on mass transfer across liquid-liquid interfaces. Lewis [1, 2], Olander and Reddy [4] as well as Sethy and Cullinan [8] employed stirred extraction cells or Lewis cells to study the effect of interfacial turbulence on the mass transfer rate. Maroudas and Sawistowski [3], Bakker *et al.* [5] and Zhang *et al.* [20] designed an extraction apparatus based on parallel flows to investigate liquid-liquid mass transfer. Experimental results for different types of contactors showed that the mass transfer enhancement factors range from 1.5 to 10. One disadvantage of these methods is that the interfacial turbulence may be affected by the characteristics of the apparatus. In order to determine the effect of electrically driven turbulence on mass transfer, Glitzenstein *et al.* [17] applied a non-flow contactor to

study the mass transfer enhancement of acetic acid across a plane kerosene/water interface. In other works countercurrent contactors were employed for mass transfer experiments across plane interfaces under electric fields [14, 15, 21]. Since liquid-droplet contactors are widely used for liquid-liquid extraction, study of single-droplets is also a common approach used. The mass transfer rate during droplet formation with interfacial turbulence was studied experimentally [10]. Interfacial turbulence was found to increase the mass transfer rate, and an enhancement factor was defined as the ratio of the overall mass transfer coefficient in the presence of interfacial turbulence to its value based on the penetration theory. Lode and Heideger [7] studied single drop mass transfer immediately following formation using a photographic technique. The drop was retained in a channel after release for photograph. High mass transfer coefficients were observed. Similarily, Wham and Byers [16] determined the influence of electric fields on mass transfer from a single droplet, which was suspended in a precisely machined expanding channel. The arrangement allows monitoring of drop size and shape in addition to photographic recording of interfacial hydrodynamics. The mass transfer rates in a hemispherical quasi-steady-state pendant aqueous droplet have been measured as a function of time in the toluene-acetone-water system [13]. The overall mass transfer coefficients are initially high in a new flowing pendant droplet but the values decrease to a steady-state value as the droplet surface ages. The extent of the initial enhancement of the coefficients over the steady-state values is dependent upon the solute concentration in the continuous phase because of the concentration dependence of Marangoni type interfacial turbulence. Mass transfer from freely moving single aqueous charged drops was also investigated under applied AC and DC voltages at constant drop size [19].

In summary, plane interfaces and pendant droplets are two of the more common methods used for investigating mass transfer in liquid-liquid systems. The benefit of the plane interfaces method is that the interfacial area may be well-controlled. For the pendant droplets method, droplets are easily to obtain in experiment and it is similar to actual environment in extraction equipments. No measurement of the mass transfer from pendant charged droplets with time has been made so far. Hence, the first objective of this part was to establish a feasible method and to measure it experimentally. An attempt was made to measure the mass transfer across a plane interface when an electric field was applied.

4.2 Experimental

4.2.1 Setup

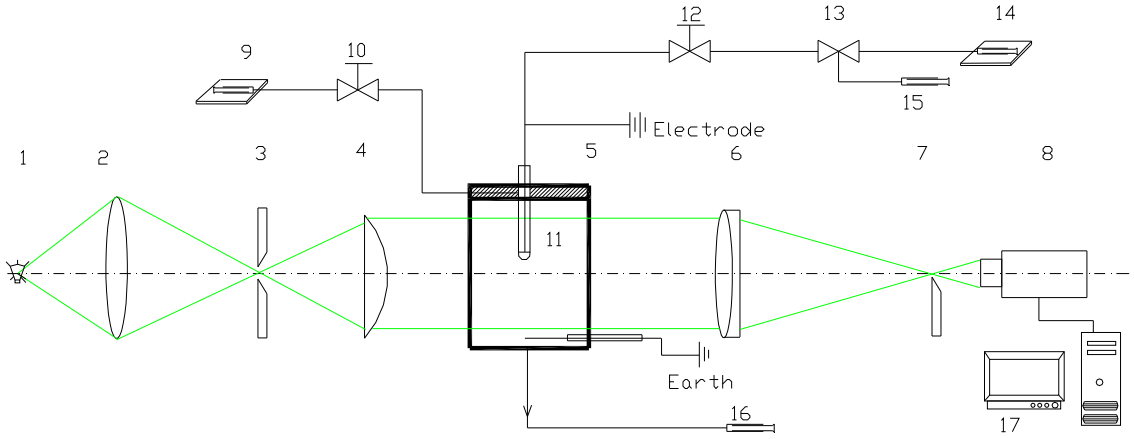

1-Light source; 2-biconvex; 3-slit; 4-planoconvex; 5- Schlieren cell; 6-achromat; 7-knife edge; 8-CCD camera; 9,14- syringe pumps; 10, 12-shut off valves; 11-concentric nozzle; 13-sampling Tee; 15, 16-syringes, 17- computer

Figure 4.1 Schematic of experimental setup for the measurement of mass transfer from a pendant droplet

The schematic of the apparatus used for the measurement of mass transfer from a pendant aqueous droplet into a continuous phase is shown in Figure 4.1. A sampling unit was added into the original optical Schlieren system. In order to obtain a sample from the outlet line, a

sampling Tee and a syringe were employed. Figure 4.2 shows the schematic of the flow cell for the pendant droplet. Its description is seen in Chapter 3.

A flow cell was used for the study of mass transfer across a plane interface as presented in Figure 4.3. The acrylic cell has dimensions of 10mm (length) ×10mm (width) ×45mm (height) with two stainless steel plate electrodes (5mm×5mm) located 15mm from the middle of the height. Two pieces of capillary tubing were attached at the one side of the cell for the inlet lines of organic phase and aqueous phase, respectively. The other two pieces of capillary tubing were attached at the other side of the cell for outlet lines. Two syringe pumps were used to infuse the two phases. The two phases were withdrawn from the cell by siphoning. The position of the interface was controlled by adjusting the height of the two outlet lines.

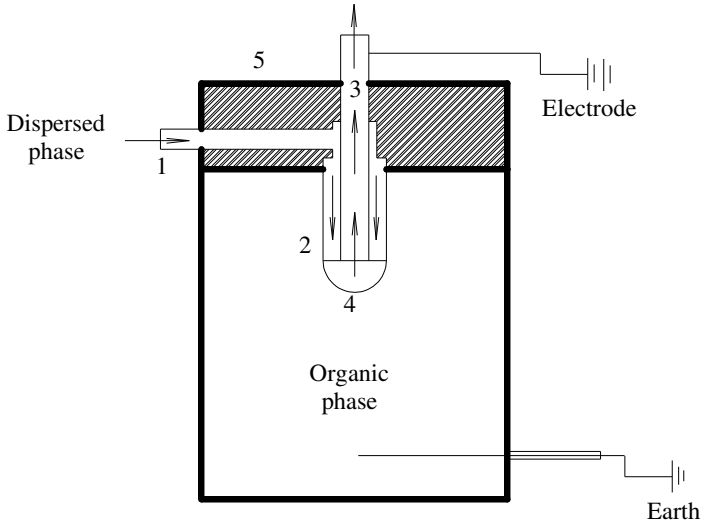

1-Inlet; 2-glass tubing; 3-hypodermic needle; 4-pendant droplet; 5-PVT lid

Figure 4.2 Schematic of flow cell for a pendant droplet

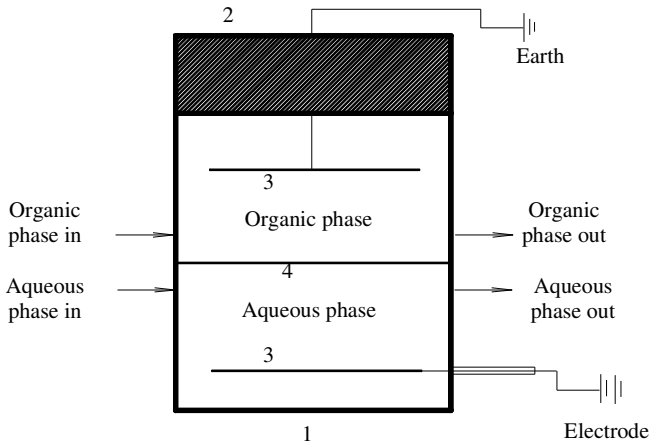

1-Cell; 2-PVC lid; 3-flat stainless steel electrode; 4 interface

Figure 4.3 Schematic of flow cell for a plane interface

4.2.2 Procedures

For the pendant droplet system, the glassware of the concentric nozzle was cleaned using chromic-sulfuric acid (Fischer Scientific), washed in deionized water and then dried before each run. The deionized water and 1-decanol phases were mutually saturated before preparing ethanol aqueous solutions. The aqueous solution of known ethanol concentration was infused to fill the inlet and outlet lines and all tubing using two syringe pumps (AL-2000, WPI, Inc., USA) so that all air bubbles were excluded. Then the nozzle was immersed into 1-decanol phase. The syringe pump connected with the inlet line was used to infuse the aqueous phase through the nozzle annulus to form a hemispherical droplet at the tip of the nozzle. This operation was carried out slowly in order to avoid any hydrodynamic disturbance to the droplet surface during formation. Once the droplet reached the predetermined hemispherical sizes, the syringe pump connected with the outlet line was started immediately with the same speed as the infusion pump speed to withdraw liquid from the droplet and thus maintain the pendant droplet at a constant size. At the same time, the high DC voltage unit (Glassman High Voltage, Inc, USA) was used to impose an electric

field on the electrodes at time t=0. After 3.5 minutes of residence time, sampling was begun by pulling a syringe back slowly in order to allow for the holdup in the outlet line. The speed of the withdrawing pump needed to be reduced to keep the droplet size constant. The time interval of each sampling was fixed at 2.5 min. About 20 samples were taken over a 1 hour period during each run with each run repeated at least three times. The samples were analyzed and the content of ethanol was determined by GC (Agilent 6890N, USA).

For the plane interface case, the aqueous phase was introduced first through the inlet line using a syringe pump. The phase level was kept at the middle height of the flow cell by using adjusting the level of the outlet line and controlling the flowrate of the effluent using a micrometer screw. After that the 1-decanol phase was introduced using the other syringe pump. Its level was controlled using the same method as the aqueous phase. Once the flow rates of the two phases and the interface level reached stable, an electric field was applied and a run was started. After some residence time, sampling was begun at a 3min interval. About 20 samples were taken over a 1 hour period during each run with each run repeated at least three times. The samples were analyzed and the content of ethanol was determined by GC (Agilent 6890N, USA).

4.3 Results and Discussion

4.3.1 Physical Properties of Liquids

Ethanol (EtOH), deionized water and 1-decanol were used as solute, the solvent of dispersed phase and continuous phase respectively. Physical properties of these pure components are shown in Table 3.2. Mutually saturated water and 1-decanol were used in order to eliminate any mass transfer between them. Aqueous solutions of different ethanol concentrations were prepared as dispersed phase. The density of these aqueous phases was

measured at 25°C using a DMA 4500 densitometer (Anton Paar, USA) and the results showing the relationship between density of composition plotted in Figure 4.4.

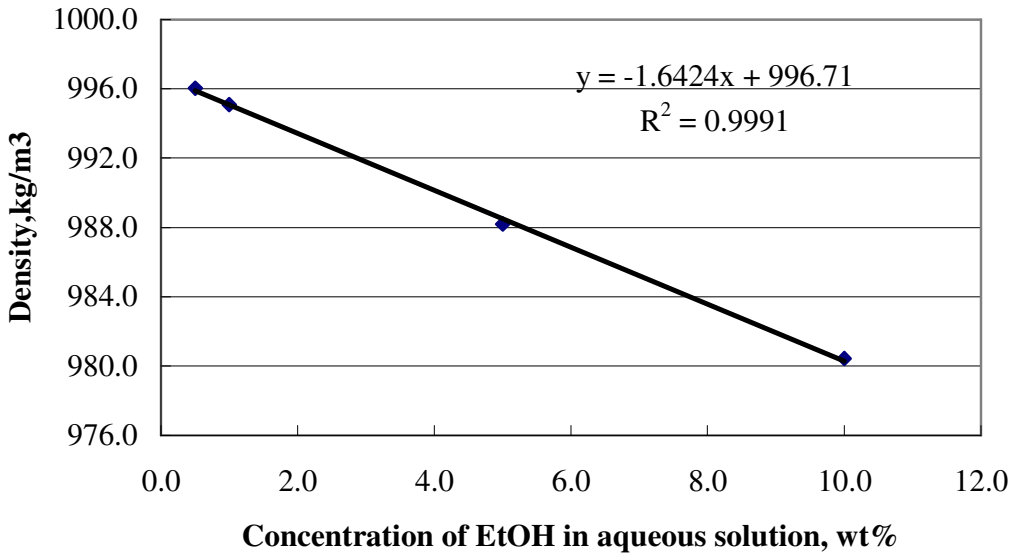

Figure 4.4 Density of dispersed phase at different EtOH concentration

4.3.2 Distribution Ratio of EtOH in Water and 1-Decanol

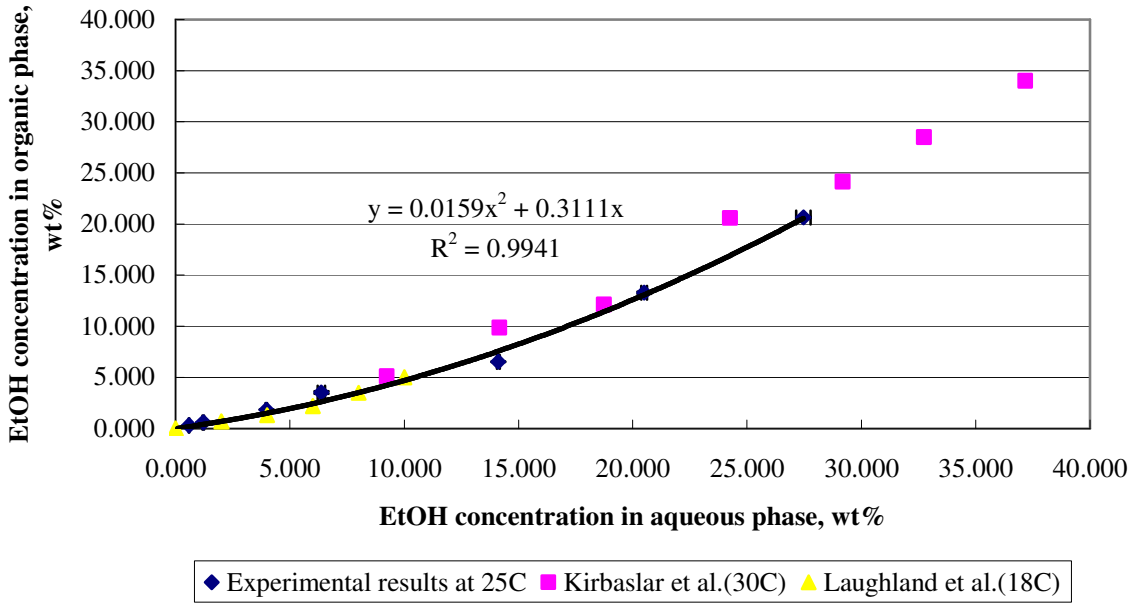

Figure 4.5 Distribution ratio curves for ethanol-water-1-decanol system

The distribution ratio of the test system is a very important parameter when mass transfer is measured. In liquid-liquid extraction, distribution ratio is often quoted as a measure of the feasibility of extraction of a particular component into a second liquid. Distribution ratio may be defined as the ratio of the concentration of solute in organic phase to its concentration in aqueous phase. The distribution ratio of ethanol in water and 1-decanol can be measured by determining the concentration of ethanol in the two phases. During experiment, the dispersed phases of different ethanol concentration were mixed with 1-decanol in 20 ml disposable vials and shaken well at 25^{o} C. The mixtures were left standing overnight to ensure complete separation of the two phases which were sampled individually by syringe. The samples were analyzed and the concentration of ethanol was detected using GC. Laughland *et al.* [22] determined the partition behavior of EtOH-water-1-decanol by a routine batch equilibrium technique at 18^{o} C. Kirbaslar *et al.* [23] published the liquid-liquid equilibrium data for the EtOH-water-1-decanol system at 30^{o} C. All these distribution ratio data are shown in Figure 4.5. The experimental data seem to be satisfactory although there are not the same as those in literatures possibly caused by the difference of temperature. The distribution ratio of ethanol in water and 1-decanol is 0.56 at 25^{o} C.

4.3.3 Mass Transfer Rate Measurement

4.3.3.1 Pendant Droplet

A quasi-steady state droplet technique [11] was used to study the time-dependent behavior of mass transfer rate in our experiment. The technique involves the formation of a suspended, aqueous pendant hemispherical droplet from a concentric nozzle in an organic continuous phase contained in a column. Figure 4.6 is a schematic diagram of flow

conditions for a quasi-steady hemispherical droplet. A mathematical model was developed to determine mass transfer coefficient based on a mass balance of solute in the droplet.

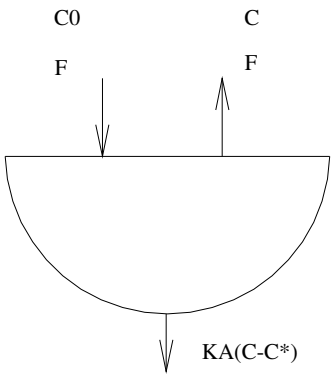

Figure 4.6 Schematic of the flow conditions for a hemispherical pendant droplet

An unsteady state mass balance for the droplet may be written:

$$F(C_0 - C) - KA(C - C^*) = V\frac{dC}{dt} \tag{1}$$

where C_0 is the concentration of dispersed phase pumped in, mol/ml

C is the concentration of ethanol in droplet, mol/ml

C^* is the equilibrium concentration of ethanol in droplet, mol/ml

F is the flow rate in inlet line and outlet line, ml/hr

K is the overall dispersed phase mass transfer coefficient, m/hr

A is the pendant droplet surface area, m^2

V is the pendant droplet volume, m^3

Assuming that the ethanol concentration in the continuous phase is negligible because of the large quantity of organic phase in the column, the concentration of ethanol in the organic phase is assumed to approach zero at all times. Thus the equilibrium concentration (C^*) of ethanol in droplet is assumed to be zero. Hence, Equation 1 reduces to

$$F(C_0 - C) - KAC = V\frac{dC}{dt} \tag{2}$$

and

$$K = \frac{F}{AC}(C_0 - C) - \frac{V}{AC}\frac{dC}{dt} \tag{3}$$

if the mass transfer coefficient K may be considered constant over a small time interval Δt, and the corresponding concentration change is ΔC, then Equation 3 becomes

$$K = \frac{F}{A\bar{C}}(C_0 - \bar{C}) - \frac{V}{A\bar{C}}\frac{\Delta C}{\Delta t} \tag{4}$$

where $\bar{C}$ is the mean concentration in the drop during this time interval Δt.

Hence, the values of the K calculated from Equation 4 can be plotted as a function of mean time $\bar{t}$ for given experimental conditions.

At steady state condition, Equation 4 can be simplified to

$$K_s = \frac{F}{AC}(C_0 - C) = \frac{F}{A}(\frac{C_0}{C} - 1) \tag{5}$$

where K_s is the overall dispersed phase mass transfer coefficient at steady state.

The ethanol concentrations in the droplet were measured, and their changes with time are shown in Figure 4.7 when the initial ethanol concentration is 5 wt% in the aqueous phase. The result indicates that the changes may consist of two kinds of trends whether or not an electric field was applied. Initially, the ethanol concentration in the pendant droplet decreases as time proceeds. Then the concentration increases and approaches a steady state value. This result seems to be different from those reported in literatures [11-13]. Three possible reasons could result in it. Firstly the actual mean residence time in outlet line may be longer than that which was measured. The use of short residence times led to higher concentration in the

samples in the early period. Secondly, the wall thickness of the needle used for withdrawing the aqueous phase was so small that some dispersed phase from the annulus of the concentric nozzle may have been withdrawn before mass transfer is complete (i.e. "short circuit" flow). This may also explain why the ethanol concentration in the droplet is high initially. Finally, the changing behavior of ethanol concentration may be related to the time-dependent nature of interfacial turbulence. As seen in Figure 4.7, the ethanol concentrations in the droplet at 1kV are lower than those in the absence of electric fields. It shows that mass transfer was enhanced by the electric field. Overall mass transfer coefficients were calculated from Equation 4 when the flow rate of dispersed phase was set to 10ml/hr. Their changes with time are shown in Figure 4.8. The trends of these curves further confirm the results observed from Figure 4.7. A about twofold increase of the equilibrium mass transfer coefficient was found.

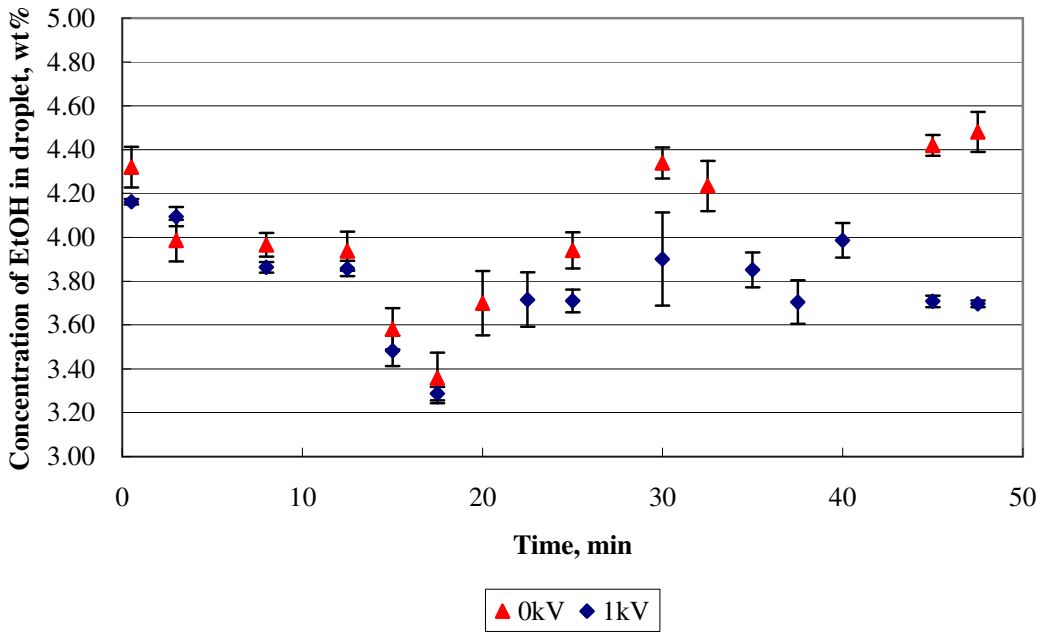

Figure 4.7 Changes of ethanol concentration in the pendant droplet with time for 5wt% solute concentration in the aqueous phase

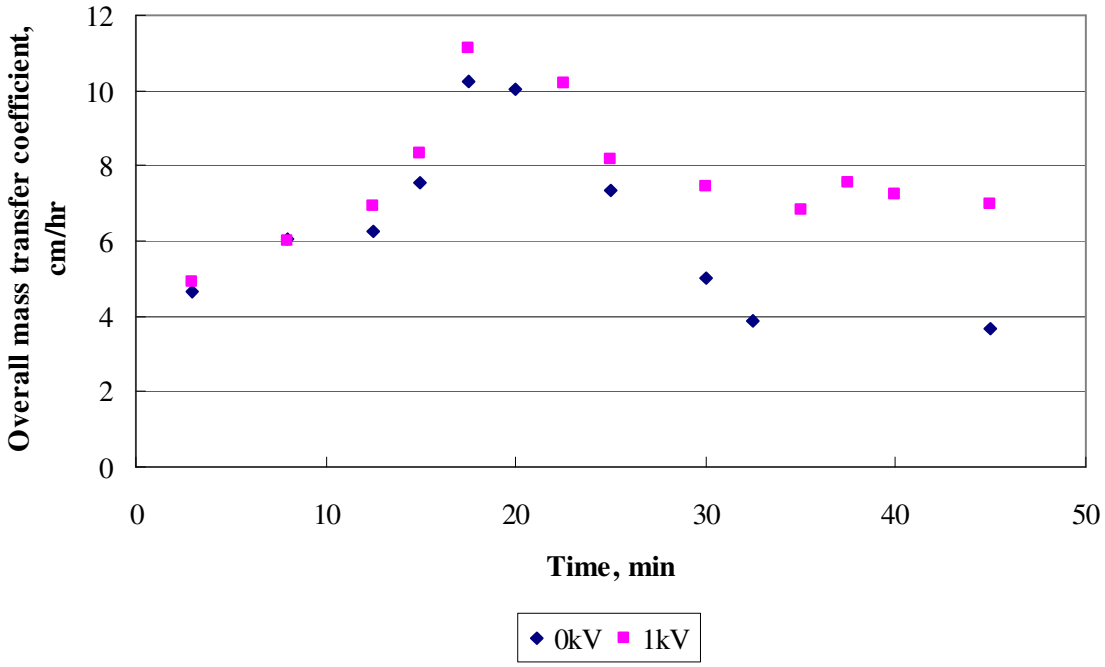

Figure 4.8 Changes of overall mass transfer coefficient with time for 5wt% solute concentration in the aqueous phase

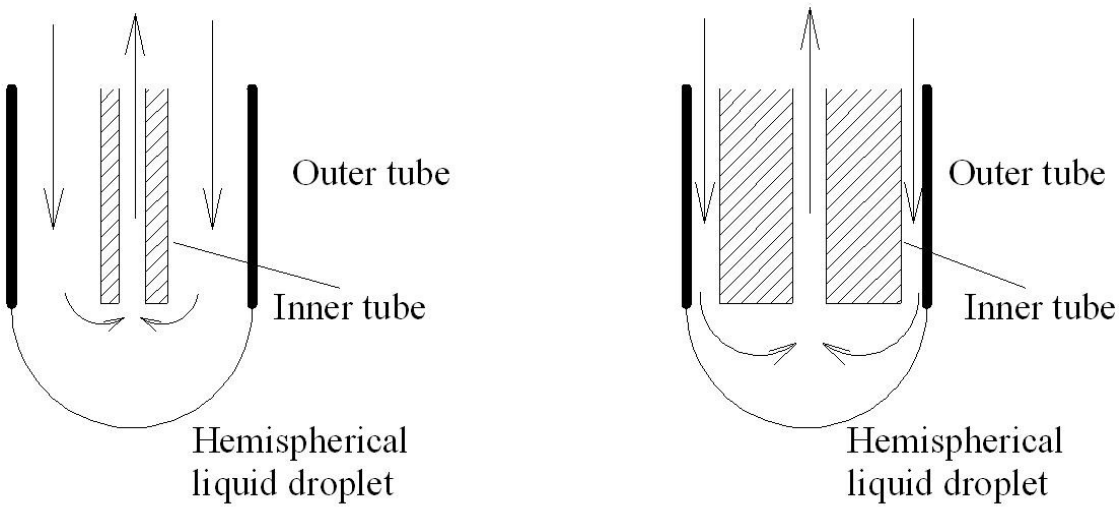

(a) Current design (b) New design

Figure 4.9 Comparison between two concentric nozzle designs

Based on experimental observation and data analysis, the current experimental method needs some modifications in order to obtain better mass transfer data. It is necessary and would be beneficial to make some changes of the sampling process. Currently a sampling Tee was used and aqueous phase was withdrawn by hand using a syringe. This technique is relatively crude and could have caused the fluctuation of the droplet size and the resulting contact area if it was not controlled carefully. One feasible way to improve this would be to remove samples by siphoning. The flow rate of effluent can be controlled precisely by micro-adjusting the level of outlet line using a micrometer screw. As we denoted earlier, another problem is the design of the concentric nozzle as shown in Figure 4.9(a). The needle used in the experiments was of 22 gauge with only a 0.3mm wall thickness, which resulted in a large annulus between the inner tube and outer tube and a very short path for the aqueous phase between them. The aqueous phase introduced may be withdrawn through the inner tube immediately before mass transfer. A sufficient wall thickness is required in order to prevent "short circuit" and a possible new design is presented in Figure 4.9(b). In this design, it takes longer time for the aqueous phase to reach the inner tube due to a thick annulus.

4.3.3.2 Plane Interface

Compared with the pendant drop method, the study of mass transfer across a plane interface has been used as an alternative because it is confined in a contactor and has a well-defined interface. Hence, some attempts were made here on the development of a laminar co-current flow channel. The flow conditions for the laminar co-current flow channel are shown in Figure 4.10.

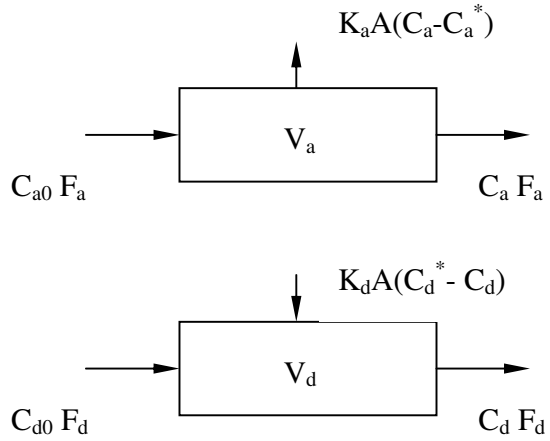

Figure 4.10 Schematic of the flow conditions for aqueous phase and 1-decanol phase of a laminar co-current flow channel

An unsteady state mass balance for the aqueous phase is:

$$F_a(C_{a0}-C_a)-K_aA(C_a-C_a^*)=V_a\frac{dC_a}{dt} \tag{6}$$

Similarly, for 1-decanol phase we have

$$F_d(C_{d0}-C_d)+K_dA(C_d^*-C_d)=V_d\frac{dC_d}{dt} \tag{7}$$

where C_0 is the concentration at the inlet of flow channel, mol/ml

C is the concentration at the outlet of flow channel, mol/ml

C^* is the equilibrium concentration, mol/ml

F is the flow rate, ml/hr

K is the overall dispersed phase mass transfer coefficient, m/hr

A is the area of plane interface, m^2

V is the volume of the two phases, m^3

a denotes the aqueous phase, and d denotes the decanol phase.

Eq. 6 and Eq. 7 can be changed into

$$K_a = \frac{F_a(C_{a0} - C_a)}{A(C_a - C_a^*)} - \frac{V_a}{A(C_a - C_a^*)}\frac{dC_a}{dt} \tag{8}$$

$$K_d = \frac{F_d(C_{d0} - C_d)}{A(C_d - C_d^*)} - \frac{V_d}{A(C_d - C_d^*)}\frac{dC_d}{dt} \tag{9}$$

If the mass transfer coefficient K may be considered constant over a small time interval Δt, and the corresponding concentration change is ΔC, then Eq.8 and Eq. 9 become

$$K_a = \frac{F_a(C_{a0} - \overline{C_a})}{A(\overline{C_a} - C_a^*)} - \frac{V_a}{A(\overline{C_a} - C_a^*)}\frac{\Delta C_a}{\Delta t} \tag{10}$$

$$K_d = \frac{F_d(C_{d0} - \overline{C_d})}{A(\overline{C_d} - C_d^*)} - \frac{V_d}{A(\overline{C_d} - C_d^*)}\frac{\Delta C_d}{\Delta t} \tag{11}$$

where $\bar{C}$ is the mean concentration in the each phase during this time interval Δt.

At steady state conditions, Equation 10 and 11 reduce to

$$K_{as} = \frac{F_a(C_{a0} - C_a)}{A(C_a - C_a^*)} \tag{12}$$

$$K_{ds} = \frac{F_d(C_{d0} - C_d)}{A(C_d - C_d^*)} \tag{13}$$

where K_{as} and K_{ds} are the overall dispersed phase mass transfer coefficients at steady state.

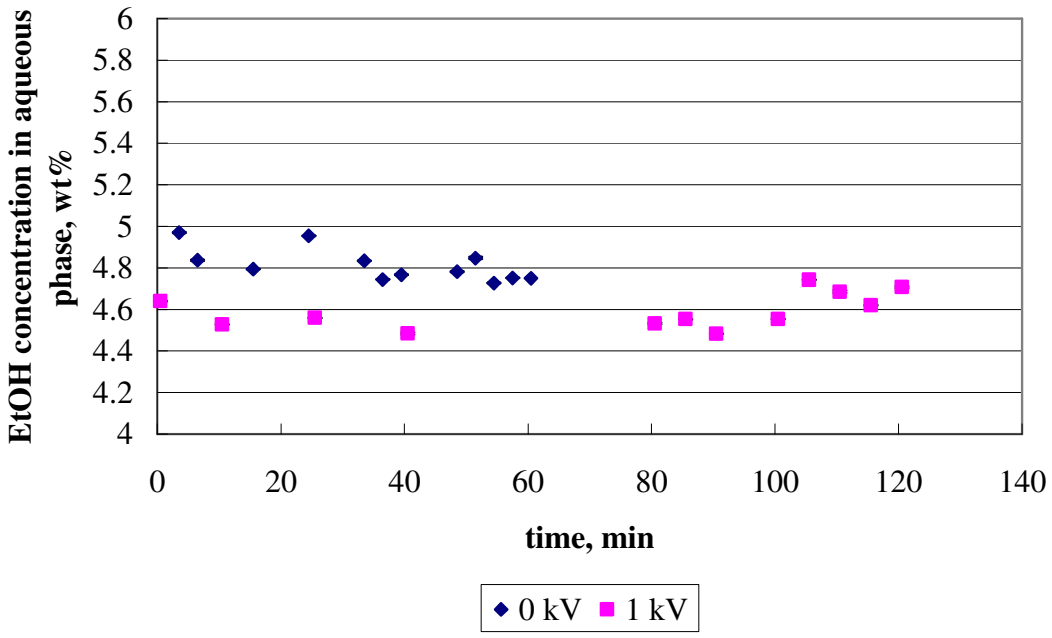

Figure 4.11 Time dependent of ethanol concentration in aqueous phase and the effect of electric fields on mass transfer across a plane interface for 5wt% solute concentration

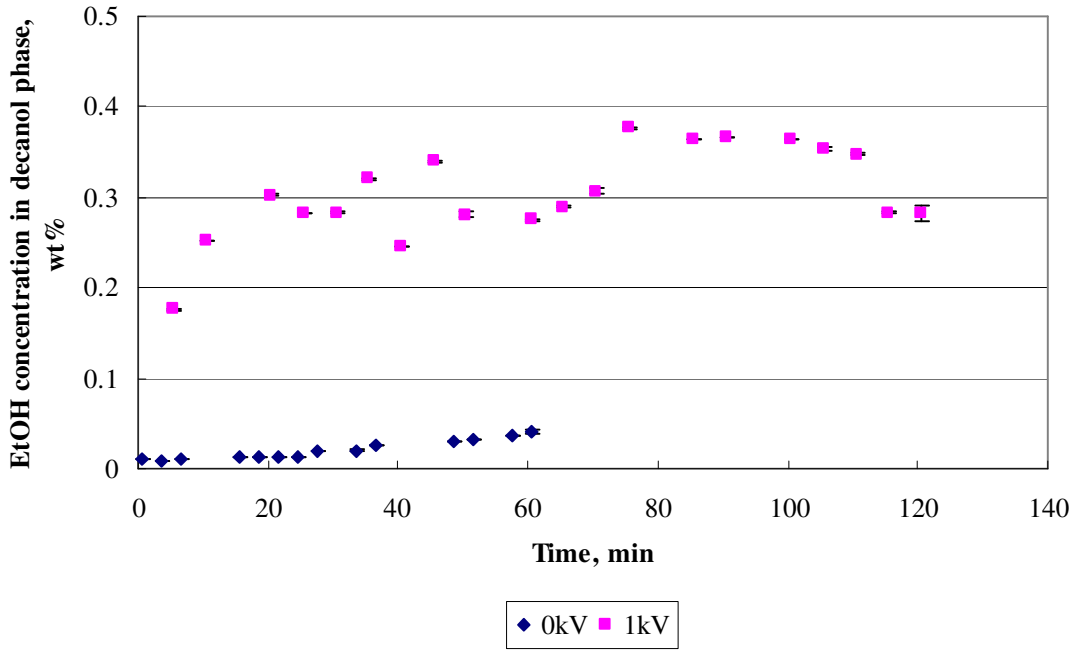

Figure 4.12 Time dependent of ethanol concentration in decanol phase and the effect of electric fields on mass transfer across a plane interface for 5wt% solute concentration

A flow cell with the dimension of 10mm×10mm×45mm is shown in Figure 4.3. Some initial experimental data were obtained for 5wt% solute concentration in the aqueous phase. The ethanol concentrations in the aqueous phase and in the 1-decanol phase were measured. The changes of ethanol concentration in the two phases with time were shown in Figure 4.11 and Figure 4.12, respectively. In the absence of electric fields, the ethanol concentration in the aqueous phase declines in a very small range during the short experimental period. Accordingly, the ethanol concentrations in 1-decanol phase are very small (less than 0.1wt%) and increase slowly with time. These data indicate that mass transfer occurred but it is very limited in the absence of electric fields. When a 1kV electric charge was applied, the ethanol concentrations in both phases have identical change trends with time as those at 0kV within the first 60 min. Then the ethanol concentration in aqueous phase increases as time proceeds, and the ethanol concentration in 1-decanol phase decreases with time. The trends are similar to those observed in the pendant droplet. Two reasons for this may be put forward. Firstly, the applied flow cell was designed to have a small interfacial area because of short length, which is not beneficial to mass transfer and did not result in large change of ethanol concentration especially in the absence of electric fields. Additionally, the transport cell has relatively big height and the outlet lines are located far from the plane interface. Hence, it could take more time to transport ethanol by interfacial convection to the location of outlet lines which would lead to even higher concentrations in aqueous phase and lower concentrations in organic phase during the early period. The data in Figures 4.11 and 4.12 clearly show that the aqueous phase retains much more of the ethanol solute in the absence of the external electric field. Correspondingly, the organic phase extracts much less ethanol in the absence of the electrical field. Thus there is clear evidence that the mass transfer is

enhanced in the presence of the electric field. The enhancement cannot be explained by increase in interfacial area since none occurs. The most likely explanation is due to enhanced interfacial turbulence and enhanced solute transport in the region of the interface.

Based on the results, the design of current flow cell needs some modifications. Firstly, it may benefit from a larger ratio of length to height as noted in some literatures [14, 15, 21]. Moreover, the locations of the outlet lines are very important for sampling. All of them will improve the mass transfer data.

4.3.3.3 Mass Transfer Mechanisms with Interfacial Turbulence

Usually it is difficult to obtain liquid-liquid mass transfer coefficient data especially when electrically induced interfacial turbulence exists. Liquid-liquid mass transfer coefficients can be predicted from transport models or by use of correlations developed using dimensional analysis and liquid physical property data, geometrical data, and experimental mass transfer data. However, the first method requires a complete understanding of interfacial mass transfer mechanisms in the presence of electric fields although some conventional transport models have been developed to predict mass transfer coefficients for liquid-liquid extraction. Two classical models include the two-film model of Lewis and Whitman [24] and the penetration theory of Higbie [25]. Other models are developed from the two classical models by assumption of dynamic film and adopting different age distributions for the surface elements including surface renewal model [26], film-penetration model [27] and modified surface renewal models [28-32].

It is very difficult for the surface renewal model to be applied in estimation of mass transfer coefficient in liquid-liquid system due to the difficulty in measurement of the age distribution of the liquid eddies. The only work which has reported surface renewal

measurement for liquid interfaces was by Thornton *et al.* [37]. They used a novel photochromic dye tracer technique to analyze the droplet surface behavior qualitatively and quantitatively. The exposure time distribution of the surface eddies was measured by the technique. The results for the droplet systems under the conditions employed in the study showed that the observed surface renewal was caused by interfacial turbulence accompanying mass transfer not by the hydrodynamic flow as assumed in the renewal models.

The surface renewal models are based on molecular diffusion. Some literature proposed eddy diffusion models [33, 34] which attempted to relate the mass transfer mechanism to turbulence through eddy diffusivity (D_E). The eddy diffusivity depends on the normal distance from the interface and the mass transfer is attributed to the structure and the sizes of the eddies [35, 36]. Although the turbulent diffusion models seem to be more fundamental by comparison with the surface renewal models because they assume the effect of turbulence in terms of the characteristics of turbulent flow, it still is difficult for them to estimate the mass transfer coefficients because of a lack of direct information about the eddy size, structure and the velocity fluctuations in the interfacial areas. Recently, laser Doppler anemometry (LDA) was used to study the turbulence structure and transport mechanism and measure the velocity fluctuations in the interfacial regions [38, 39]. However, it is not possible to formulate a unified theory which properly represents the real mechanisms of transfer until a lot more information is available concerning the hydrodynamic behavior at and near to the interface.

In the presence of an electric field, interfacial turbulence is initiated and then develops into the organic phase in our system. After some time, the fluid eddies meet each other and they can travel back to the interface. The situation is more complicated than that in the

surface renewal model. First, the surface renewal is induced by interfacial flow due to interfacial tension gradients other than hydrodynamic flow. In addition, it becomes more difficult to measure the exposure time distribution of fluid eddies due to the diversity of interfacial flows.

According to the turbulence diffusion model, the eddy diffusion varies in magnitude with the normal distance from the interface. At the interface the eddy diffusion is damped by the interfacial tension forces and transfer is by molecular diffusion alone. For the systems where interfacial turbulence or Marangoni effect is present, the assumption is not exact any more. Moreover, the structures and sizes of fluid eddies are more complicated because the eddies show them in many forms including eruptions, surface rippling and agitation.

Due to complexity of the mass transfer mechanism when interfacial turbulence happens, a general model has not been developed to evaluate the mass transfer coefficient enhancement due to the interfacial turbulence. Correlation may provide a simpler method to predict the mass transfer coefficients in liquid-liquid systems because they can be expressed as a function of the liquid properties and the dimensions of the contactors. Lewis [1, 2] applied successfully this method to calculate the individual mass transfer coefficients for liquid-liquid systems in his Lewis cell. Takeuchi and Numata [9] correlated the amount of solute transferred and the contact time to determine the mass transfer coefficients for the acetic acid-water-isobutyl alcohol system, where interfacial turbulence occurred. Glitzenstein *et al.* [17] predicted the Sherwood Number in the presence of an electric field using the Sherwood-Grashof correlation based on the data acquired in the absence of an electric field. The Sherwood Number was then used to calculate the mass transfer coefficient in the organic phase. Results on a system involving extraction of acetic acid across a plane kerosene/water

interface proved to be a promising example of this approach. While this approach is feasible it can be significantly limited to a narrow range of systems operating under well specified conditions.

4.4 Conclusions

In this chapter, a number of different types of apparatus were explored for the study of interfacial liquid-liquid mass transfer in the presence of an electrostatic field. Two experimental methods were employed to study interfacial mass transfer: (1) a pendant droplet and (2) a plane interface. Two corresponding experimental setups were built. Ethanol-water-1-decanol was selected as the test system. Mass transfer was investigated for the system in the two different setups by measuring ethanol concentrations and deducting the mass balance of ethanol in two phases. Initial data of mass transfer coefficients were obtained for the mass transfer from a pendant droplet. Changes in ethanol concentrations in both phases and the corresponding mass transfer coefficients show a time-dependent nature which correlated closely with the Schlieren images described in Chapter 3. Mass transfer measurements in a small flow cell provided further evidence of the above phenomena. Moreover, all data show that mass transfer can be intensified by the application of electric fields. A about twofold enhancement of mass transfer of ethanol was observed from the aqueous pendant droplet into 1-decanol phase when 1kV DC was applied. The result is reasonable compared to those obtained by Iyer and Sawistowski [15] although they used the different systems. Finally, in order to obtain mass transfer coefficients under electric fields based on current mass transfer models, mass transfer mechanism with electrically induced interfacial turbulence should be investigated. Some considerations about it were discussed. Correlation may be a good means to calculate mass transfer coefficients.

Some initial data and results have been obtained in my experiment, but they are not good as expected. Some proposals have been provided and may improve the data quality. These ideas include a new design of the concentric nozzle and the flow cell, and development of a more accurate sampling method.

4.5 References

1. J. B. Lewis, The mechanism of mass transfer of solutes across liquid-liquid interfaces Part I: The determination of individual transfer coefficients for binary systems, Chem. Eng. Sci., 3 (1954) 248-259.
2. J. B. Lewis, The mechanism of mass transfer of solutes across liquid-liquid interfaces Part II: The transfer of organic solutes between solvent and aqueous phases, Chem. Eng. Sci., 3 (1954) 260-278.
3. N.G. Maroudas and H. Sawistowski, Simultaneous transfer of two solutes across liquid-liquid interfaces, Chem. Eng. Sci., 19 (1964) 919-931.
4. D.R. Olander and L.B. Reddy, The effect of concentration driving force on liquid-liquid mass transfer, Chem. Eng. Sci., 19 (1964) 67-73.
5. C.A.P. Bakker, F.H. Fentener van Vlissingen and W.J. Beek, The influence of the driving force in liquid-liquid extraction –a study of mass transfer with and without interfacial turbulence under well-defined conditions, 22 (1967) 1349-1355.
6. E. Ruckenstein, Mass transfer in the case of interfacial turbulence induced by the Marangoni effect, Int. J. Hat Mass Transfer, 11 (1968) 1753-1760.
7. T. Lode and W.J. Heideger, Single drop mass transfer augmented by interfacial instability, Chem. Eng. Sci., 25 (1970) 1081-1090.

8. Sethy and H.T. Cullinan, Transport of mass in ternary liquid-liquid systems, AIChE J., 21 (1975) 571-582.
9. H. Takeuchi and Y. Numata, The effect of interfacial turbulence on liquid-liquid mass transfer rates, Int. Chem. Eng., 17 (1977) 468-474.
10. Y. Nakaike, T. Mizukoshi, T. Aonuma, T. Tadaki, Mass transfer accompanied by interfacial turbulence during droplet formation in a liquid-liquid system, Int. Chem. Eng., 24 (1984) 527-535.
11. K.H. Javed and J.D. Thornton, Time dependent mass transfer rates in a liquid-liquid system exhibiting interfacial turbulence, I. Chem. E. Symposium Series, 88 (1984) 203-216.
12. D. Rogers, P.J. Thompson, J.D. Thornton, The time dependence of the mass transfer of uranyl nitrate between nitric acid and tri-butyl phosphate, I. Chem. E. Symposium Series, 103 (1987) 15-27.
13. K.H. Javed, J.D. Thornton, T.J. Anderson, Surface phenomena and mass transfer interactions in liquid-liquid systems: Part 2, AIChE J., 35(1989) 1125-11136.
14. L.J. Austin, L. Bancyk, and H. Sawistowski, Effect of electric field on mass transfer across a plane interface, Chem. Eng. Sci., 26 (1971) 2120-2121.
15. P.V.R. Iyer and H. Sawistowski, Effect of electric field on mass transfer across a plane interface, Proceedings of the international solvent extraction conference, Lyon, (1974) 1029-1046.
16. R.M. Wham and C.H. Byers, Mass transfer from single droplets in imposed electric fields, Separation Sci. and Techno. 22 (1987) 447-466.

17. Glitzenstein, A. Tamir, and Y. Oren, Mass transfer enhancement of acetic acid across a plane kerosene/water interface by an electric field, The Canadian J. of Chem. Eng., 73 (1995) 95-102.
18. W. He, M.H.I. Baird, and J.S. Chang, The effect of electric field on mass transfer from drops dispersed in a viscous liquid, The Canadian J. of Chem. Eng., 71 (1993) 366-376.
19. Gneist, H.-J. Bart, Influence of high-frequency AC fields on mass transfer in solvent extraction, J. of Electrostatics, 59 (2003) 73-86.
20. S.H. Zhang, Z.M. Wang and Y.F. Su, Mass transfer and interfacial turbulence in a laminar film, study of transferring two solutes separately and simultaneously through liquid-liquid interface, Trans. IChemE, 68 (1990) 84-92.
21. S. Wolf and J. Stichlmair, The influence of the Marangoni-effect on mass transfer, ISEC, Melbourne, Australia, (1996) 51-56.
22. G.J. Laughland, M.K. Millar, and L.R. Weatherley, L. R., Electrostatically enhanced recovery of ethanol from fermentation liquor by solvent extraction, IChemE symposium series no. 103, EFCE publication series no. 347 (1987) 263-278.
23. Kirbaslar, S. Cehreli, D. Ustun and E. Keskinocak, Equilibrium data on ethanol-water-solvent ternaries, Braz. J. Chem. Eng., 17 (2000) 191-197.
24. W.K. Lewis and W.G. Whitman, Principles of gas absorption, Ind. Eng. Chem., 16 (1924) 1215-1220.
25. R. Higbie, The rate of adsorption of a pure gas into a still liquid during short periods of exposure, Trans. Am. Inst. Chem. Eng., 31 (1935) 365-389.
26. P.V. Danckwerts, Significance of liquid film coefficients in gas absorption, Ind. Eng. Chem., 43 (1951) 1460-1467.

27. H.L. Toor and J.M. Marchello, Film penetration model for mass and heat transfer, AIChE J., 4 (1958), 97-101.

28. D.D. Perlmutter, Surface renewal models in mass transfer, Chem. Eng. Sci., 16 (1961) 287-296.

29. P. Harriott, A random eddy modification of the penetration theory, Chem. Eng. Sci., 17 (1962) 149-154.

30. L.B. Koppel, R.D. Patel, and J.T. Holmes, Statistical models for surface renewal in heat and mass transfer: Part I. Dependence of average transport coefficients on age distribution, AIChE J., 12 (1966) 941-946.

31. T.F.C. Benjamin, L.T. Fan, and C.L. Hwang, Surface renewal and penetration models in the transient state, AIChE J., 17 (1971) 154-160.

32. D. Rambabu and G. Narsimhan, A Surface Renewal Model for Unsteady-State Transfer Processes, The Chem. Eng. J., 20 (1980) 169-175.

33. V.G. Levich, Physiochemical hydrodynamics, Prentice-Hall, Englewood cliffs, N.J., (1962).

34. C.J. King, Turbulent liquid phase mass transfer at free gas liquid interface, Ind. Eng. Chem. Fundamentals, 5 (1966) 1-8.

35. G.E. Fortescue and J.R.A. Pearson, On gas absorption into a turbulent liquid, Chem. Eng. Sci., 22 (1967) 1163-1176.

36. J.C. Lamont and D.S. Scott, An eddy cell model of mass transfer into the surface of a turbulent liquid, AIChE J. 16 (1970) 513-519.

37. J.D. Thornton, T.J. Anderson, K.H. Javed and S.K. Achwal, Surface phenomena and mass transfer interactions in liquid-liquid systems, Part 1: Droplet formation at a nozzle, AIChE J., 31(1985) 1069-1076.
38. S. Komori, H. Ueda, F. Ogino, Mizushina, Turbulence structure and transport mechanism at the free surface in an open channel flow, Int. J. Heat Mass Transfer, 25 (1982) 513-521.
39. S. Luke and Y.H. Lee, Mass transfer in eddies close to air water interface, AIChE J., 32(1986) 1546-1554.

Chapter 5 Biodiesel Production using Electrostatic Liquid Spraying

5.1 Introduction

Biodiesel is mainly synthesized through alkali-catalyzed transesterification of alcohol with vegetable oils or animal fats, which was discussed in Chapter 2. The process involves a liquid-liquid two-phase system, where reaction rate is limited by mass transfer between the alcohol rich phase and the oil phase. The efficiency of the contact or mixing between the feed oil and alcohol is crucial to achieving high interfacial mass transfer rate and large contact area, and leading to high reaction rate, short residence time and improved production efficiency. Conventionally, the enhancement of mass transfer rate and a large turbulent interfacial area can be achieved by mechanical agitation in a stirred tank. This mixing can help droplets break up and promote turbulence in the mixture. However, mechanical agitation is low in energy efficiency [1]. Additionally, liquid droplet size cannot be controlled carefully and excessive agitation can produce droplets which are so small that they form stable emulsions. It reduces the efficiency of product separation and diminishes the throughput of the process. It is well known that high voltage electric fields can enhance mass transfer rates and phase separation in liquid-liquid systems [2-6]. This improvement is due to higher specific interfacial area, induced interfacial turbulence and enhanced rates of interfacial shear and is attributed to fast drop coalescence. The technique employing electric fields involves charged droplet formation at a nozzle and the electrostatic spraying of dispersed phase into a continuous phase at high velocity.

5.1.1 Mechanism of Electrostatic Liquid Spraying

The discovery of electrostatic spraying can be traced back to the mid 18th century. Abbe Nollet performed experiments in which a water vessel with an outlet nozzle on the base was charged by a hand-rubbed, rotating glass ball. The emerging water which had previously dripped slowly from the nozzle then began to spray [7]. Due to the lack of any commercial application, the sprayer was not developed for any practical purpose. In the 1950's Vonnequt and Neubauer [8] produced sprays of water, ethanol, lubricating oil and sugar solutions from positively charged glass capillaries. Additional experiments on the spraying of dyed liquids produced the first ink jet printer. Since then there have been a number of interests in the study of electrostatic spraying, but they concentrated mostly on liquid/air systems not on liquid/liquid systems [9]. Many investigators have studied the formation of droplets in electric fields including uniform and non-uniform fields [2, 10-13]. Thornton [14] proposed two regimes responsible for the droplet formation and dispersion in electric fields: a discrete drop regime and an electrostatic spraying regime. As shown in Figure 5.1, a system comprising a single droplet of dispersed phase issuing from a conducting nozzle held at some potential will be used to explain the two regimes.

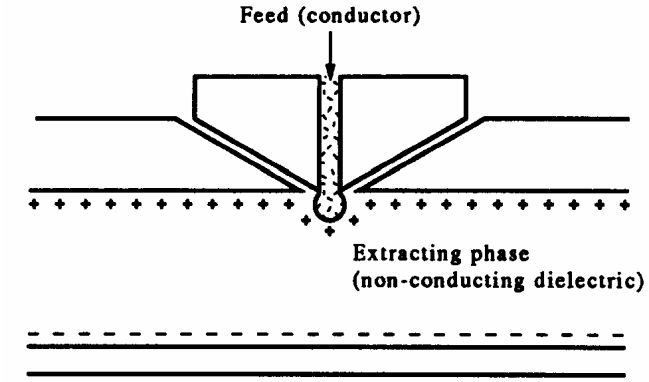

Figure 5.1 Charge induced on a conducting droplet in a uniform electric field [15]

- **Discrete drop regime**

At low to medium field strengths, the electrical force reduces the effective interfacial tension resulting in smaller droplet size. When the gravitational force exceeds the effective interfacial tension, the droplet will detach from the formation nozzle and travel as a single charged droplet whose motion is determined by the electrostatic force acting on the droplet at the moment of detachment. The electrostatic force is a complex function of the surface charge trapped within the drop, the droplet shape and the local field strength near the nozzle. The electrostatic force for a uniform field and the resulting effective interfacial tension may be expressed, respectively as follows [2, 15]:

$$F_e = \frac{\sigma^2}{2\varepsilon\varepsilon_0} \tag{1}$$

$$\gamma' = \gamma - \frac{\sigma^2 \bullet d}{8\varepsilon\varepsilon_0} \tag{2}$$

where F_e is the electrostatic force, N/m^2, ε is the dielectric constant of liquids, ε_0 is the permittivity of free space, σ is the charge density for an isolated spherical droplet, d is the equivalent sphere diameter, γ is interfacial tension and γ' is the effective interfacial tension, N/m.

- **Electrostatic Dispersion Regime**

At higher voltages the droplet surface is subjected to a high electrostatic stress that causes the interface to become elongated and unstable. When the voltage is further increased to a certain critical value, the droplet surface forms into a conical shape and a continuous stream of highly charged small droplets is produced and emitted from the tip of the nozzle. This is referred to as a Taylor cone, after Geoffrey Taylor, who investigated the stability of charged water droplets in air [16]. Figure 5.2 shows how the pendant droplet's profile changes in the electric fields at different field strengths. Figure 5.3 summarizes the different droplet

behaviors when the field strength of the applied electric field is increased from zero to a critical value.

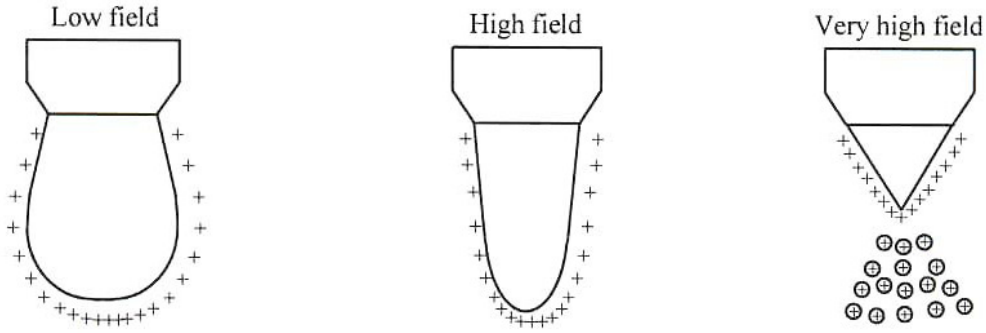

Figure 5.2 Effect of increasing potentials on pendant droplet profile [2]

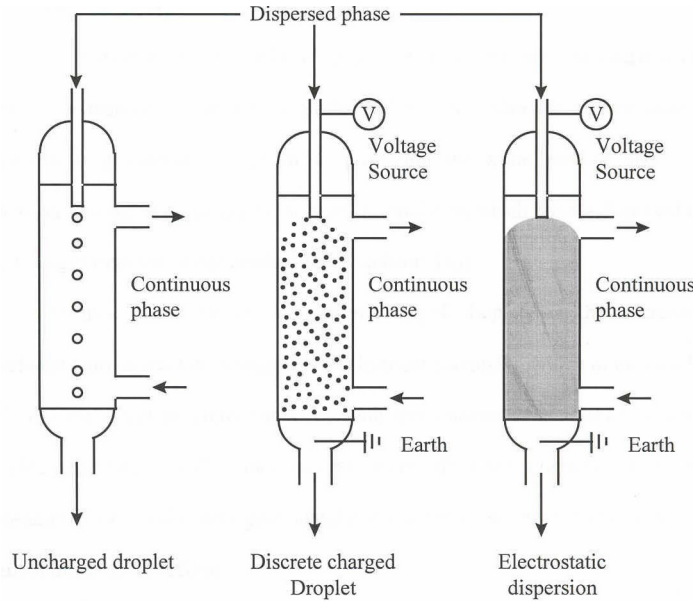

Figure 5.3 Electrostatic spraying [17]

The fluid dynamics of the electrostatic spraying process is governed by the speed at which the liquid can respond to the electrostatic forces. This is determined by the liquid viscosity and surface tension. The mechanism of electrostatic spraying is derived from the interaction between the surface charge on the liquid meniscus and the externally applied electric field. This surface charge arises from the sudden exposure of an imperfectly

conducting liquid to an electric field. Droplet surface charge will depend on the physical properties of the system and the electric field strength. The rate of charge transfer to the dispersed liquid at the nozzle and the droplet formation time determines the amount of charge on the droplet, and hence provides certain limits as regards to which liquids gain most charge. The rate of charge transfer is dependent on the initial charge, the dielectric constant and conductivity of the liquid presented in Equation 3[2].

$$Q = Q_0 \exp(-t/\tau) \tag{3}$$

where Q *and* Q_0 are the charge and initial charge, τ is the relaxation time.

The relaxation time τ may be expressed by [2]:

$$\tau = \frac{\varepsilon\varepsilon_0}{k} \tag{4}$$

where k is the electrical conductivity of the liquid.

Equation 4 governs the rate of charge transfer to the pendant droplet, if the conductivity is low, then the relaxation time is long and if the formation time is less than the relaxation time, then the drop may not acquire the maximum possible charge before detaching from the nozzle [2]. Also, the electrical properties of the liquid determine how much charge is lost during droplet fall/rise through the continuous phase. Hence, it is necessary in the practical application to assume that [2]:

(a) The surface of a droplet forming on an electrified nozzle attains the same potential as the nozzle, i.e. the droplet becomes charged during formation;

(b) After the droplet has detached and is moving through the continuous phase it retains its charge, i.e. no charge should be lost by conduction through the continuous phase.

From these requirements, the range of conductivities of the phases, in which the application of charged droplets is feasible, is stated as [2]:

Continuous phase: $k < 10^{-11}\ \Omega^{-1}\ m^{-1}$; (5)

Dispersed phase: $k > 10^{-10}\ \Omega^{-1}\ m^{-1}$. (6)

This shows that the dispersed phase needs to be a "good" conductor (e.g. water, alcohols or ketones), and the continuous phase should be a "poor" conductor (e.g. silicone oil, n-decyl alcohol).

As mentioned above, effective interfacial tension decreases when an electrostatic force acts on a pendant droplet. This leads to the reduction of droplet size and hence increases surface area or contacting area between the droplets and continuous phases. Due to extra electrostatic force on droplets, terminal velocity may be enhanced in most cases when droplets are falling. The electric field tends to increase the internal motion of the droplets, thus decreasing the dispersed phase mass transfer resistance. Due to the enhanced velocity of the droplets, there is increased relative motion between the two phases, which can lead to droplet oscillation [14]. Additionally, interfacial turbulence is promoted by interfacial tension gradients resulting from the variation of charge density across droplet surface. The charge density of a spherical drop in a uniform electric field is a combination of free charge on the sphere and the charge induced by the field, and can be expressed by [2]

$$\sigma = \frac{Q}{\pi d^2} + 3\varepsilon\varepsilon_0 E\cos\theta \tag{7}$$

where θ is the colatitude angle.

From Equation 7, the charge density is at a maximum for $\theta = \pi = 180^\circ$, i.e. at the front of the droplet. Figure 5.4 presents the distribution of charge density. All these reasons lead to significant enhancement of interfacial mass transfer.

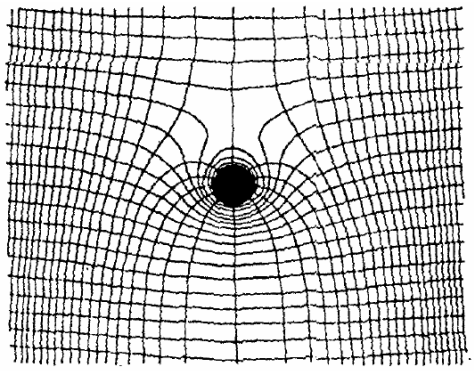

Figure 5.4 Electric field lines around a charged droplet in a uniform electric field [2]

Besides improved mass transfer rate, the energy in this case is efficiently utilized since the electric field acts at the droplet/continuous interface rather than throughout the bulk of the liquid phases. An emulsion which is produced electrostatically has a narrower size distribution than one produced by mechanical means. The stability of the emulsion may be controlled since the droplet size of the resulting dispersion is a function of the field strength and the electrical and physical properties of the two phases [18].

5.1.2 Applications of Electrostatic Liquid Spraying

Since Thornton [14] proposed the use of electric fields in liquid-liquid systems to improve mass transfer, investigation of possible applications concerned with electrically enhanced liquid-liquid extraction and reactions have been taken.

- **Electrostatically Enhanced Liquid-Liquid Extraction**

Thornton [14] investigated the extraction of benzoic acid from toluene by charged aqueous droplets and found the relative extraction rate was increased rapidly for electric field strengths greater than 1.5 kV/cm, with a threefold improvement for electric field strength of 3.25 kV/cm. The power consumed was small, as the continuous phase conductivity was small and the energy consumption was mainly governed by the total charge carried by the disperse phase droplets. Bailes [19] examined the extraction of copper (II) by hydroxyamines in an

electric field. The rate of mass transfer at different voltages showed that charged droplets of the same size had different extraction rates depending on the polarity of the voltage applied. Using droplet size and velocity data, Vu & Carleson [20] developed a mass transfer correlation to predict the mass transfer coefficient and there was calculated a 50 % increase in the extraction efficiency for the dispersed phase controlled resistances and a 90 % increase for the continuous phase controlled resistances in a field of 5 kV/cm. Wham and Byers [21] found that droplet oscillation increased the mass transfer coefficient by 35% even though the increase in interfacial area was less than 1%.

Weatherley *et al.* [22] examined the enhanced extraction of penicillin from buffer solution and from whole broth into dichloromethane using electric fields. For pure penicillin G buffer solution there was a sharp transformation between discrete and spray regime at 10 kV, and a corresponding increase in mass transfer and a similar pattern with corn steep show broth extraction. Reduction of voltage from the critical value resulted in maintenance of spraying at lower voltages due to change in column conductance. No transfer of solid material into the organic phase was observed during the whole broth extraction, along with little sign of entrainment or emulsification unlike the behavior of a stirred system. The extraction was found to increase with time and then plateau off due to attainment of hold-up maximum. An enhancement factor of 4-5 was achieved. The semi-continuous extraction of benzyl penicillin from a sodium phosphate buffer into methylene chloride was also enhanced using electric fields. The variation in conductance was measured in order to determine magnitude of space charge effects. The conductance of penicillin G in buffer increased with time due to extraction of penicillin. The presence of the dispersion under high penicillin concentration was found to make only minor contribution to the conductance. After

termination of spraying the conductance was found to decrease due to coalescence and then to increase slightly due to reversal of space charge migration. Precharging the column was found to result in lower minimum dispersion voltage at each flowrate and the minimum dispersion voltage was a linear function of nozzle diameter [23].

The extraction of ethanol from an aqueous phase into TBP-heavy distillate was studied by Millar & Weatherley [24]. The system examined consisted of a premixing stage, where the aqueous phase was dispersed into the organic phase under the application of electric fields. The aqueous phases examined were solutions of ethanol and ethanol in malt extract liquor. The resulting dispersion was fed tangentially to a settling chamber, where the two phases separate out. An increase in voltage increases the mass transfer, with a difference of 30 % after 2 hours for an electric field of 3 kV/m for the whole broth system. The applied voltage was limited as current discharge resulted at high voltages with high aqueous hold-ups, due partly to the small inter-electrode distance of 5 cm.

- **Electrostatically Enhanced Liquid-Liquid Reactions**

The dispersions or emulsions formed by electrostatic dispersion may be used not only for solvent extraction but also for chemical reactions. Slaughter *et al.* [25] found that the enzyme catalyzed hydrolysis of vegetable oil was enhanced in a spray column using electric fields. After 10 hours over 80 % hydrolysis had been achieved, with the activity of the enzyme 80-86 % of that of the fed solution. With a positively charged electrode the hydrolysis was 4-5 % after 9 hours, which was less than for uncharged runs. The recovery of the enzyme was not affected by polarity. Stirred systems resulted in the formation of emulsions and after centrifugation the activity of the lipase appeared to be much lower.

The biodesulphurization of kerosene oil and crude oil by sulphate reducing bacteria was

enhanced in a sprayed system by the application of electric fields [26-28]. The system used an emulsion phase contactor (EPC) which consisted of a spray chamber in which the bacteria in a suitable medium was dispersed into the oil phase and a column through which the dispersion falls. The droplets produced by the spray nozzle were over an order of magnitude smaller than those produced in a stirred tank at an agitation speed of 450 rpm. The bacteria viability was found to be unaffected by the electric fields. The EPC is expected to have tremendous impact on reactor operation costs.

The aim of this chapter is to explore the feasibility of a novel intensification technology based on electrostatic liquid spraying for improvement of biodiesel production. A novel electrostatically intensified reactor-electrostatic spraying contactor was developed for more efficient production of biodiesel. In the new contactor relatively uncontrolled mechanical agitation was replaced by electrostatic dispersion of the alcohol/caustic mixture into a continuous stream of the oil phase, and the results were discussed. Firstly, the plane interface contactor, which was developed in Chapter 3 for visualization of interfacial turbulence, was employed to investigate the interfacial reaction kinetics during biodiesel synthesis. The factors controlling the reaction were provided. Secondly, a preliminary experimental study was carried out on a new designed process consisting of an electrostatic spray contactor and a product separation unit.

5.2 Experimental

5.2.1 Feedstocks and Chemicals

In the experiments, canola oil and methanol were the primary feedstocks, with sodium hydroxide catalyst. Canola oil was purchased from a local grocery shop (Dillons, USA). Anhydrous methanol, sodium hydroxide, 1N hydrochloric acid and anhydrous sodium sulfate

were ordered from Fisher Science Company. Sodium methoxide solutions were prepared by dissolving sodium hydroxide into methanol and shaking them. Some properties of canola oil and methanol are shown in Table 5.1.

Table 5.1 Some properties of the feedstocks

	Molecular weight	Density, kg/m^3 (20°C)
Canola oil	959.04	914
Methanol	32.04	792

5.2.2 Experimental Setup, Operation Procedures and Sampling Methods

5.2.2.1 Batch Stirred Reactor

The batch stirred reactor system comprised a 250 ml conical flask, a magnetic stir bar and a mechanical stirrer.

Under the conditions of 6:1 molar ratio of methanol to canola oil and 1 wt% sodium hydroxide in canola oil, the reactor was charged with 85 g of canola oil following which 17.85 g of methanol and sodium hydroxide mixture were added to the base of the reactor to prevent the evaporation of methanol. The reaction was timed immediately after finishing the addition of the reagents and starting the stirrer. Reaction was carried out at room temperature. 2ml of samples were withdrawn at preset time intervals from the sample port using a micropipette. They were collected into 15ml test tubes, to which two droplets of 1N hydrochloric acid were immediately added in order to neutralize the catalysts and stop the reaction. 4ml of deionized water were added to wash the samples and then the samples were centrifuged to ensure a thorough separation. The top layers were used for further analysis.

5.2.2.2 Fixed Plane Interface Cell

The schematic of the fixed plane interface cell is shown in Figure 5.5. The cell was described in Chapter 3.

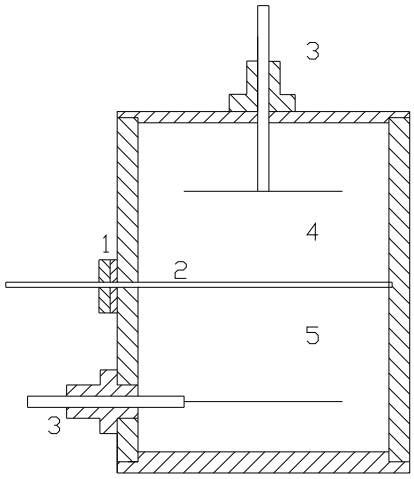

1- Rubber sheet; 2- slideable plexiglass plate; 3-stainless steel gauze electrodes; 4-methanol phase; 5- oil phase

Figure 5.5 Schematic diagram of a plane interface cell for alkali-catalyzed transesterification reaction in the presence of electric fields

The transesterification reactions were carried out in the cell under the conditions of 6:1 molar ratio of methanol to canola oil and 1 wt% sodium hydroxide in canola oil at the room temperature. 85g of canola oil were added slowly into the clean plane interface cell. At this point, the slideable plexiglass plate was pushed carefully into the cell, thus dividing the cell into two sections, the lower section now charged with the canola oil. All the remains at the top of the slide were wiped off using lab tissue paper. 17.85g of sodium methoxide solution were carefully introduced into the top part of the cell. The cover was replaced. Once the top phase attained a quiescent state, typically after 10 minutes, the plate was pulled back slowly to bring the two liquids into contact but at the same time minimizing any hydrodynamic disturbances. The high voltage unit was started and the reaction timed. During the reaction,

the transesterification takes place at the interface between the oil phase and methanol phase. The two phase liquid-liquid mixture which remains after reaction comprises a light layer of biodiesel and a heavy layer, rich in glycerol and side products.

At preset times corresponding to the end of each run, 20 ml of 1N HCl was immediately added to neutralize the sodium hydroxide in the top phase and terminate the reaction. The two phase mixture was transferred into a flask and shaken gently. The mixture was further centrifuged for 20min at 2000rpm and separated into two phases using a separating funnel. Soap and remaining methanol were removed through washing the top oil phase using hot tap water for successive three times. Some anhydrous sodium sulfate was added to the washed methyl ester phase to remove residual water. Pure and dry biodiesel products were obtained for analysis after further filtration.

5.2.2.3 Electrostatic Spraying Contactor

Based on prior preliminary work a co-current column contactor was initially tested as a possible conceptual design for eventual scale-up. This design [29, 30] has been successfully developed and used for co-current reaction of water and triglyceride esters undergoing enzymatic hydrolysis. That system is physically and chemically quite similar to the biodiesel system. In that system, water (and enzyme) were electrostatically sprayed into the oil phase while a stable high voltage electrical field was maintained across the oil phase. High rates of equilibrium conversion were achieved, and good phase separation was observed post-reaction. When it was applied to biodiesel production, the methanol/sodium hydroxide mixture was successfully electrostatically dispersed into canola oil from the bottom of column due to its lower density than canola oil. However, a number of problems were encountered. An unreacted methanol-rich layer tended to form at the top of the column.

Different from water phase in enzymatic hydrolysis, the charged layer of methanol has a high volatility and may cause an explosion hazard. Another problem concerned the byproducts of glycerol and soap. During the reaction, glycerol and soap were produced and tended to accumulate on the outer surface of the drops in the dispersion. This gave rise to difficulties in phase separation. The charged droplets made the bulk oil phase conductive and produced electric arcing, thus affecting the stability of the electrical conditions inside the column.

In light of the problems with the column contactor it was decided to seek an alternative solution. Some contactors with different configurations have been used. A centrifugal contactor was designed and applied where a central electrode was charged and the aqueous feed was introduced through an earthed electrode [24]. However, due to high dispersed phase hold-up problems with arcing were found and it was not possible to maintain a voltage greater than 5 kV. An alternative design of contactor was based on a simple but compact spray nozzle system [24]. The system comprised a two stage dispersion and reaction process, achieved using a dispersion stage consisting of a nozzle, a high voltage electrode and an oil feed inlet. The aqueous phase is dispersed through a nozzle into the fast moving organic stream with the advantage that there is no build-up of aqueous phase in the system. The dispersion is then fed to a reactor. A similar set-up was used by Tsouris *et al.* which consisted of a dispersion stage leading to a column [26, 27]. This design greatly reduces the size of the actual reaction volume, at the same time providing improved hydrodynamic conditions. More important, this flow arrangement also has the advantage of reducing the volumetric hold-up of the dispersed phase in the vicinity of the electrical field and preventing arching.

Based on this system, a novel two-stage configuration consisting of a cruciform

electrostatic spraying contactor and a phase separator was developed as shown in Figure 5.6. The dimensions of the cruciform glass contactor are included in this figure. Figure 5.7 shows the experimental setup. The oil phase is pumped vertically upwards through the vertical section of the cruciform reactor vessel. The horizontal section is equipped with an electrode shown on the right hand side. This is attached to a high voltage supply unit. The sodium methoxide phase is injected through stainless steel tubing (1/16×0.02×10cm, Upchurch scientific) located in the left hand horizontal section of the reactor. The tubing is grounded and thus an electrical field is established across the region of reactor where the two liquid streams come into contact. Under appropriate conditions, the sodium methoxide forms a very fine and turbulent electrostatic spray which is very favorable for biodiesel production. Following intimate contact of the electrostatic spray of sodium methoxide and the canola oil, the resulting two-phase mixture is discharged into a separator. Here the dispersed droplet phase coalesces at the top of the separator and is discharged through an upper port. The other second liquid phase, in the case the oil phase descends to the bottom of the column and is discharged through a lower port. In the experimental arrangement used here both phases were recycled. The separator comprised a cylindrical vessel of 10-cm internal diameter and 30-cm length. A rectangular baffle is located close to the inlet port to even out the flow of the mixed phase entering the separator and to minimize contact of the mixture and separated two phases. The principle of operation of the separator involved the droplets flowing evenly around the inlet baffle to subsequently coalesce at the liquid-liquid interface located in the right hand section of the separator. Coalesced light phase (in this case sodium methoxide) was pumped from the top of the separator into a buffer vessel for recycling back into the reactor. Likewise, heavy phase was withdrawn from the bottom of the separator into the canola oil container for

recycling and further conversion.

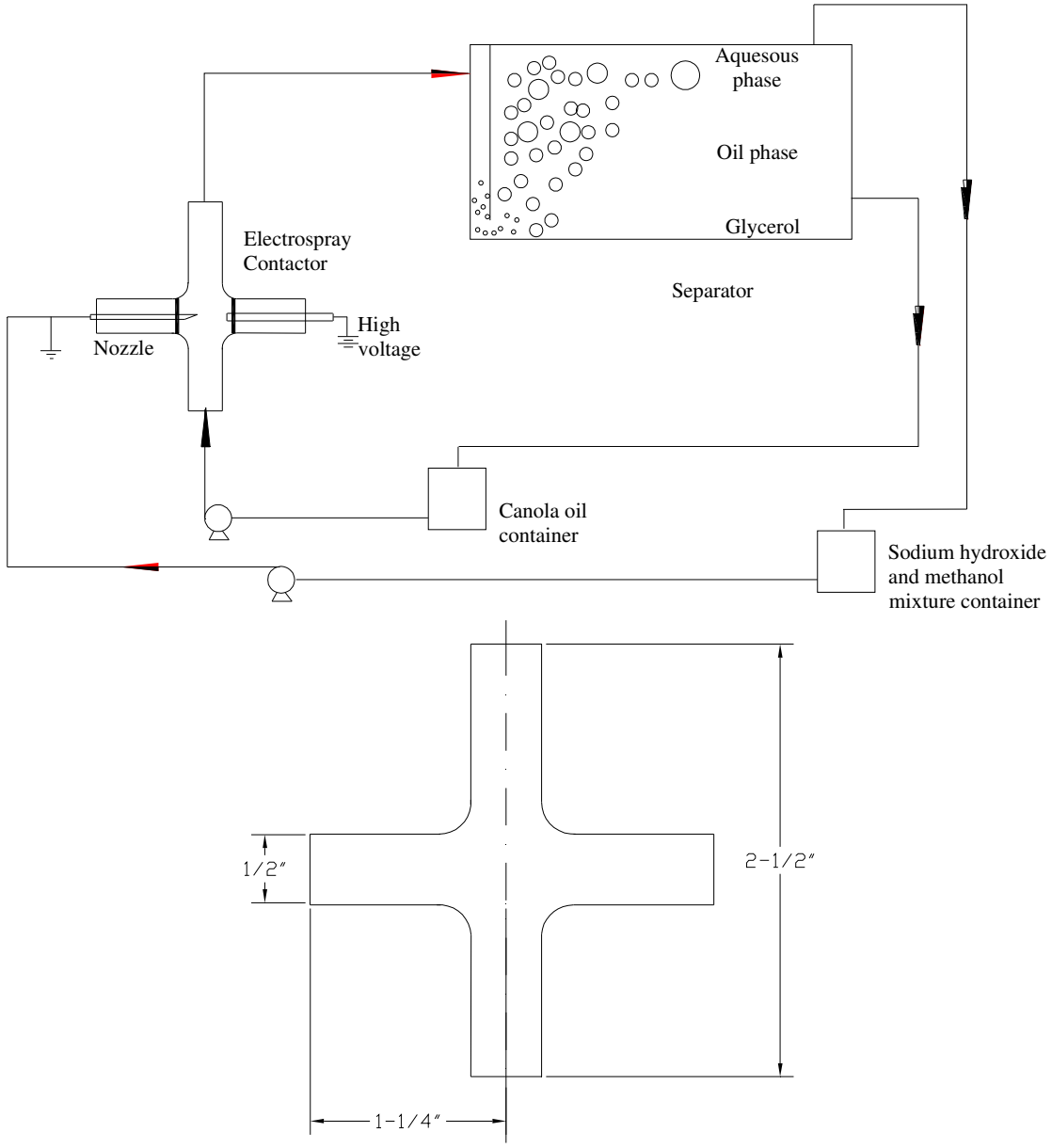

Figure 5.6 Schematic diagram of two-stage system including the electrostatic spraying contactor and separator for biodiesel production (Dimensions shown in bottom figure)

During the course of the development of the design specifically for biodiesel reaction, several important modifications were made. These included the redesign of the phase separator, and the employment of an external insulated electrode. The nozzle itself was

experimentally optimized by variation of the nozzle shape, diameter and the interelectrode distance until a stable but good quality continuous spray of sodium methoxide was formed. In order to prevent dispersed phase from contacting directly the electrode and eliminate arching, an angled end different from flat end was investigated in the experiment. The nozzle tip was closer to the electrode than other regions of the nozzle, which resulted in the maximum surface charge density at the apex of the nozzle. Therefore, the highest electric field generated by the potential difference between the nozzle and the electrode was achieved at the nozzle apex, indicating the spray position. Hence, a deviation of the spray emission from the angled end nozzle was observed and no deviation from the flat end nozzle. However, there was no apparent difference on reaction conversions found. All these modifications allowed us to operate the reactor for extended periods without static discharge or breakdown and thus obtain feasible levels of conversion on which we could judge the potential of the technique.

For the experimental runs reported here the following procedure was adopted. Initially 870g of canola oil was recirculated through the system using a peristaltic pump (Watson-Marlow, England) at a flowrate of 155ml/min. Continuous recycle from the separator and feedstock vessel was by means of a second peristaltic pump (Watson-Marlow, England) operated at the same flowrate as the feed pump The sodium methoxide feed comprised a 180g mixture of sodium hydroxide in methanol and this was metered using a smaller peristaltic pump (Watson-Marlow, England) to the injection nozzle attached to the reactor at a flow rate of 2ml/min. The molar ratio of methanol to canola oil was 6:1, and the weight percent of sodium hydroxide in canola oil was 1wt%. A further peristaltic pump (Watson-Marlow, England) was employed to recycle the sodium methoxide rich phase from the buffer

vessel located close to the outlet of the separator. The sampling point was located at the outlet line of oil phase from the separator. Sampling was commenced 10minutes after starting the experiment. 2 ml of sample were continuously collected at the sampling point into a 15 ml centrifuge tube. The tube was pre-filled with 5 ml deionized water and was refrigerated prior to use. The sample was quenched in the centrifuge tube by placing the tube into ice water. The samples were shaken gently to stop reaction and were washed. Upon washing, unreacted methanol, sodium hydroxide and glycerol were assumed to be present in the heavy phase, and the FAMEs and bound glyceride in the light phase. The liquid phases were further centrifuged at 3000 rpm for 20 min to ensure a thorough separation. The top layer of the samples was analyzed.

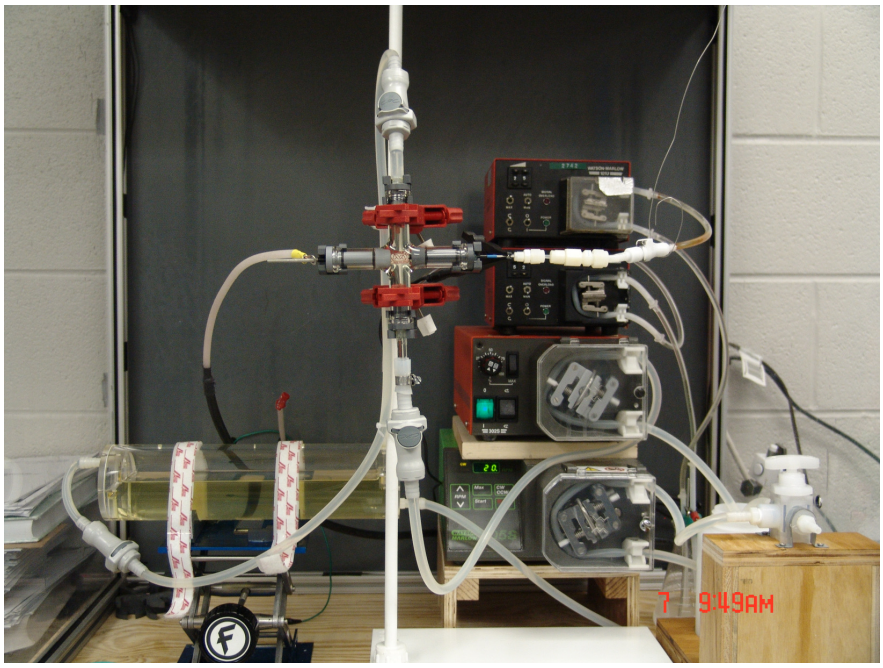

Figure 5.7 Experimental setup for biodiesel production comprising an electrostatic spraying contactor and a phase separator

5.2.3 Sample Analysis

In order to calculate the conversion of canola oil during the tranesterification, the methyl esters in biodiesel samples were separated by Gas chromatography (GC) and their concentration in products measured. The GC (HP Agilent 6890N Series) was equipped with a split/splitless injection, a flame-ionization detector, and HP ChemStation software (Hewlett-Packard, USA). The column was a 15 m x 0.32 mm, 0.25 μm HP-INNOWax capillary column (Agilent, USA). The analytical method and the conditions were used as follows:

Carrier gas flowrate: He at 25 ml/min;

Split ratio: 50:1;

Injector and detector temperatures: 250°C;

Oven temperature program: 150°C for 2 min, increased to 220° C at a rate of 5°C/min, and held at this temperature for 15 min;

Internal standard: Eicosane;

Solvent: hexane;

Reference standards: methyl palmitate, methyl stearate, methyl linoleate, methyl oleate, and methyl linolenate.

Figure 5.8 shows the GC spectrum of a typical biodiesel sample. The response factors of all methyl esters are shown in Table 5.2.

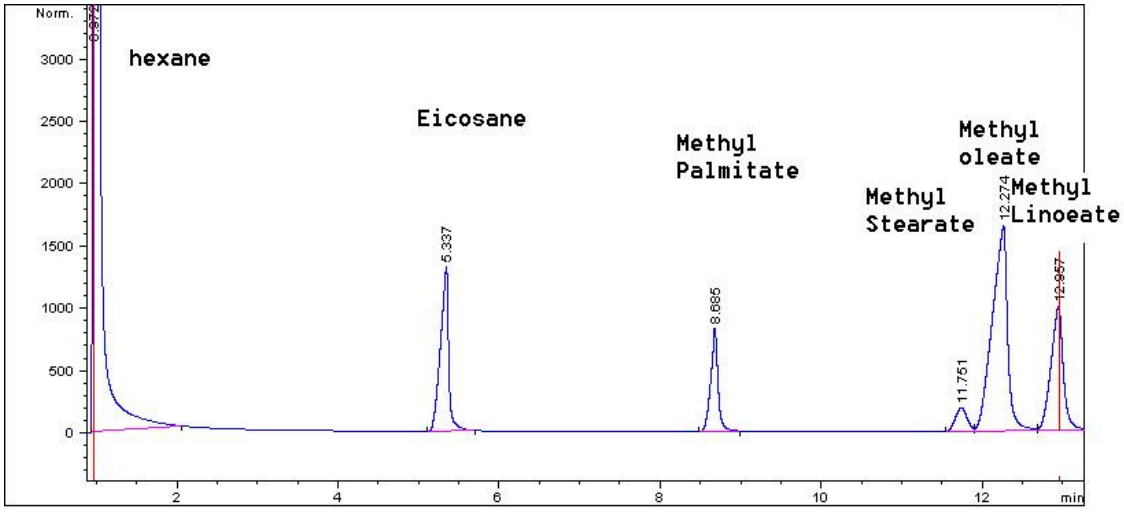

Figure 5.8 GC spectrum of a biodiesel sample

Table 5.2 Response factors of methyl esters

Methyl palmitate	Methyl stearate	Methyl oleate	Methyl linoleate	Methyl linolenate
0.7671	0.8061	0.7999	0.7857	0.7652

5.2.4 Conversion Rate Calculation

The conversion rate of canola oil is defined as follows.

$$\text{Conversion } \% = \frac{\text{The quantity of fatty acid methyl esters (mol)}}{3 \times \text{the amount of canola oil (mol) added}} \times 100\% \qquad (8)$$

5.3 Results and Discussion

5.3.1 Transesterification in the Stirred Reactor

The conversion rates of transesterification at the different reaction times in the stirred batch system are shown in the Figure 5.9. The stirrer speed is about 250 rpm. The reaction took about 20 min to reach equilibrium with the maximum conversion yield of approximately 70%. The reaction is relatively fast although the conversion is a little lower than that required

in industry because the reaction took place at room temperature compared to 65ºC in a commercial process.

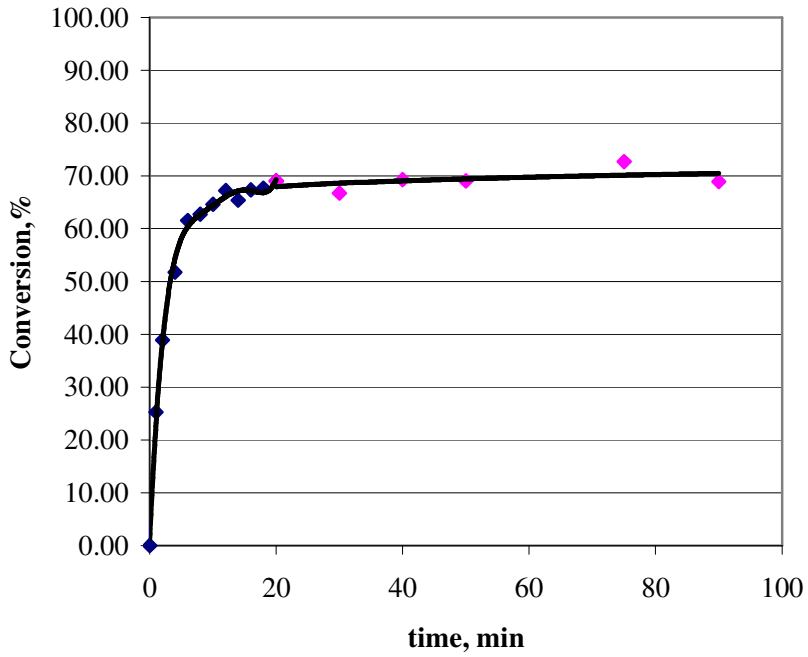

Figure 5.9 Transesterification of canola oil with methanol/sodium hydroxide in a stirred batch system (250 rpm) at 25℃

5.3.2 Transesterification in the Plane Interface Cell

The results from this part of the study are in two parts. Firstly the interfacial disturbances and changes during reaction periods were visualized and recorded using the optical Schlieren technique as described in Chapter 3. The effect of the electrical fields on interfacial turbulence or bulk turbulence was examined. Secondly the reaction rate under different applied potentials was measured and the influence of applied electric fields was investigated.

5.3.2.1 Visualization of Interfacial Turbulence

Figures 5.10, 5.11 and 5.12 show single frame shots of the liquid-liquid interface during the biodiesel reaction in the presence of an electrical field. In Figure 5.12, the thickness of

the interface is increasing with the reaction time which would tend to increase the resistance of mass transfer of the two phases at the interface. Simultaneously, some visible slow settling fine particles or drops which were produced at the interface close to the oil phase are noted. These particles are possibly made of glycerol and soap produced during the reaction. The progress of the transesterification reaction with respect to time is shown in Figure 5.11 and Figure 5.12 for 4kV and 10kV electric fields, respectively. The feature to note in these pictures is the strong circulation which is apparent in the oil phase which is attributed to the electric fields. The resulting turbulence may in some cases enhance mass transfer and thus accelerate the overall observed rate of conversion.

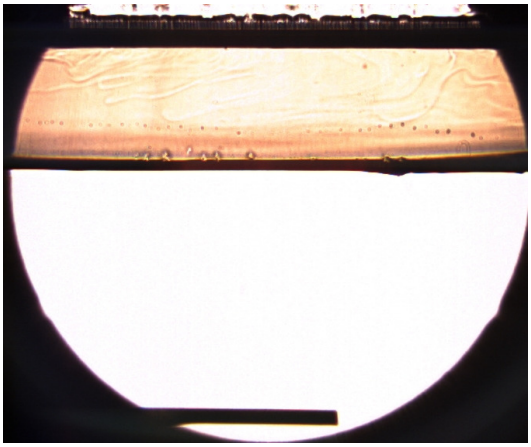

10 seconds

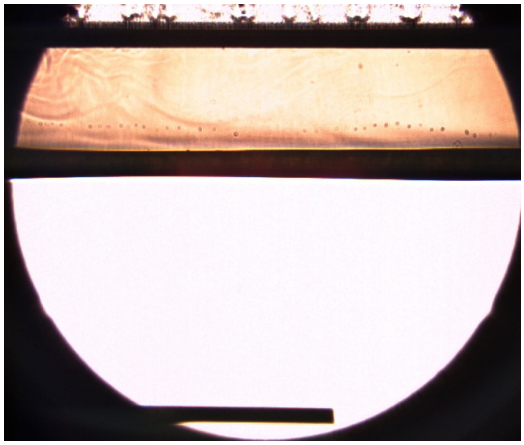

10 min

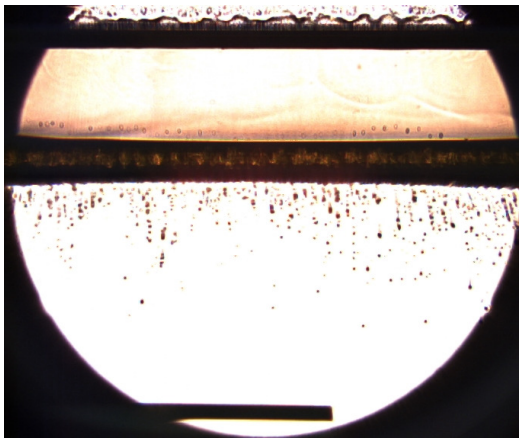

30min

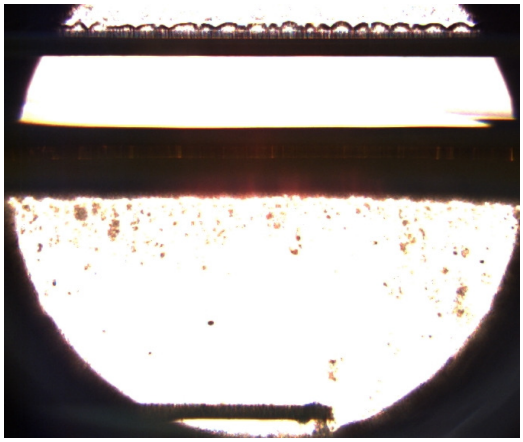

2hr

Figure 5.10 Schlieren images during the transesterification in the absence of electric fields

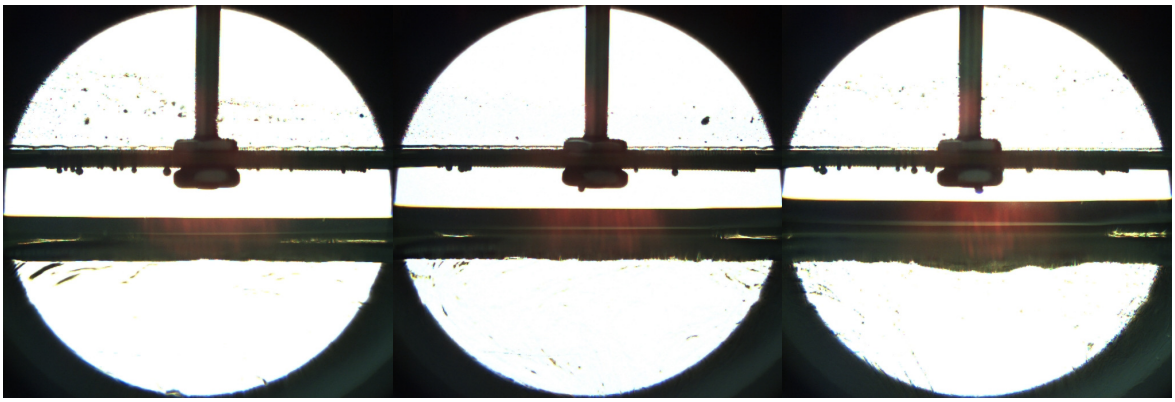

2hrs 4hrs 6hrs

Figure 5.11 Schlieren images during the transesterification at 4kV DC electric field

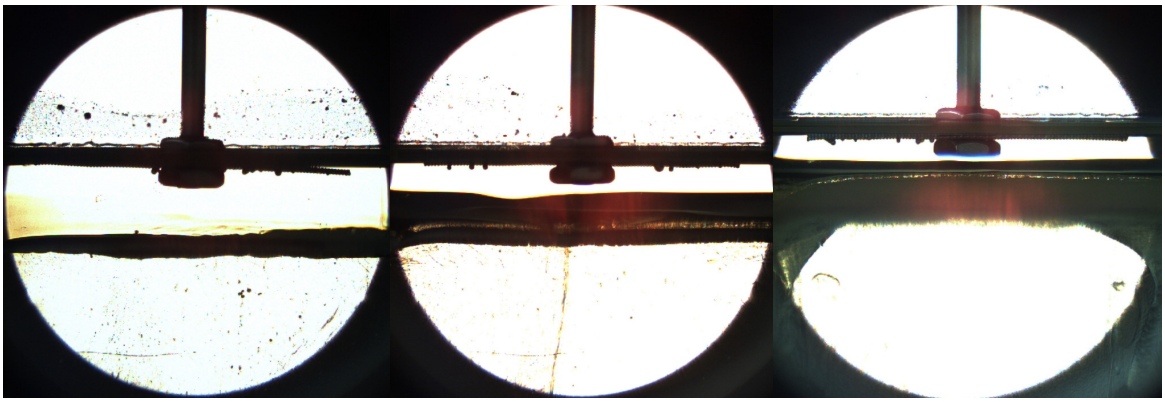

2hrs 4hrs 6hrs

Figure 5.12 Schlieren images during the transesterification at 10kV DC electric field

5.3.2.2 Reaction Kinetics

The conversion yields of alkali-catalyzed transesterification at the different reaction times for the various electric field strengths are shown in Figure 5.13. The results show that the conversion rates during transesterification were increasing with time at each value of applied electric voltage. Examination of the data in Figure 5.13 indicates clearly that the reaction was greatly enhanced at an applied voltage of 10kV. Typically the conversion values at 10kV are

6-7 times that at 0kV at a range of individual reaction times. The results do show some anomalous behaviors which were exhibited at intermediate applied voltages in the range below 10kV. At applied voltages in the range of 4-5kV, the conversion-time characteristics appear to show a negative influence of increasing voltage. There are two possible reasons for this apparent anomaly. The relationship between the degree of turbulence and applied voltage may be one factor. The second possibility is connected to the migration of CH_3O^- anion during the reaction. Some CH_3O^- was produced when the sodium hydroxide catalyst was dissolved into methanol. This follows from the mechanism upon which the base-catalyzed transesterification of vegetable oils is based. It is hypothesized that these ions are negatively charged and would migrate towards the positively charged electrode in the cell under the influence of the electrostatic force. At low values of applied voltage, electrically driven turbulence increases with the magnitude of electric fields, but it is still limited near to the interface. In the mean time, the migration rate is too small for the ions to pass through the canola oil phase and reach the bottom electrode. Hence, the applied voltages have a positive effect on the conversion of canola oil. But when the electric field is increasing to 4kV or more, the migration of the anion is enhanced and thus reduces the concentration of CH_3O^- at the interface which results in a reduction in the overall transesterification rate. At higher electrical fields (10kV), the strong electric force deformed the interface and intensified the contact between the two phases significantly. This would explain the switch over from reduction in rate to increase in rate.

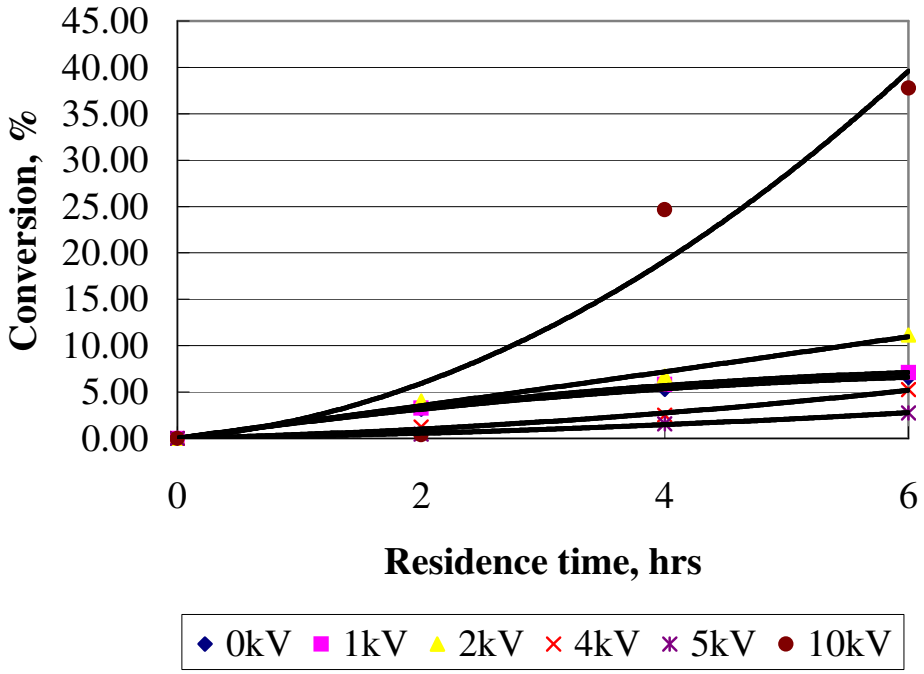

Figure 5.13 Conversion yields of canola oil during transesterification with sodium methoxide vs. reaction time in the plane interface cell

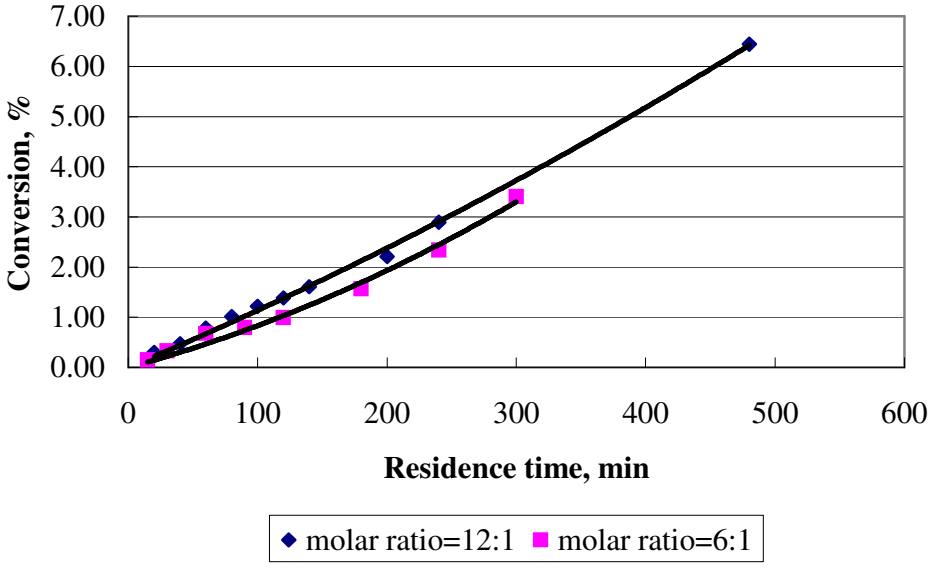

Figure 5.14 Effect of molar ratio of methanol to oil on the transesterification at 4kV DC electric field

5.3.3 Transesterification Reactions in the Electrostatic Spraying Contactor

In order to investigate transesterification reactions in the new contactor, the first task was to achieve good electrostatic spraying of sodium methoxide into canola oil. Continuous and ideal electrostatic spraying was observed through the optimization of experimental conditions. Figure 5.15 shows electrostatic spraying under different applied potentials during the course of experiment. In the absence of electric fields, the dispersed phase appears in the form of big droplets from the tip of the nozzle and no disturbance was observed. When a -20kV DC electric field was applied, sodium methoxide was sprayed into smaller droplets but they were still visible. When the magnitude of applied charge was increased to -30kV, strong spraying was observed with strong turbulence. The dispersed droplets were too small to determine their size by eye. As the experiment proceeded, the properties of the oil phases were influenced due to the production of the byproducts of glycerol and soap as well as entrainment of unseparated methanol. The oil phases become conductive and affected the stability of electric fields. Thus, the spaying was also affected as shown in the last image of Figure 5.15. The stability of electric conditions can be improved by employing pulsed DC [26, 27] and intensifying the product separation in the phase separator by electrostatic coalescence technology [31].

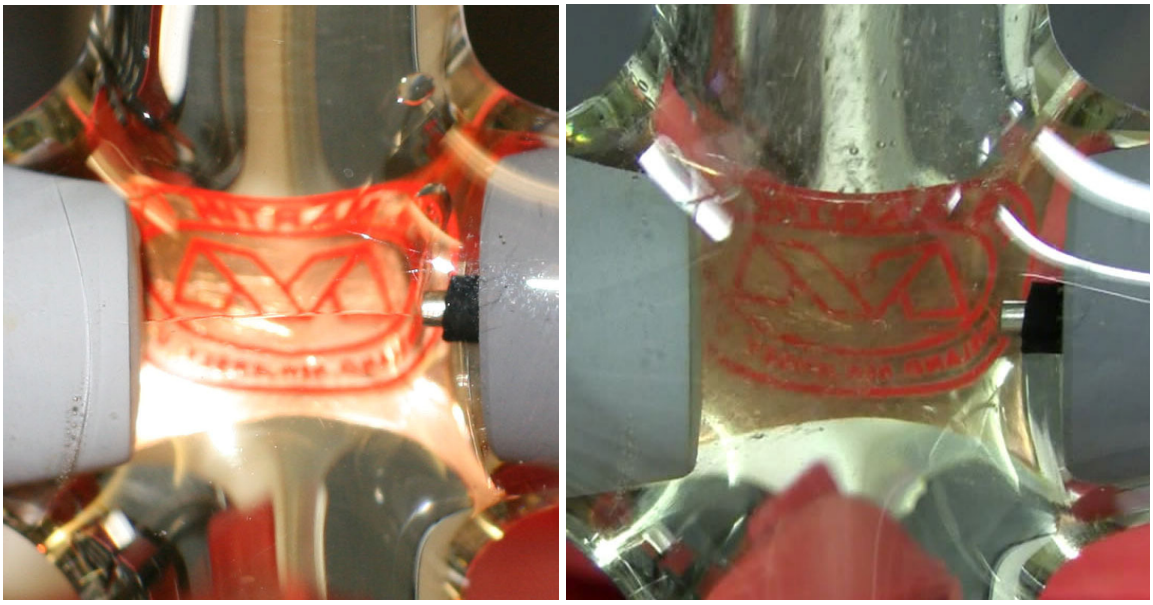

(a) 0kV (b) -20kV DC

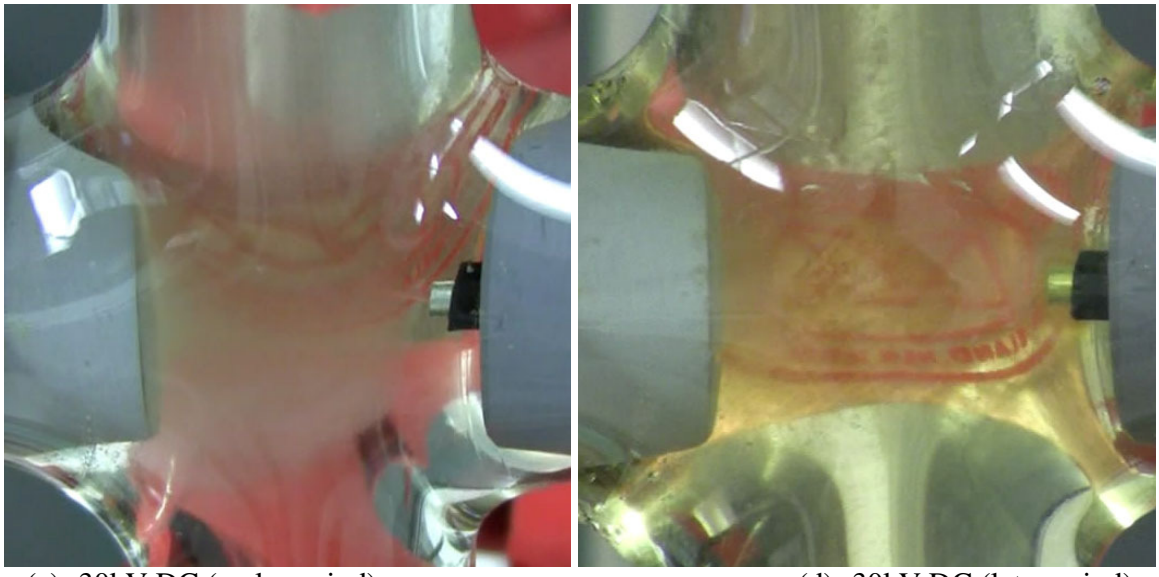

(c) -30kV DC (early period) (d) -30kV DC (late period)

Figure 5.15 Electrostatic spraying of sodium methoxide into canola oil for biodiesel production

The reaction was conducted under electrostatic spraying conditions and the overall rate of conversion followed with time for fixed inventories of canola oil and sodium methoxide. The control experiment involved the same flowrates, molar ratios and catalyst concentrations but with no applied electrical field. The comparison is shown in Figure 5.16 and shows a clear

and significant enhancement of biodiesel production rate in the presence of the applied electrical field. For example after 100 minutes reaction time, the electrostatic spraying contactor at -35kV DC yielded approximately 40% conversion compared to 3% conversion in the absence of the field. Further experiments are required to extend the range of variables including applied electrical field strength, and inter-electrode distance.

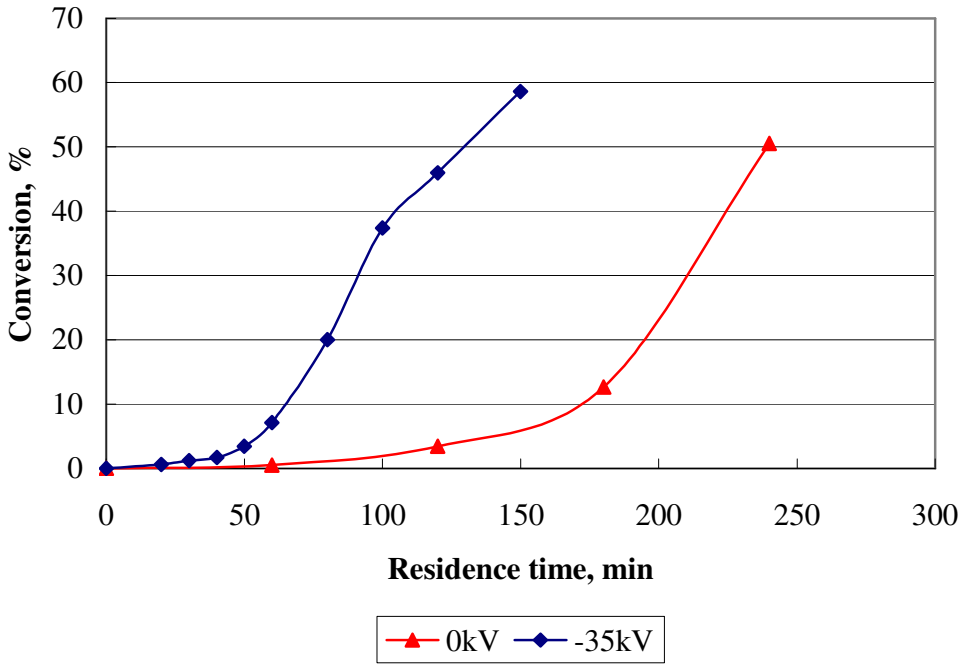

Figure 5.16 Conversion yields of biodiesel vs. time at -35 kV and without electric field

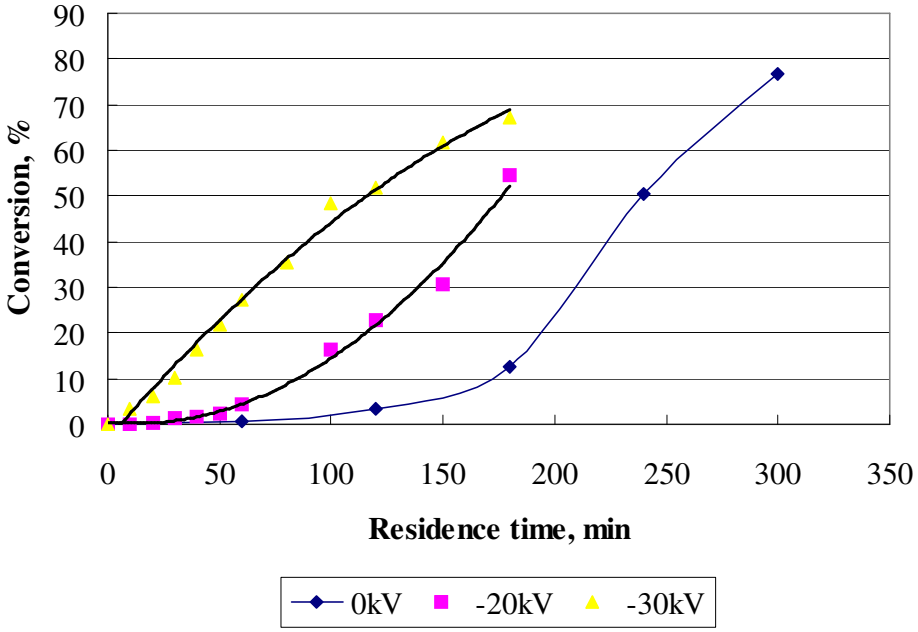

Figure 5.17 Effect of electric field strength on the conversion yield of biodiesel

Figure 5.17 shows conversion yields of canola oil obtained in the continuous electrostatic spraying contactor and they are compared with the results for the reaction in the absence of the electric field. The conversion rates of methyl esters were very low when the reaction time was less than 50min at –20kV DC. The reaction rate was increasing after 60min. The conversion reached 20% when reaction time was 120min and reached approximately 30% after 150min. In the presence of an electric field of –30kV DC, the reaction rate was apparently faster than at –20kV DC. The biodiesel yield was approximately 50% after 120min. The yield can be improved if electrostatic spraying conditions are optimized. In contrast to electrostatic spraying, there were almost no reactions in the first hour when no electrostatic field was applied. The yield was only 3.4% at 120min. Although the reaction rate was increasing faster after 3hrs, the conversion was still only about 50% at 4hrs. The enhancement of conversion of canola oil had strong relationships with the large specific surface areas and strong disturbances observed in Figure 5.15.

Figure 5.18 shows the effect of the distance between the tip of nozzle and the electrode on the conversion yield of biodiesel. The different result is due to the weaker strength of electric field when the distance is bigger.

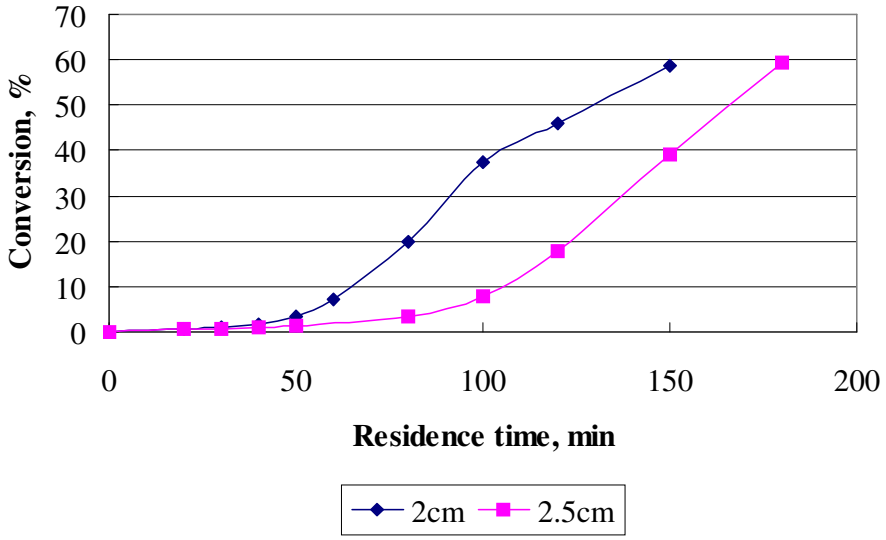

Figure 5.18 Effect of the distance between the tip of nozzle and the electrode on conversion yields of biodiesel at -35kV DC

Electrostatic coalescence of the dispersed phase was explored briefly in the phase separator. Figure 5.19 illustrates the coalescence phenomena which occurred around the electrode charged at –5kV DC. Small droplets of the dispersed phase aggregated together and formed big droplets, and thus the phase separation was apparently enhanced. The results can be integrated with electrostatic spraying data into the novel system in the future.

Here it must be stressed that the concentration of biodiesel is dependent on the location of the sampling point. In our experiments, the sampling point was located close to the canola oil vessel. Biodiesel product was diluted by the oil in the phase separator after reaction. This led to low biodiesel concentration and resulting conversion yields especially in the early period. Actually the conversion should be higher if the product samples were taken close to the

outlet of the contactor. However, the performance comparisons at different applied potentials remain valid.

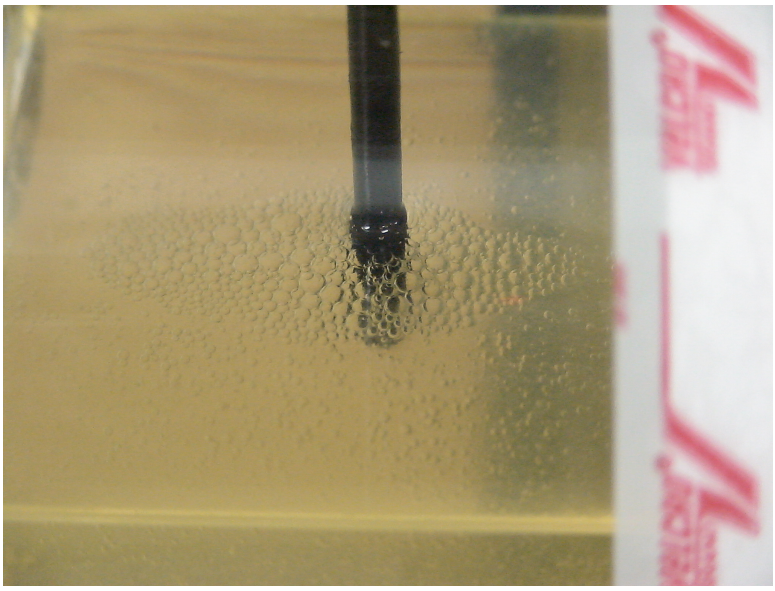

Figure 5.19 Electrostatic coalescence in the phase separator during transesterification of canola oil with sodium methoxide at 5kV DC

5.4 Conclusions

Electrostatic enhancement technology was investigated in this chapter for biodiesel production. A novel intensive contactor was developed using the principle of electrostatic spraying. The reaction rate of transesterification of canola oil with sodium methoxide is significantly enhanced by the application of an electrical field across the liquid-liquid plane interface. Typically a fourfold enhancement was observed at an applied voltage of 10kV. The enhancement may be due to enhanced interfacial hydrodynamic disturbances and this is supported by the visible gradients in refractive index which were observed. Other possible mechanism includes electrokinetic acceleration of reactant and products in the vicinity of the interface. The change in rate of reaction may not be a continuous function of applied electric field strength and some anomalous behavior was observed at applied fields in the range 0-

4kV. Further study of the relationship between electric field and interfacial tension is required. Also the enhanced accelerated migration of anionic fatty species under the influence of the electric field requires further investigation.

The co-current column reactor did not perform well for biodiesel synthesis due to undesirable accumulation of unreacted methanol on the top surface of the oil phase. The methanol layer is hazardous because of high volatility. The co-current reactor was also badly affected by the formation of glycerol and soaps during the reaction because they reduced stability of the output of high voltage unit.

The exploitation of electrospraying for continuous enhanced biodiesel production was successfully demonstrated using a compact intensified reactor design. Typical enhancements showed a ten-fold increase in conversion rate. The design was based on simple tubular geometry with horizontal injection of an electrostatic spray of sodium methoxide. Control of the dispersed phase hold-up, and the use of partially insulated electrodes were critical to stable performance of the design. The use of a pulsed electric field may be good option for sustained good electrostatic spraying. The design has potential for scale up either by direct geometrical scale-up, or by the development of a multi-module system with a number of reactors operating in parallel. Further work is required to establish in detail the relationships between applied voltages, drop size, hold-up, and residence time. This will enable us to establish the essential parameters for the development of a design method.

5.5 References

1. A. Green, B. Johnson, A. John, Process intensification magnifies profits, Chemical Engineering, Dec., (1999) 66-73.

2. G. Stewart and T.D. Thornton, Charge and velocity characteristics of electrically charged droplets. Part I. Theoretical considerations, Int. Chem. Engng. Symp. Ser., 26(1967a) 29-36.
3. G. Stewart and T.D. Thornton, Charge and velocity characteristics of electrically charged droplets. Part II. Preliminary measurements of droplet charge and velocity, Int. Chem. Engng. Symp. Ser., 26(1967b) 36-41.
4. P.J. Bailes and J.D. Thornton, Electrically augmented liquid-liquid extraction in a two component system, I. Single droplet studies, Proceeding of the international solvent extraction conference, 2 (1971) 1431-1439.
5. P.J. Bailes and J.D. Thornton, Electrically augmented liquid-liquid extraction in a two component system, II. Multidroplet studies, Proceeding of the international solvent extraction conference, 2 (1974) 1011-1027.
6. L.J. Austin, L. Bancyk, and H. Sawistowski, Effect of electric field on mass transfer across a plane interface, Chem. Eng. Sci., 26 (1971) 2120-2121.
7. N.J. Felici, Recent developments and future trends in electrostatic generation, Direct Curr., 4 (1959) 192-201.
8. B. Vonnequt and R.L. Neubauer, Production of monodisperse liquid particles by electrical atomization, J. Colloid Sci., 7 (1952) 616-622.
9. A.G. Bailey, The theory and practice of electrostatic spraying, atomization and spraying technology, 2 (1986) 95-134.
10. S. Ogata, T. Kawashima, O. Nakaya, O. Shinohara, Stability of a charged drop issuing from a fine capillary, J. Chem. Eng. Japan, 9 (1976) 440-444.

11. T. Takamatsu, M. Yamaguchi, T. Kataymama, Formation of single charged drops in a non-uniform electric field, J. Chem. Eng. Japan, 16 (1983) 267-272.
12. C. Byres, J. Perona, Drop formation from an orifice in an electric field, AIChE J., 34 (1988) 1577-1580.
13. T. Takamatsu, Y. Hashimoto, M. Yamaguchi, T. Kataymama, Theoretical and experimental studies of charged drop formation in a uniform electric field, J. Chem. Eng. Japan, 14 (1981) 178-182.
14. J.D. Thornton, Electrically enhanced liquid-liquid extraction, Brimingham University Chem. Eng. J., 27 (1976) 6-13.
15. L.R. Weatherley, Electrically enhanced mass transfer, Heat recovery systems & CHP, 13 (1993) 515-537.
16. G. Taylor, Disintegration of water drops in an electric field, Proc. R. Soc. London, A280 (1964) 383-397.
17. L.R. Weatherley, Electrokinetic processes for biochemical extractions, IChemE symposium series, 119 119-146.
18. T. Scott, O. Basaran, C. Byers, Characteristics of electric field induced oscillations of translating liquid droplets, Ind. Eng. Chem. Res., 29 (1990) 901-909.
19. P.J. Bailes, Solvent extraction in an electrostatic field, Ind. Eng. Chem. Process Des. Dev., 20(1981) 564-570.
20. N. Vu and T.E. Carleson, Electric field effects on drop size and terminal velocity in liquid-liquid systems, AIChE J. 32 (1986) 1739-1742.
21. R.M. Wham and C.H. Byers, Mass transport from single droplets in imposed electric fields, Sep. Sci. and Techno., 22 (1987) 447-466.

22. L.R. Weatherley, I. Campbell, D. Kirton and J.C. Slaughter, Electrically enhanced extraction of Penicillin G into dichloromethane, J. Chem. Tech. Biotechnol., 48 (1990) 427-438.

23. L.R. Weatherley, I. Arnott, J.C. Slaughter and I. Campbell, Solvent extraction of penicillin-a study of electrostatic spraying behaviour during enhanced extraction in a spray column, Trans. IChemE, 69 (1991) 83-90.

24. M.K. Millar and L.R. Weatherley, Whole broth extraction in an electrically enhanced liquid-liquid contact system, Chem. Eng. Res. Des., 67 (1989) 227-231.

25. J.C. Slaughter, L.R. Weatherley, and A. Wilkinson, Electrically enhanced enzymatic hydrolysis of vegetable oils using lipase from Candida Rugosa, Enzyme and Microbial Techno., 15 (1993) 293-296.

26. C. Tsouris, H.M. Lizama, M.A. Spurrier, T.L. Takeuchi and T.C. Scott, Hydrodynamics of bioreactor systems for liquid-liquid contacting, Applied Biochemistry and Biotechnology, 57 (1996) 581-592.

27. C. Tsouris, S.H. Neal, V.M. Shan, M.A. Spurrier and M.K. Lee, Comparison of liquid-liquid dispersions formed by a stirred rank and electrostatic spraying, Chem. Eng. Comm., 160 (1997) 175-197.

28. E.N. Kaufman, J.B. Harkins, M. Rodriguez Jr., C. Tsouris, P.T. Selvaraj and S.E. Murphy, Development of an electro-spray bioreactor for crude oil processing, Fuel Processing Techno., 52 (1997) 127-144.

29. L.R. Weatherley and D. Rooney, Enzymatic catalysis and electrostatic process intensification for processing of natural oils, Chem. Eng. J., 135 (2008) 25-32.

30. J. Petera, L.R. Weatherley, D. Rooney, K. Kaminski, A finite element model of enzymatically catalyzed hydrolysis in an electrostatic spray reactor, Computers and Chemical Engineering 33 (2009) 144-161.
31. C.D. Henricks and S. Sadek, Electric field enhanced coalescence of drops in liquid emulsions, IEEE Transactions on Industry Application, 13 (1977) 489-493.

Chapter 6 Biodiesel Production Using an Intensified Spinning Disc Reactor

6.1 Introduction

Spinning disc reactors (SDR) are one of process intensification technologies employing high gravity field. It is mainly aimed at fast and very fast liquid/liquid reactions involving large heat effects, such as nitrations, sulfonations, and polymerizations [1]. Figure 6.1 shows a design of the spinning disc reactor developed by Ramshaw's group at Newcastle University (Newcastle, U.K.) [2]. High gravity field–centrifugal force is created by rotation of a disc surface in spinning disc reactors. When a liquid is introduced onto the disc surface at or adjacent to the spin axis, the liquid flows radially outward under the centrifugal force in the form of a thin film as seen in Figure 6.2. At up to approximately 1,000 rpm, these films are less than 100 microns thick and so offer a short diffusion path length [3]. The film is unstable and forms waves at the gas-liquid interface. Unsteady film surface waves on the disc surface, coupled with the shearing action of the rotating surface, ensure that micro mixing and excellent mass and heat transfer are achieved. Extensive mass and heat transfer studies using this technology have shown that convective heat transfer coefficients as high as 14kWm^{-2} K and mass transfer coefficients, K_L values as high as 30×10^{-5} ms^{-1} and K_G values as high as 12×10^{-8} ms^{-1}, can be achieved whilst providing micro-mixing and an appropriate fluid dynamic environment for achieving faster reaction kinetics [4]. Residence times on the spinning disc range from a few seconds down to fractions of a second, and it is therefore well

suited to fast processes where the inherent reaction kinetics are of the same order or faster than the mixing kinetics [5]. The SDR has the following characteristics:

- Intense mixing in the thin liquid film;
- High heat and mass transfer coefficients;
- Short residence time;
- Plug flow characteristics.

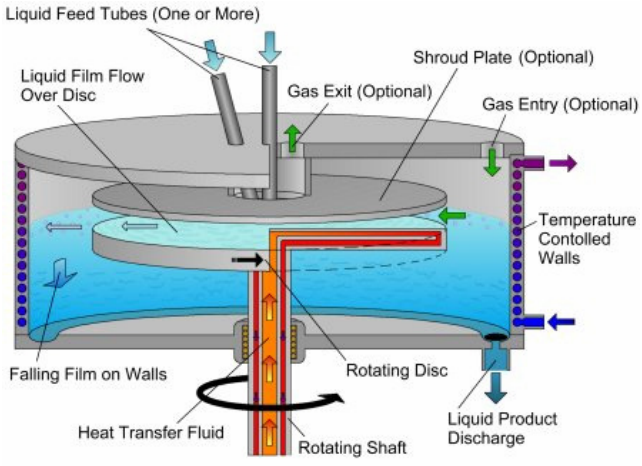

Figure 6.1 Schematic view of a typical spinning disc reactor [2]

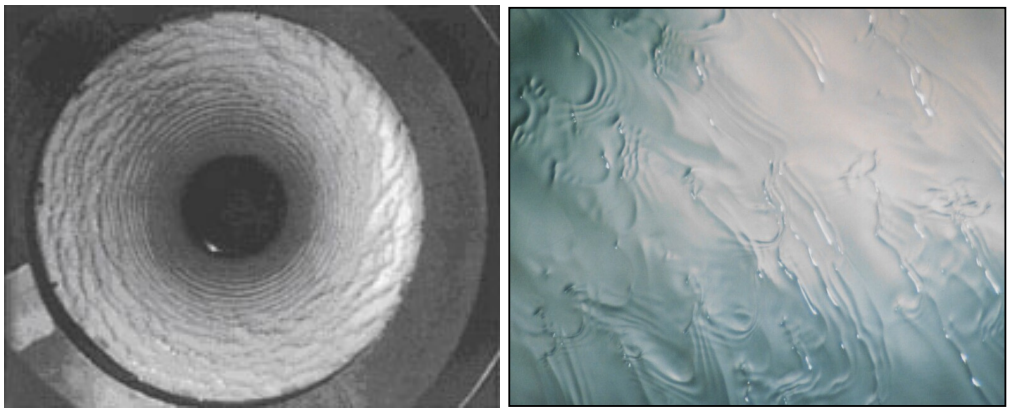

Figure 6.2 Thin wavy film formations on the spinning disc [6]

A wide range of applications of SDRs has been explored including polymerization reactions that involve condensation, free radical and ionic mechanisms [7-9]. Significant enhancements in polymerization rates have been obtained within the thin films generated on the rotating reaction surface, compared to classical stirred tank reactors. The distribution of molecular weight properties was also improved. A different application of SDRs also being studied is for the continuous production of nano- and micro-size particles via reactive crystallization [10, 11]. Due to the short residence times, the micro-mixing time is less than the induction time for clustering of particles, encouraging the formation of the very smallest particles.

These applications are limited to fast reactions with large heat effects or requiring short residence time. In light of the characteristics of spinning disc reactors, they can potentially be used to intensify liquid-liquid reactions due to their excellent mass transfer and uniform micro mixing, and achieve good temperature control of systems due to their high heat transfer rate between films and the rotating discs. However, less work has been reported on the application of spinning disc reactors to liquid-liquid two-phase systems, for example transesterfication reactions for biodiesel production. However, short residence times in the spinning disc reactors may be in a dilemma for liquid-liquid reactions. On the one hand, short residence time may improve production efficiency and make continuous processes be possible. On the other hand, residence time is too short to allow slow liquid-liquid two-phase reactions to reach high conversion yields. In order to attain high reaction rates within a very limited several seconds, high speed, intense and forced molecular inter-diffusion of the reactant molecules is required. Some attempts on change the designs of spinning disc reactors have been made to enhance liquid-liquid mass transfer and reaction rate. One kind of reactor

involves two impinging jets into rotating and stationary discs through two simple nozzles which are directed toward each other as shown in Figure 6.3. The reactor combines the impinging process with high rate shear forces acting the phases. However, the effect of the impinging jet on the conversion is small at higher rotating speeds, especially when gap between two discs is very small.

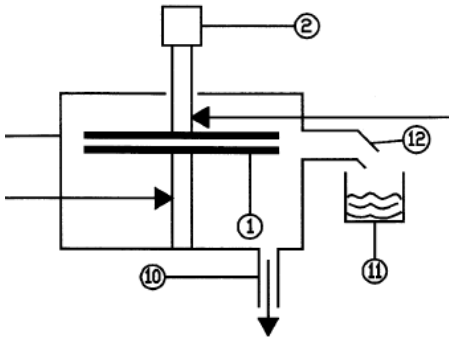

Figure 6.3 Schematic of SDR with impinging jets [12]

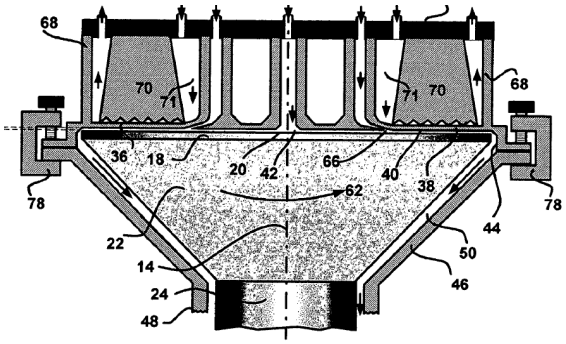

Figure 6.4 Cross section of a SDR with a special feed system

Holl [5] invented another kind of reactor based on spinning disk technology shown in Figure 6.4. The reactor uses a small spinning cylinder to facilitate high reaction rate. A special feed system was provided which is suitable for two or more immiscible reactants. Each reactant is introduced to the respective entry. The first inlet is located above the disc surface at the center of disc, which is similar to that in gas-liquid SDR. The second reactant is fed into the first film developed by the first reactant via an annular venture nozzle located

at some distance from the first entry, and the arrangement can realize respective feed of more than two liquids. The reactor also utilizes a retaining surface coextensive with the disc surface. The thickness of the gap between the disc surface and retaining surface can be adjusted to less than 1.00mm. The retaining surface is used as heat exchange means to control the reactants' temperatures passing in the gap. The reactor can effect the uniform mixing of two or more liquids within several milliseconds and the mixing length is les than 5mm. The forced inter-diffusion from the high shear rates can allow a very rapid encounter of all reactant molecules as immediately as possible, thus accelerate the observed reaction rate. However, it may be very difficult to inject liquids through a venture nozzle into so small gap size and the energy consumption may be high. Additionally, it may be unnecessary because the effect of jet is small as mentioned in the first configuration.

In this chapter, a novel intensive spinning disc reactor will be investigated to explore the possibility of improving the efficiency of biodiesel production. The modified SDR includes a stationary disc, which is coaxially spaced adjacent to a rotating parallel disc separated by only a fraction of a millimeter. Rather than high speed jet, liquid-liquid two phases are pumped from the centers of the stationary disc and the rotating disc, respectively. The performance of the new spinning disc reactor will be discussed by examining the effects of separation distance between the discs, rotational speeds, flowrates of two phase and designs of the rotating disc. Additionally, reaction conditions will be optimized to determine the values of molar ratio of methanol to oil, reaction temperature and catalyst concentration which result in the highest biodiesel conversion. A grooved disc design was provided to obtain longer residence time and its influence on biodiesel synthesis was discussed. Finally,

the performance of the intensified spinning disc reactor will be compared with that of stirred tank reactors.

6.2 Experimental

6.2.1 Chemicals

Canola oil (ConAgra Foods, USA), anhydrous methanol, and sodium hydroxide (Fisher) were used in the biodiesel synthesis. Sodium methoxide was prepared by dissolving sodium hydroxide in methanol. The amounts of sodium hydroxide and methanol were determined based on the molar ratio of methanol to oil and also based on the catalyst concentration in oil phase. Methyl esters standards for fatty acid analysis included methyl palmitate (Fluka), methyl oleate, methyl stearate methyl linoleate, and methyl linolenate (Sigma). The internal standard used was eicosane (Aldrich) and hexane (Fluka) was used as the solvent. All these reagents were GC grade (≥99%). Decaglycerol monooleate (Polyaldo 10-1-0 KFG, CAS #67784-82-1) was kindly provided by Lonaza Inc., USA.

6.2.2 Design of the Novel Intensive Spinning Disc Reactor

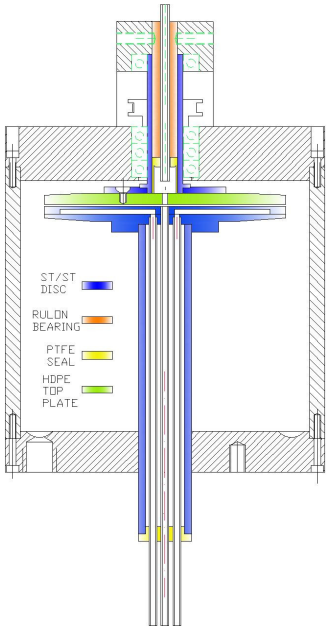

Figure 6.5 Design of the intensified spinning disc reactor

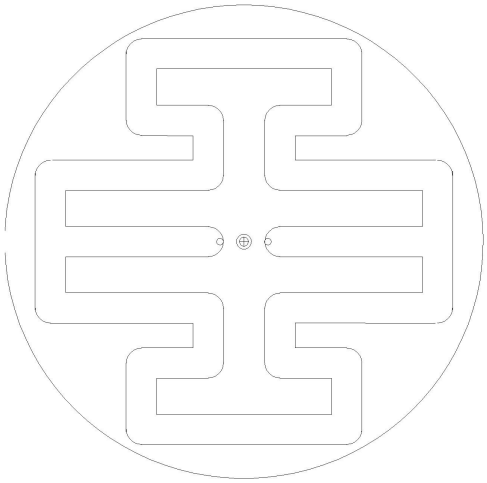

Figure 6.6 Heating/cooling pattern inside the bottom disc

The design of new intensified spinning disc reactor was shown in Figure 6.5. It comprises two very narrowly apart discs of a 10cm diameter located within a cylindrical containment, which is used to collect liquid mixture sprayed from the gap between two discs. The upper part of the reactor consists of a rotating disc made of HDPE mounted on a hollow shaft. The stainless steel shaft is supported by a ball bearing (15mm×28mm×7mm, 6902RS, McMaster) assembly and a plexiglass cover sitting above the cylindrical containment. The rotation of the top disc can be achieved when the shaft is driven by a 90V DC motor (Dayton 4Z825, Grainger) via a pulley (McMaster) and a belt (McMaster). The rotational speed is adjustable using a DC variable speed control (15DVE, Dart Controls, USA). The oil phase can be pumped into an entry at the center of the rotating disc through a glass tube coaxially installed through a rulon bearing. The lower part of the reactor comprised a stainless steel stationary disc also mounted on a hollow shaft. Small gap sizes (about several hundred microns) need very high precision on machining of disc surface and the degree of parallel between discs.

The inner structure of the stationary disc was configured as shown in Figure 6.6 in order to increase heat transfer area. Two steel tubes were welded to the low part of the bottom disc for the introduction of heating media supplied by a bath circulator (Isotemp 3016p, Fisher

Scientific). Another stainless steel tube was connected to an entry located at the center of the bottom disc to allow sodium methoxide to be introduced into the narrow reaction zone. The stationary disc was adjustable to allow variation of the separation distance between two discs.

The mean residence time in a spinning disc reactor can be increased by grooving the rotating discs's inner surface [13]. A new grooved rotating disc was designed in order to obtain longer mean residence time than the smooth disc in the novel spinning disc reactor. The rotating disc comprises eight grooves. The width and depth of each groove were designed to be 5mm and 0.5mm, respectively. The dimension and structure of the grooved disc is shown in Figure 6.7.

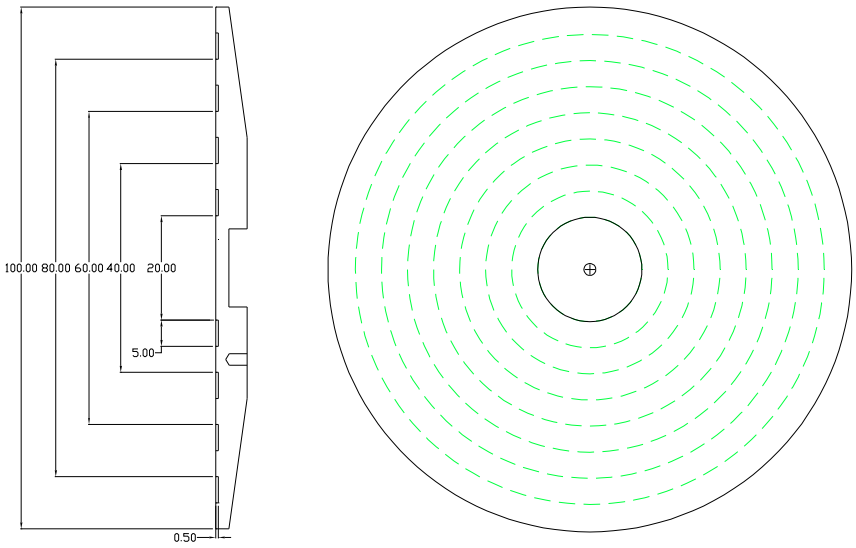

Figure 6.7 Dimension and structure of the grooved rotating top disc

6.2.3 Experimental Setup, Procedures and Sampling Method

Figure 6.8 presents the schematic of experimental setup for biodiesel synthesis. It mainly comprises an intensive spinning disc reactor, a feed system and a temperature control system.

At the beginning of each experiment, the heating circulator was turned on and the temperature was preset to the required reaction temperature, and the gap between two discs was adjusted to be predetermined value using a feeler guage (England). When the temperature in circulator reached the setpoint, DC motor was started and the rotational speed was adjusted to setpoint by the power controller and measured using a laser photo digital tachometer (VC265981, Neiko Tools, USA). The canola oil and sodium methoxide were continuously charged into the upper inlet and lower inlet of the spinning disc reactor at fixed flowrates using a peristaltic pump (101U, Watson-Marlow, England) and a piston pump (A0024753, Cole-Parmer, USA), respectively. The flowrates of these two phases were determined based on the desired molar ratio of methanol to oil. The oil phase was preheated near to the reaction temperature via a heating tape located around the inlet line. A digital thermometer (14-648-44, Fisher Scientific) was used to measure the temperature of the product stream from the reaction zone. Upon the attainment of the steady state, timing of each run was commenced. Every five minutes, 2 ml of sample were continuously collected at the sampling point into a 15 ml centrifuge tube. The tube was pre-filled with 5 ml deionized water and was refrigerated prior to use. The sample was quenched in the centrifuge tube by placing the tube into ice water. Totally four samples were collected within about 20 minutes. The samples were shaken gently to stop reaction and wash fatty acid methyl esters (FAMEs). Upon washing, unreacted ethanol, sodium hydroxide and glycerol were assumed to be present in the heavy phase, and the FAMEs and bound glyceride in the light phase. The liquid phases were further centrifuged at 3000 rpm for 20 min to ensure a thorough separation. The upper layer was samples and analyzed using GC. The analysis method and the calculation of conversion yields are seen in Chapter 5. The actual experimental setup is

shown in Figure 6.9, and the running DC motor and reactor is shown in Figure 6.10.

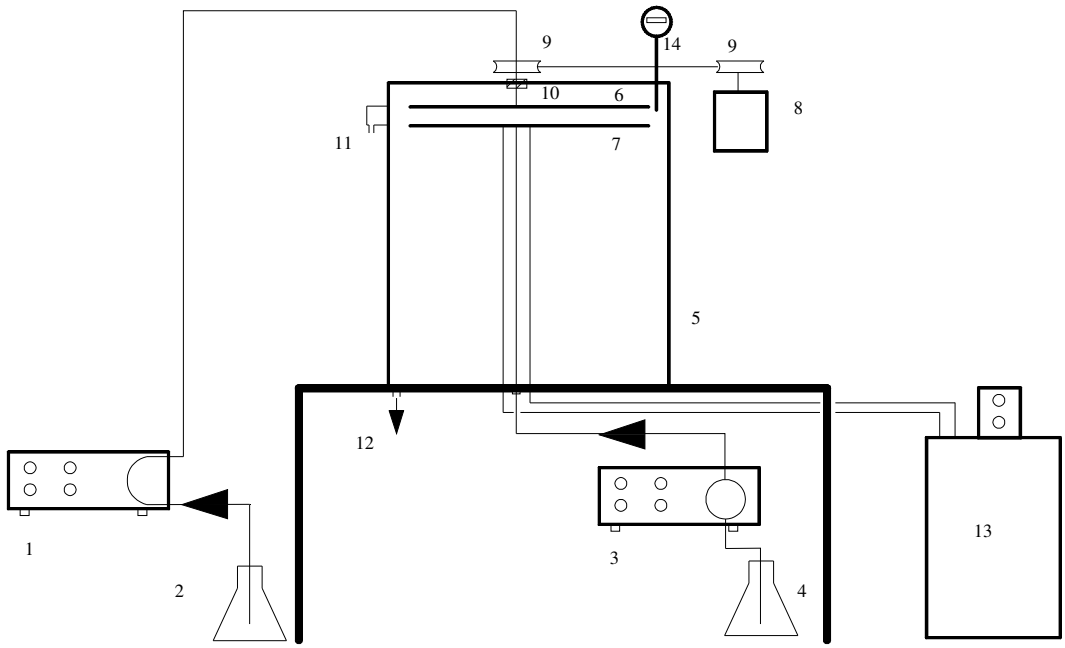

(1) Peristaltic pump; (2) canola oil vessel; (3) digital piston pump; (4) sodium methoxide vessel; (5) cylinder; (6) rotating disc; (7) stationary disc; (8) variable-speed DC motor; (9) pulley; (10) bearing assembly; (11) sampling point; (12) products drainage; (13) heating circulator; (14) thermometer

Figure 6.8 Schematic diagram of the experimental setup for biodiesel synthesis

As a control experiment with which the performance of the spinning disc could be compared, a stirred reactor was used to measure the conversion of canola oil in batch mode. Comparisons between the stirred tank reactor and the intensive spinning disc reactor were conducted at different reaction temperatures. Rather than the stirred reactor in Chapter 5, this reactor consists of a 1000 ml three-neck round bottom flask, a water bath and a condenser. An isotemp stirrer (Fisher Scientific) was used to provide heating and mixing. A thermometer was inserted inside the flask through a neck to monitor the temperature of mixture. Tubing connected with a syringe was put into flask through another neck for

sampling. The glass condenser was installed through the center neck of the flask to cool the methanol vapor. Prior to experiment, 100g of canola oil and magnetic stirrer bar (50mm length×9.35m width×9.35mm height) were poured into the clean flask. The isotemp stirrer was set to the desired values of temperature and stirring speed to heat and agitate the oil. Once the temperature reached, sodium methoxide was introduced gently into the flask to avoid strong disturbance. At this point the reaction begun and the timing started. The sampling method is identical to that used in the spinning disc reactor. Time intervals should be short in the initial 10 min because the reaction is very fast. The samples were separated by a centrifuge and analyzed using GC.

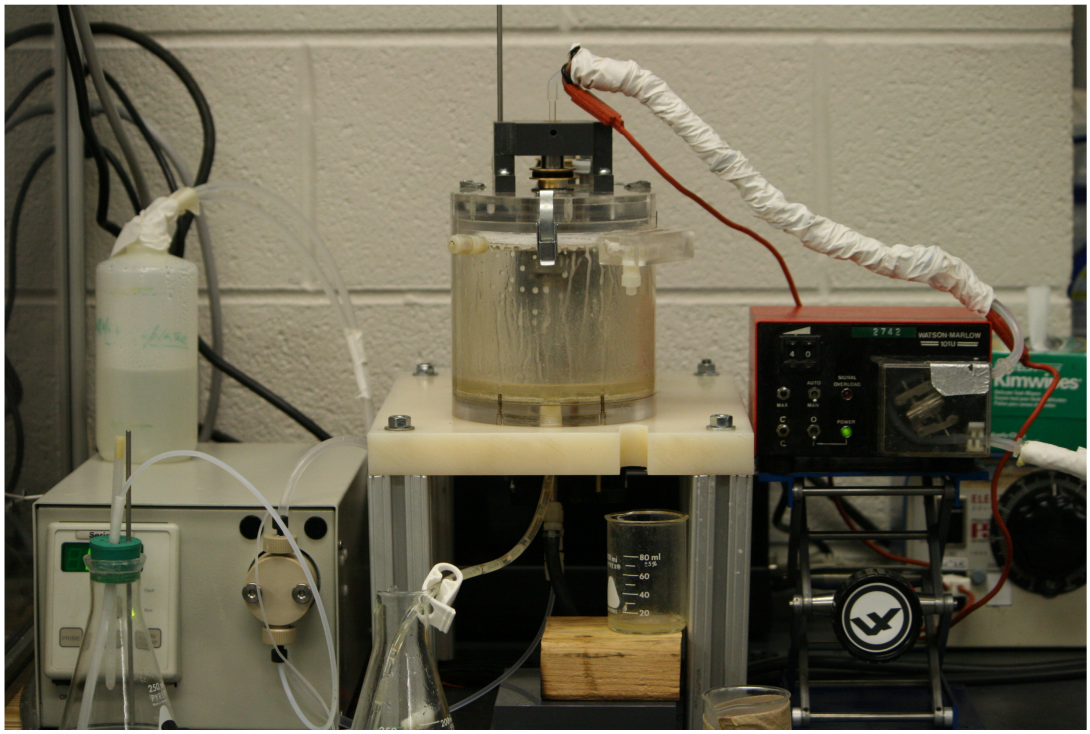

Figure 6.9 Experimental setup of the intensive spinning disc reactor for biodiesel synthesis

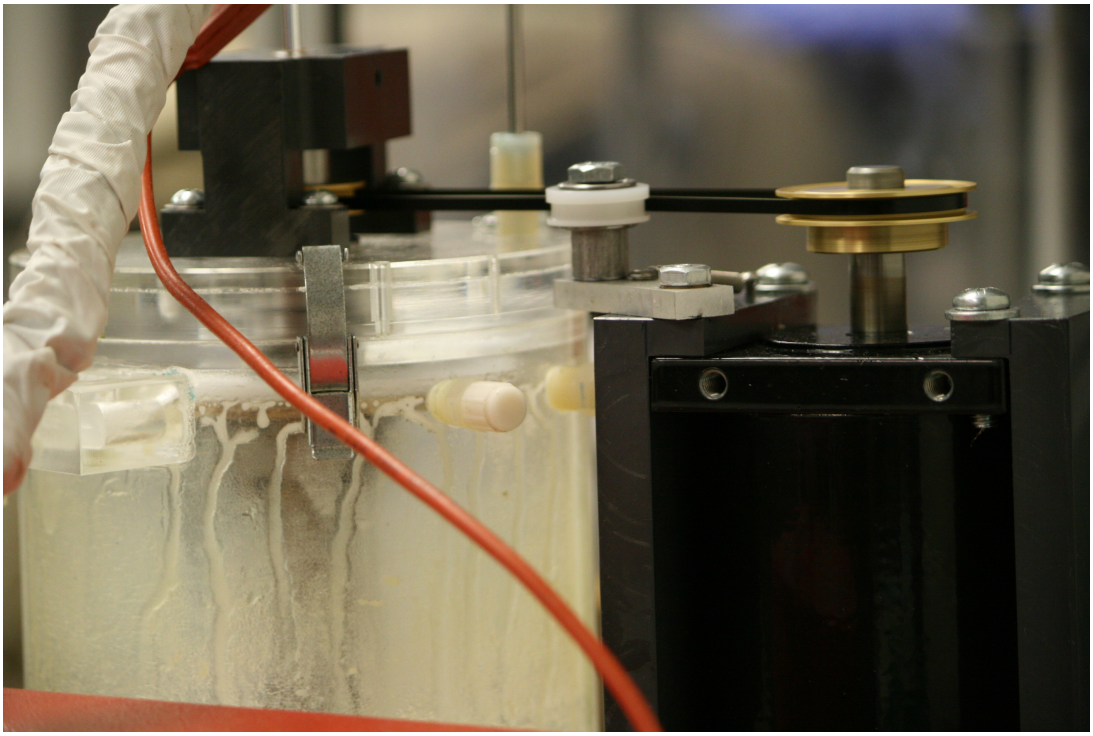

Figure 6.10 Running DC motor and intensive spinning disc reactor

In order to study the mixing produced by the new spinning disc reactor and compare its performance with that in the stirred tank reactor, mixing experiments were carried out in the two reactors without catalyst of sodium hydroxide. Decaglycerol monooleate was used a dispersant and was pre-dissolved into methanol to slow down droplets coalescence process. It has been verified to be the best dispersant to stabilize the droplets for size distribution measurement [14, 15]. During experiments, the molar ratio of canola oil to methanol was 1:1 in order to lower the turbidity of the dispersions which prevented reproducible droplet size measurements. The concentration of decaglycerol monooleate was 0.1wt% in canola oil and methanol. In the stirred tank reactor, the emulsions were prepared with 50g of canola oil and 1.72g of the mixture of decaglycerol monooleate and methanol solution at room temperature. The stirring speed was 1000 rpm. 3ml of emulsion samples were removed by a syringe for droplet size measurement at different times. In the spinning disc reactor, the emulsions were

prepared by charging canola oil phase and methanol phase with the predetermined flowrates at room temperature. The gap size was set to 0.2mm. 3ml of emulsion samples were collected for droplet size measurement. Size distributions were determined by photon correlation spectroscopy of quasi-elastically scattered light using a 90 plus/BI-MAS particle size analyzer (Brookhaven Instruments Corporation, USA).

6.3 Results and Discussion

6.3.1 Effect of Some Parameters on the Performance of the Novel Spinning Disc Reactor

- **Gap Size**

Shear stress is inversely proportional to the separation distance between two discs or gap size when rotational speeds are constant. It means that the degree of mixing can be enhanced by smaller gap sizes. Figure 6.11 shows the effect of the gap sizes on the biodiesel yield. The yield of biodiesel from canola oil at the lower flowrate of canola oil and room temperature was increased from about 25% to 55% when the gap size decreased from 0.40mm to 0.10mm at a rotational speed of 1000rpm. This could be explained by higher mixing intensity brought about at the smaller gap size. It would be expected that shear stress be inversely proportional to separation distance between two disks at a constant rotational speed resulting in more intensive mixing. On the other hand operation at a smaller gap size might reduce the effective mean residence time of the reactor, which would lead to a reduction in conversion. The results in Figure 6.12 perhaps throw some light on the opposing effect. When the rotational speed was increased to 1600rpm, the conversion rate at a 0.2mm gap size exceeded that at 0.15mm of gap size. In this case it may indicate that the reduction in residence time has a significant influence upon conversion. The conversion rate has reached about 55% at 0.1mm

gap and 25 ℃. It is very high at only several seconds of residence time although it is not as high as perhaps would be desirable in commercial production. It will be promising if reaction temperature is increased to 60℃ or higher.

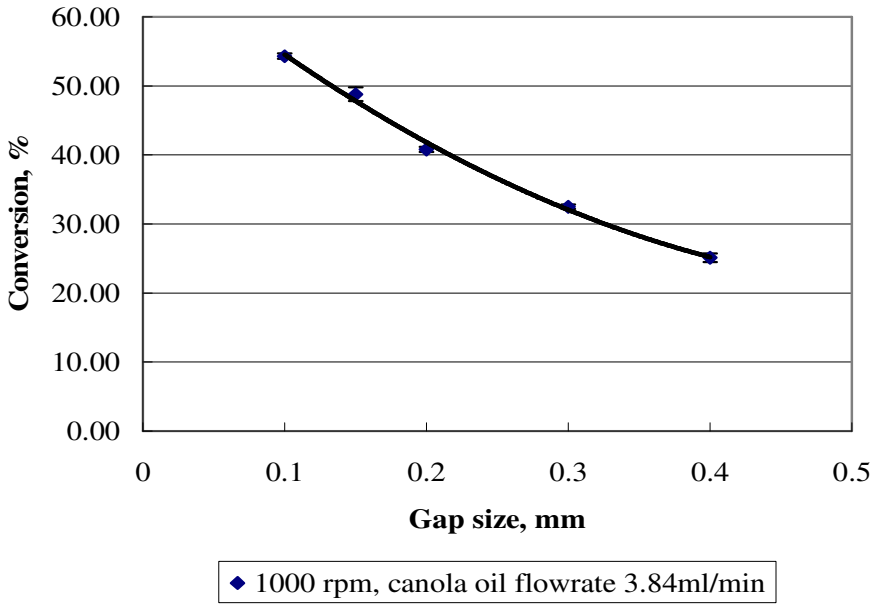

Figure 6.11 Effect of the gap sizes on the conversion of canola oil at 25℃

- **Rotational Speed**

Rotational speeds can affect shear stress and thus mixing intensity. Biodiesel conversion yields were measured at the different rotational speeds when experiments were conducted at 25℃. The flowrate of canola oil was set to 3.84ml/min. Three different results were observed in Figure 6.12. At a gap size of 0.40mm, the percent of conversion showed little changes with respect to rotational speeds. When the gap size was 0.2mm the conversion increased with respect to the rotational speeds. The increase in conversion with respect to rotational speed at a gap width of 0.2mm is consistent with improved mixing and interfacial transport processes because of enhanced shear stress. However, at gap sizes ranging from 0.1mm to 0.15mm, the

conversions decreased with increasing rotational speeds. It is difficult to explain qualitatively. Given that the liquid volume between the disks is constant, continuity dictates that the average residence time will not change except if the volumetric flowrate changes. Another explanation may be that rotational speed influenced fluid flow and residence time distribution inside the inter-disc space in a manner which can only be determined by simulation of the hydrodynamics.

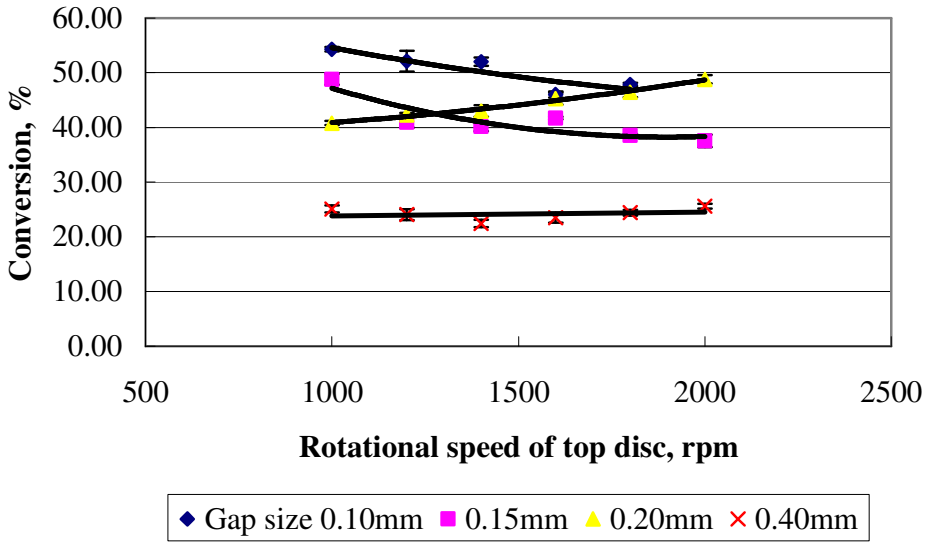

Figure 6.12 Effect of the rotational speeds on the conversion of canola oil at 25℃

- **Flowrate of Canola Oil Phase**

The flowrate of canola oil phase influences directly the mean residence time in the reactor. The flowrate of sodium methoxide phase is determined from the flowrate of canola oil phase by the molar ratio of methanol to canola oil. Hence, only the effect of the flowrate of canola oil phase was considered. Some results about the relationships between the flowrate of canola oil phase and conversions are shown in Figure 6.13 and Figure 6.14. Overall the data show that conversions reduced with respect to increase in the flowrate of canola oil, which is consistent with a reduction in mean residence time.

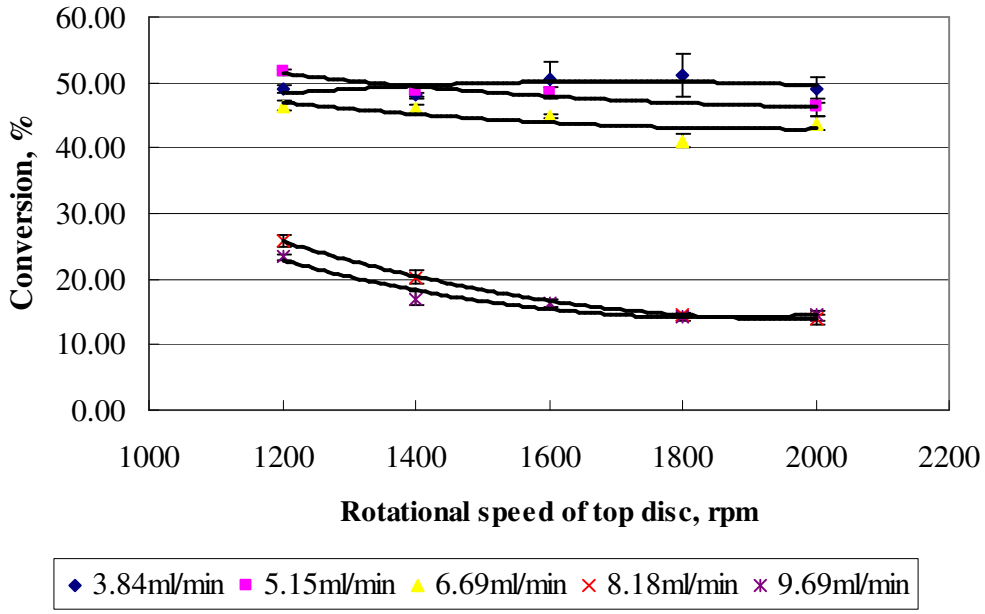

Figure 6.13 Conversions at the different flowrates of canola oil phase when gap size is 0.25mm at 25℃

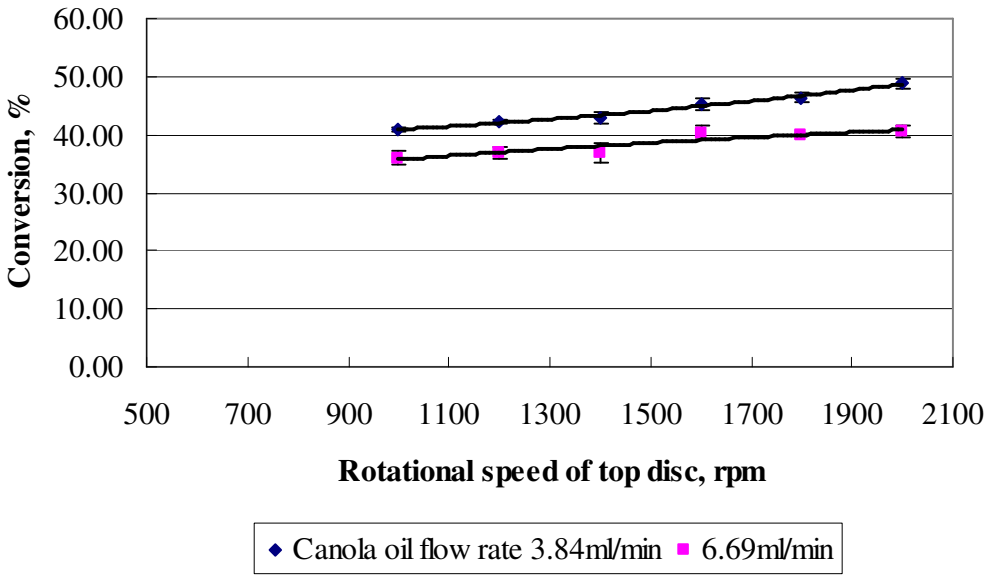

Figure 6.14 Conversions at the different flowrates of canola oil phase when gap size is 0.20mm at 25℃

6.3.2 Effect of Surface Topography of the Rotating Disc

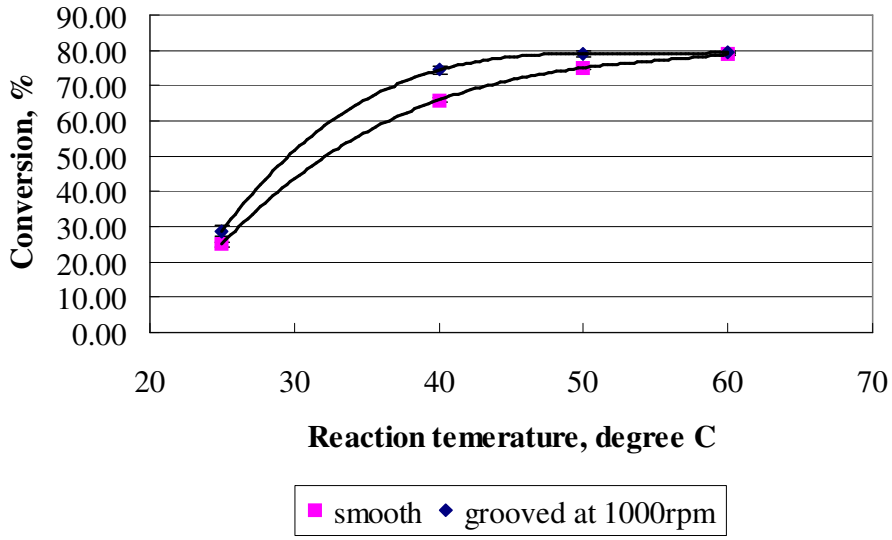

Figure 6.15 Effect of the grooved rotating surface on conversion when gap size is 0.40mm

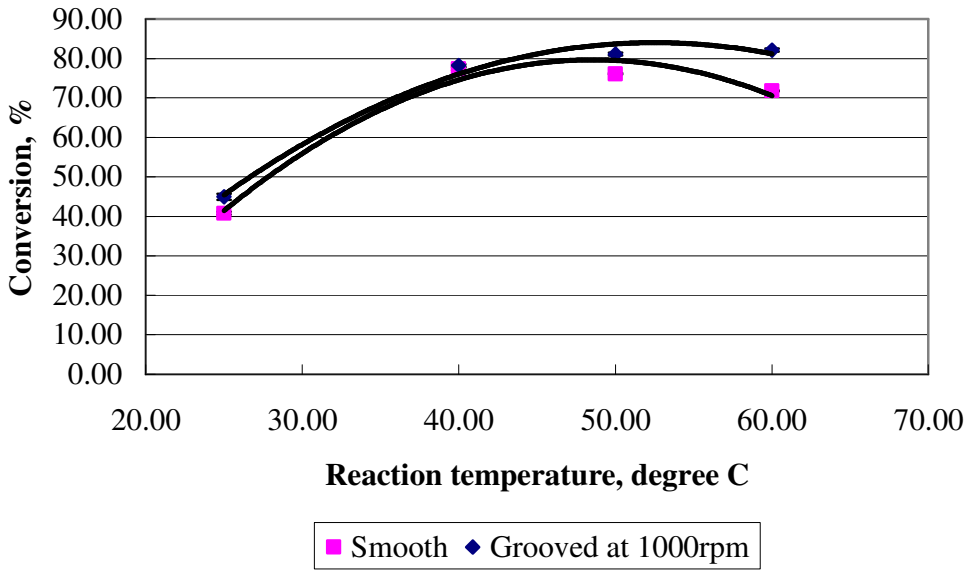

Figure 6.16 Effect of the grooved rotating surface on conversion when gap size is 0.20mm

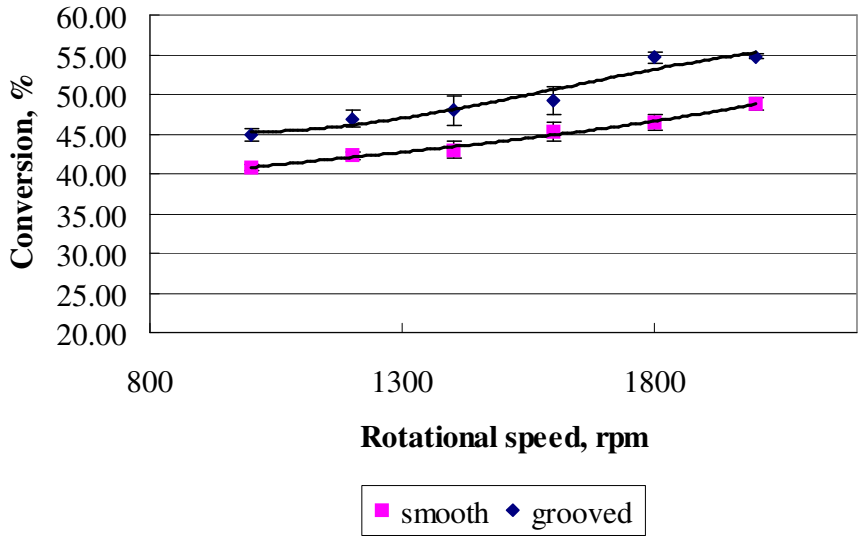

Figure 6.17 Effect of the grooved rotating surface on the conversion when gap size is 0.2mm at 25℃

Based on the above results, the canola oil conversions were relatively lower than desired for commercial production although the actual reaction temperature was as low as 25℃. One possible reason is that the residence time in the spinning disc reactor was so short that the transesterification reactions were unfinished. Grooved discs can provide longer mean residence time than smooth discs in a spinning disc reactor. Figure 6.15 presents the effect of the grooved surface on conversion rate when gap size is 0.40mm. The conversions for the grooved surface are higher than those for the smooth surface at low reaction temperatures, and then they approach to some value at 60℃. Some reasons might lead to this result. First the groove itself increased the distance between two discs, which led to smaller shear stress acting on fluids and lower conversion. It was also possible that grooved surface not only increased mean residence time but also affected residence time or radial velocity distribution. The change of residence time or radial velocity distribution might be different at different

reaction temperatures because of the change of viscosity of fluids. Similar results were observed when gap size is 0.2mm as shown in Figure 6.16. Figure 6.17 shows that the grooved surface was in favor of the conversion rate with the rotational speeds when the reaction temperature was 25℃ and the gap size was 0.2mm. These assumptions need to be further confirmed by experiments and numerical simulation.

6.3.3 Optimization of Reaction Conditions

- **Reaction Temperature**

Transesterification is an endothermic reaction. Increase in reaction temperature is in favor of reaction rate and conversion. Additionally, increasing reaction temperature decreases reactants' viscosity, which reduces shear stress and mixing intensity in the new spinning disc reactor. As mentioned previously, the change of the properties of reactants may affect their flow (such as back mixing) in the reactor. Therefore, the conversion achieved in the reactor was also studied at a range of temperatures. The purpose was to find how high the conversion rate reached when temperature went up to 60℃. The temperature of the product stream leaving the inter-disc gap was measured in the experiment. In order to maintain a constant temperature, the canola oil phase in the inlet line to the reactor was preheated to the reaction temperature via a heating tape located around the inlet line.

As shown in Figure 6.18, there is a steep increase in conversion with respect to temperature in all cases as expected. Biodiesel conversion reached about 80% when reaction temperature increased from 25℃ to 60℃ for all gap sizes at 1000rpm of rotational speed. When the gap size was 0.2mm, the conversion approached to 80% at 40℃. At this point, it is not necessary to further increase reaction temperature.

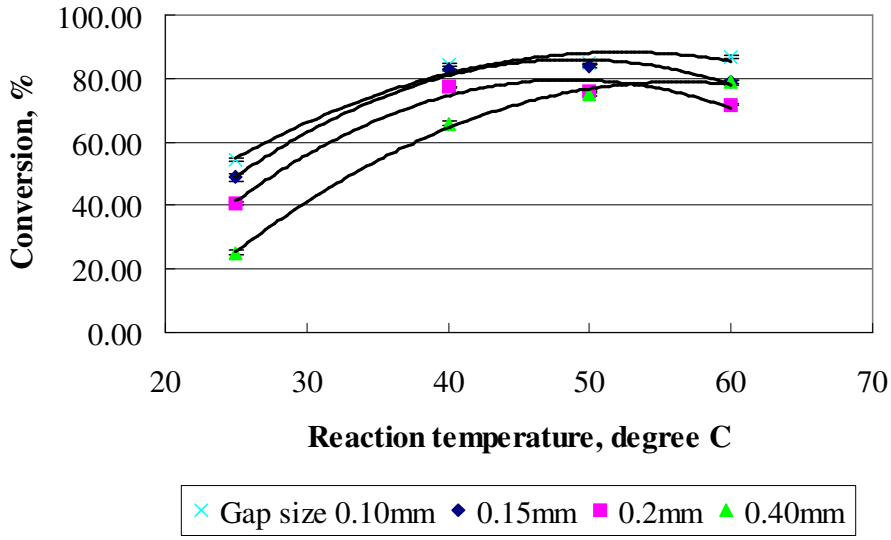

Figure 6.18 Effect of reaction temperature on the conversion at 1000rpm

- **Molar Ratio**

Molar ratio of methanol to oil is another important variable for biodiesel synthesis during transesterification reaction. High molar ratio favorably makes the reversible transesterification reaction go towards products side leading to higher conversion and faster reaction rates. However, the excessive use of methanol not only increases production cost but also makes the downstream processing more difficult. Hence, usually the molar ratio of methanol to oil is 6:1 in industrial production.

The effect of molar ratio on conversion of canola oil in the new spinning disc reactor was investigated when the concentration of catalyst was fixed to1 wt% in canola oil. The result is shown in Figure 6.19 for 0.2mm gap size and 40℃ reaction temperature. In the new spinning disc reactor, the quantity of methanol increased as the molar ratio went up. On the one hand, excessive methanol led to higher conversion in thermodynamics. On the other hand, increased quantity of methanol resulted in higher flowrate of reaction mixture and shorter residence time, which lowered conversion in kinetics. Hence, conversion rates might

decrease in the modified spinning disc reactor after increasing initially. As shown in Figure 6.19 the conversion reached a maximum value of 80% when the molar ratio was about 6 in the new spinning disc reactor.

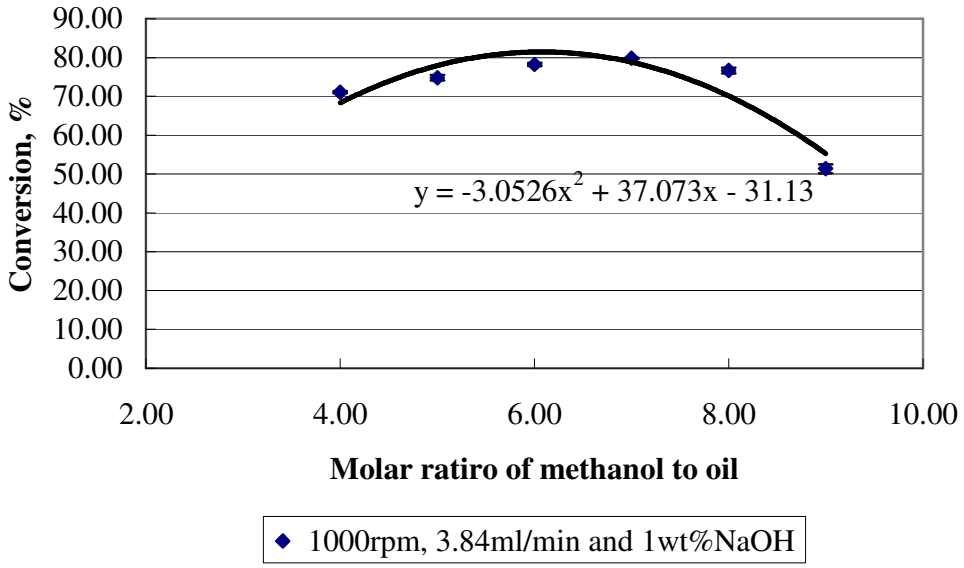

Figure 6.19 Effect of molar ratio on the conversion when gap size is 0.20mm at 40℃

- **Catalyst Concentration**

The effect of catalyst NaOH concentration in canola oil on the conversion was examined and the result is presented in Figure 6.20. The conversion rate is continuously increasing when the concentration of NaOH changes from 1 wt% to 1.5 wt%, but high NaOH concentrations bring about more soap formation. Hence, high catalyst concentration is not suggested.

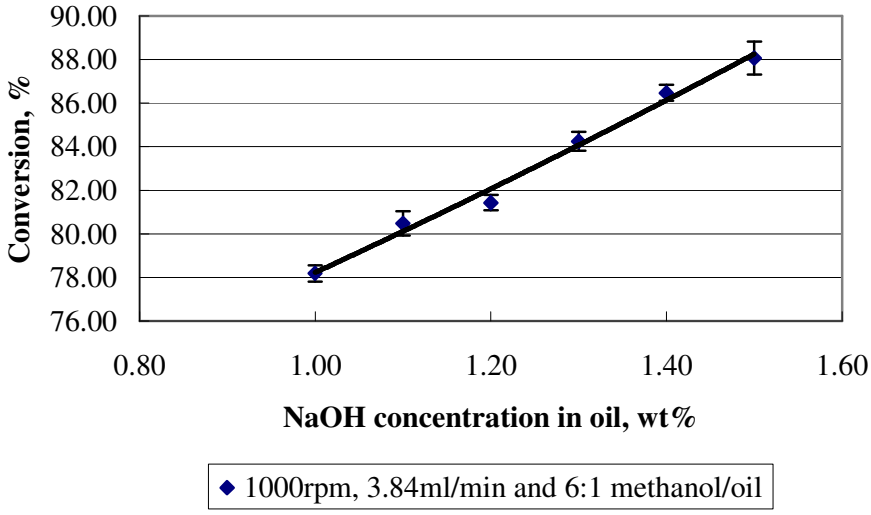

Figure 6.20 Effect of NaOH concentration on the conversion when gap size is 0.20mm at 40℃

6.3.4 Comparisons with the Stirred Tank Reactor

In order to investigate the degree of enhancement in the modified spinning disc reactor for biodiesel synthesis, some results were compared with those obtained in a stirred tank reactor based on the conversion and liquid droplet size distribution.

- **Conversion**

Figure 6.21 shows the conversion vs. residence time curves in the stirred tank reactor at the reaction temperatures in the range of 25-60℃. Figure 6.22 presents the ratio of conversion to equilibrium conversion against residence time. Reactions were carried out under the conditions of 6:1 molar ratio, 1wt% NaOH in oil and 1000rpm stirring speed. When reaction temperature was 40℃, it took two minutes for the reaction conversion to achieve about 80% in the stirred tank reactor. Under the same conditions, it only took several seconds to achieve the same conversion in the new spinning disc reactor as shown in Figure 19. The reaction rate was enhanced due to good performance of the new reactor.

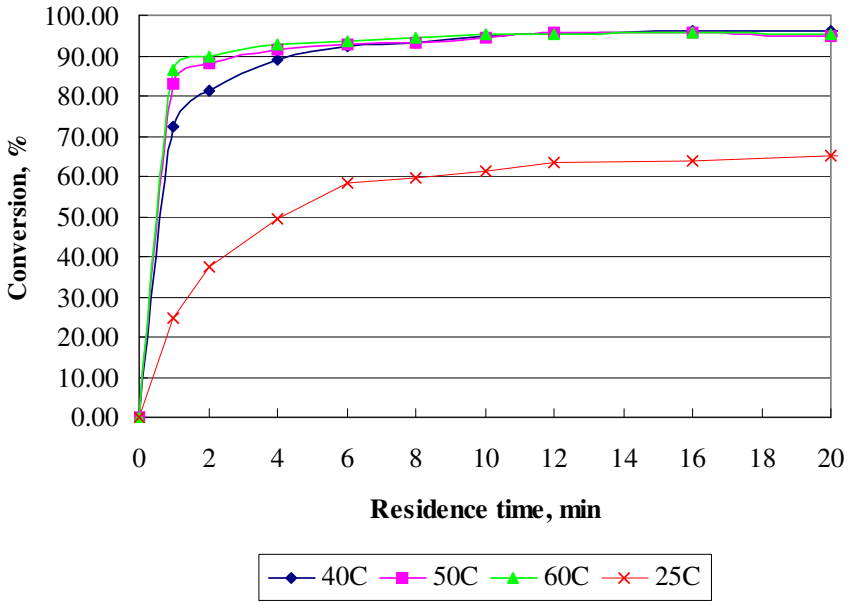

Figure 6.21 Conversion vs. residence time at difference reaction temperatures under the conditions of 6:1 methanol/oil, 1wt%NaOH and 1000rpm stirring speed (250 rpm for 25 ℃) in the stirred tank reactor

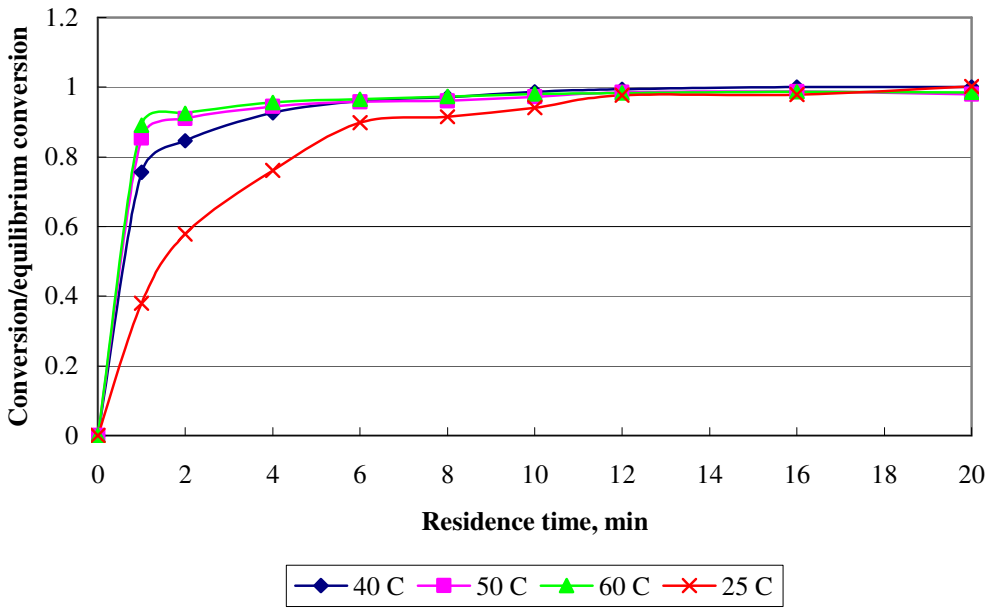

Figure 6.22 Conversion/equilibrium conversion vs. residence time at difference reaction temperatures under the conditions of 6:1 methanol/oil, 1wt%NaOH and 1000rpm stirring speed (250 rpm for 25 ℃) in the stirred tank reactor

- **Droplet Size Distribution**

Figure 6. 23 showed the cumulative droplet distributions for the stirred tank reactor at the different residence time. The droplet size at 10 seconds had a wider distribution. Increasing residence time narrowed the distribution. Simultaneously, the mean droplet size decreased with time. The mean droplet size was 434 nm at 10 seconds, and only 166 nm after 1 hr of residence time. Considering the residence time in the spinning disc reactor is only several seconds, the droplet size distribution at 10 seconds in the stirred tank reactor was compared with that in the modified spinning disc reactor. Figure 6.24 presented the results. The mean droplet size was 257 nm at 1000 rpm of rotational speed by the spinning disc reactor, approximately a half of that in the stirred tank reactor. Furthermore, the droplet size distribution by the spinning disc reactor was narrower. It can be concluded that the mixing efficiency was improved greatly by the spinning disc reactor and conversion rate was increased significantly.

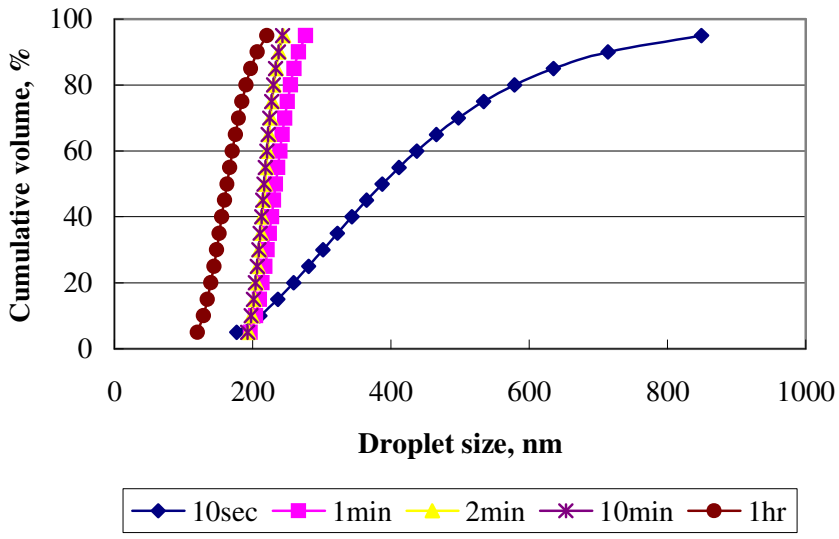

Figure 6.23 Cumulative droplet size distributions for the stirred tank reactor at the different residence times (1:1 of Molar ratio of methanol to canola oil and 25℃)

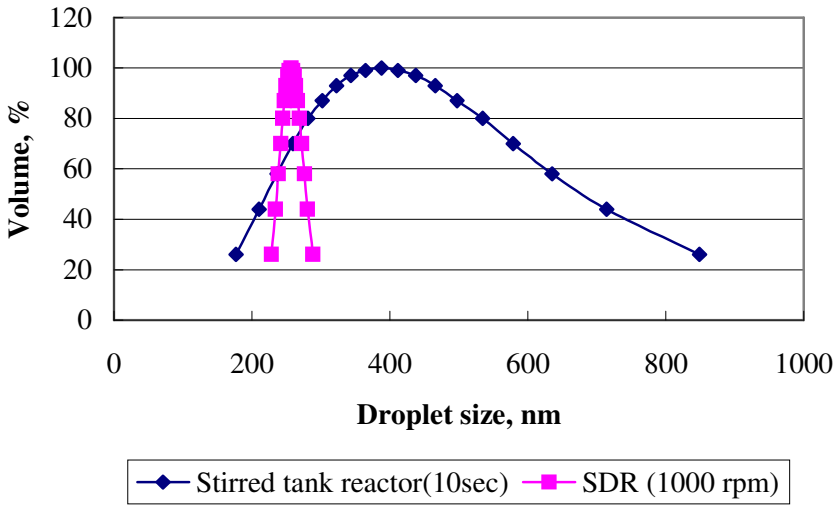

Figure 6.24 Comparison of droplet size distributions for the stirred tank reactor and the spinning disc reactor

6.4 Conclusions

In this chapter a modified spinning disc reactor was developed for intensified synthesis of biodiesel. In order to produce intense and forced micromixing of liquid-liquid two phase and achieve high conversion within a short time, the novel reactor was designed to comprise two flat discs, located coaxially and parallel to each other with a very small gap between the discs. The gap size is only about a fraction of millimeter. Simultaneously, a grooved rotating disc was used to increase residence time allowing relatively slow transesterification reaction to be as complete as possible. Compared with other spinning disc reactors, the new design is simpler and may be lower in energy consumption.

The performance of the new spinning disc reactor was investigated for the biodiesel synthesis from canola oil and methanol in the presence of a sodium hydroxide catalyst. The conversion achieved in the reactor was significantly influenced by the size of inter-disc gap, the rotational speed, the canola oil phase flowrate, the surface topography of the rotating disc,

and the reaction temperature. These factors determined the residence time, mixing intensity and fluid dynamics in the new spinning disc reactor and consequently biodiesel yields. The gap size showed the strongest influence on reactor performance with a clear improve in performance as the gap size was decreased. This is partially explained by the increase in local shear stresses and mixing intensity as the gap is decreased. The influence of rotational speed of the top disc was less clear, showing a decrease in performance with respect to disc speed at smaller gap sizes and at higher phase flowrates, the reverse being the case at larger gap size and lower phase rates. Increasing flowrate of reactants definitely decreases biodiesel conversion in our novel reactor. The grooved disc surface had a clear influence on reactor performance, with a marked increase in conversion achieved compared with a smooth disc. A very marked increase in reactor performance was noted as temperature was increased in the range 25-60℃. The increase in this range was observed at all gap sizes studied in the range 0.1-0.4mm. High temperature can aid to biodiesel yield but it may bring about more soap formation and resulting difficulty of downstream processing.

The experimental conditions were optimized including the molar ratio of two phases and catalyst concentration. The optimum value of molar ratio of canola oil to methanol was 6:1. Larger molar ratios decreased the canola oil conversion possibly due to shorter residence times. High catalyst concentration was in favor of high conversion, but it should be limited due to the resulting increased production cost.

The two-disc, spinning disc reactor demonstrated greatly increased rates of reaction for biodiesel synthesis from canola oil and methanol, at a range of temperatures when compared with a stirred tank reactor. One of reasons is that the new spinning disc reactor produced smaller droplet sizes and narrower distribution than conventional agitation, leading to more

interfacial area for the reaction to occur. The two-disc spinning disc reactor at 0.2mm of gap size and 1000 rpm of rational speed produced dispersions with average droplet sizes 40% smaller than those generated using the stirred tank reactor at room temperature.

Fluid hydrodynamcs influenced the performance of the new spinning disc reactor, but it is still unclear and some results have not been well explained. These phenomena include the effect of gap size and rotational speed on fluid flow and mixing, and thus residence time distribution. There are some difficulties in the experiment due to too small gap. Computational fluid dynamics (CFD) is a good approach. Fluid flow can be investigated by numerical simulation using professional CFD software. Some initial work has been started in a good way.

6.5 References

1. A. Stankiewicz and A.A.H. Drinkenburg, Process intensification: History, philosophy, principles, in: Re-engineering the chemical processing plant process intensification, edited by A. Stankiewicz and J.A. Moulijn, Marcel Dekker, Inc., 2004.
2. http://www.protensive.co.uk/pages/equipment/category/categoryid=SDR
3. A. I. Stankiewicz, J.A. Moulijn, Process intensification: transforming chemical engineering, Chem. Eng. Pro., 96 (2000) 22-34.
4. R. Jachuck, Process intensification for responsive processing, Trans IChemE, 80 (2002) 233-238.
5. R.A. Holl, Methods of operating surface reactors and reactors employing such methods, Patent US 7,125,527 B2, 2006.

6. C. Ramshaw, The spinning disc reactor, in: Re-engineering the chemical processing plant process intensification, edited by A. Stankiewicz and J.A. Moulijn, Marcel Dekker, Inc., 2004.
7. K.V.K. Boodhoo and R.J. Jachuck, Process intensification: spinning disk reactor for styrene pol, Applied Thermal Engineering, 20 (2000) 1127-1146.
8. K.V.K. Boodhoo and R.J. Jachuck, Process intensification: spinning disk reactor for condensation polymerization, Green Chemistry, 2 (2000) 235-244.
9. K.V.K. Boodhoo, W.A.E. Dunk, M. Vicevic, R.J. Jachuck, V. Sage, D.J. Macquarrie, J.H. Clark, Classical cationic polymerization of styrene in a spinning disc reactor using silica-supported BF_3 catalyst, J. of Applied Polymer Science, 101 (2006) 8-19.
10. R.J. Jachuck, M.J. Scalley, Process technology for continuous production of nano-micron size particles, AICHE Spring National Meeting, 2003.
11. C. Y. Tai, C. T. Tai, H. S. Liu, Synthesis of submicron barium carbonate using a high-gravity technique, Chem. Eng. Sci., 61 (2006), 7479-7486.
12. A.M. Dehkordi, Liquid-liquid extraction with chemical reaction in a novel impinging-jets reactor, AIChE J., 48 (2002) 2230-2239.
13. R. Jachuck, Process intensification: smaller, smarter and cleaner process plants for a sustainable environment, 2005.
14. P. Wu, Y. Yang , J. A. Colucci and E. A. Grulke, Effect of ultrasonication on droplet size in biodiesel mixtures, J. Am. Oil Chem. Soc., 84 (2007) 877–884.
15. Z. Wen, X. Yu, S.-T. Tu, J. Yan, E. Dahlquist, Intensification of biodiesel synthesis using zigzag micro-channel reactors, Bioresour. Technol. 100 (2009) 3054-3060.

Chapter 7 Conclusions and Future Work

To overcome inefficient liquid-liquid mixing in stirred tank reactors, this work put forward two process intensification technologies: liquid spraying in the presence of electrostatic field and the two-disc spinning disc reactor. They were firstly applied to enhance biodiesel synthesis. Interfacial turbulence is one of the important factors involved in electrically enhanced mass transfer. To understand the mechanics of interfacial turbulence or Marangoni phenomena, the Schlieren optical technique was developed and the experimental setup was built for the visualization of interfacial phenomena in the ethanol-water-1-decanol system. Two Schlieren cells were designed and fabricated, and were successfully used for the interrogation of interfacial disturbances in pendant droplets and at plane interfaces. At the lower concentrations of ethanol in aqueous phases, no interfacial convection was observed in the absence of electric fields. However, electric fields were able to promote interfacial turbulence in the ethanol-water-1-decanol system easily even when the concentration of ethanol was low. The intensity of interfacial turbulence was affected by the applied potential, becoming intense with increasing potentials. It was shown that interfacial mass transfer could be enhanced by electrostatic fields. For the ethanol-water-1-decanol system, interfacial convection originated at the interface and spread into the 1-decanol phase for both pendant droplets and plane interfaces. Some weak interfacial convection was also observed in the aqueous phase for the plane interfaces. The interfacial convection clearly exhibited time-dependency with evidence of attainment of interfacial equilibrium after some finite time.

Interfacial turbulence is a complicated phenomenon in the presence of electric fields. The current effort is not enough to understand its effect on mass transfer. It needs more works to

do in the future. These tasks may include the investigation of interfacial turbulence in the presence of pulsed DC and for other liquid-liquid systems with different viscosities and interfacial tensions, study of the influence of surface active agents. In our work, interfacial turbulence was observed for non-flow two phases. Hence, another possible task is to explore the interfacial turbulence when the both phases are flowing under controlled conditions.

Two corresponding experimental setups were built to study liquid-liquid interfacial mass transfer from an aqueous pendant droplet and across a plane interface into 1-decanol phase under applied electric fields. Initial data of mass transfer coefficients were obtained for the mass transfer from a pendant droplet. Changes in ethanol concentrations in both phases and the corresponding mass transfer coefficients showed a time-dependent nature which correlated closely with the Schlieren images described in Chapter 3. Mass transfer measurements in a small flow cell provided further evidence of the above phenomena. Moreover, all data show that mass transfer can be intensified by the application of electric fields. Some initial data and results have been obtained in my experiment, but they are not good as expected. Some proposals have been provided and may improve the data quality. These ideas include a new design of the concentric nozzle and the flow cell, and development of a more accurate the sampling method for the pendant droplets.

To improve production efficiency in bidoesel synthesis through alkali-based transesterfication, a novel intensive contactor was developed using the principle of electrostatic spraying in Chapter 5. Firstly, the reaction rate of transesterification of canola oil with sodium methoxide was investigated in the plane interface contactor discussed in Chapter 3. Typically a fourfold enhancement was observed at an applied voltage of 10kV DC. The enhancement may be due to enhanced interfacial hydrodynamic disturbances and

electrokinetic acceleration of reactant and products in the vicinity of the interface. The change in rate of reaction may not be a continuous function of applied electric field strength and some anomalous behavior was observed at applied fields in the range 0-4kV. Further study of the relationship between electric field and interfacial tension is required. Also the enhanced accelerated migration of anionic fatty species under the influence of the electric field needs further investigation.

Secondly, a compact electrostatic spraying reactor was designed to enhance biodiesel synthesis. Typical enhancements showed a ten-fold increase in conversion rate. The design was based on simple tubular geometry with horizontal injection of an electrostatic spray of sodium methoxide. Control of the dispersed phase hold-up, and the use of partially insulated electrodes were critical to stable performance of the design. The use of pulsed electric field will be good option for sustained good electrostatic spraying. The design has potential for scale up either by direct geometrical scale-up, or by the development of a multi-module system with a number of reactors operating in parallel. Further work is required to establish in detail the relationships between applied voltages, droplet size, hold-up, and residence time. This will enable us to establish the essential parameters for the development of a design method.

The spinning disc reactor was innovated and developed for intensified synthesis of biodiesel in Chapter 6. In order to produce intense and forced micromixing of liquid-liquid two phase and achieve high conversion within a short time, the novel reactor was designed to comprise two flat discs, located coaxially and parallel to each other with a very small gap between the discs. A grooved rotating disc was integrated to increase residence time allowing relatively slow transesterification reaction to be as complete as possible. Compared with

other spinning disc reactors, the new design is simpler and may be lower in energy consumption. The conversion achieved in the reactor was significantly influenced by the size of inter-disc gap, the rotational speed, the canola oil phase flowrate, the surface topography of the rotating disc, and the reaction temperature. These factors determined the residence time, mixing intensity and fluid dynamics in the new spinning disc reactor and consequently biodiesel yields. The gap size showed the strongest influence on reactor performance with a clear improve in performance as the gap size was decreased. This is partially explained by the increase in local shear stresses and mixing intensity as the gap is decreased. The influence of rotational speed of the top disc was less clear, showing a decrease in performance with respect to disc speed at smaller gap sizes and at higher phase flowrates, the reverse being the case at larger gap size and lower phase rates. Increasing flowrate of reactants definitely decreases biodiesel conversion in our novel reactor. The grooved disc surface had a clear influence on reactor performance, with a marked increase in conversion achieved compared with a smooth disc. A very marked increase in reactor performance was noted as temperature was increased in the range 25-60^{o}C. The increase in this range was observed at all gap sizes studied in the range 0.1-0.4mm. High temperature can aid to biodiesel yield but it may bring about more soap formation and resulting difficulty of downstream processing. The experimental conditions were optimized including the molar ratio of two phases and catalyst concentration. The optimum value of molar ratio of canola oil to methanol was 6:1. Larger molar ratios decreased the canola oil conversion possibly due to shorter residence times. High catalyst concentration was in favor of high conversion, but it should be limited due to the resulting increased production cost.

The two-disc spinning disc reactor demonstrated greatly increased rates of reaction for biodiesel synthesis from canola oil and methanol, at a range of temperatures when compared with a stirred tank reactor. One of reasons is that the new spinning disc reactor produced smaller droplet sizes and narrower distribution than conventional agitation, leading to more interfacial area for the reaction to occur. The two-disc spinning disc reactor at 0.2mm of gap size and 1000 rpm of rational speed produced dispersions with average droplet sizes 40% smaller than those generated using the stirred tank reactor at room temperature.

Fluid hydrodynamcs influenced the performance of the new spinning disc reactor, but it is still unclear and some results have not been well explained. These phenomena include the effect of gap size and rotational speed on fluid flow and mixing, and thus residence time distribution. There are some difficulties in the experiment due to too small gap. Computational fluid dynamics (CFD) is a good approach. Fluid flow can be investigated by numerical simulation using professional CFD software such as Fluent. Preliminary work has been done and some results are included in appendix.

Appendix

Table A. 1 Physical properties of canola oil and sodium methoxide

	Canola oil	**Sodium methoxide**
Molecular weight	959.04	-
Density (25°**C**), g/ml	0.914	0.83761
Viscosity, mPa.s		
25°**C**	63.7	1.70
30°**C**	50.7	1.27
40°**C**	34.8	0.90
50°**C**	24.4	0.56
60°**C**	17.8	0.38
Surface tension, mN/n		
25°**C**	1.70	-
30°**C**	1.27	-
40°**C**	0.90	-
50°**C**	0.56	-
60°**C**	0.38	-

Part A. 1 Process Simulation of Alkali-based Transesterification for Biodiesel Synthesis

Table A.2 Kinetic parameters for transesterification reactions [1]

	Reaction activation energy (cal/mol)	*k* values at 50 °C (l/mol · min)
TG ⟶ DG	13145	0.050
DG ⟶ TG	9932	0.110
DG ⟶ MG	19860	0.215
MG ⟶ DG	14639	1.228
MG ⟶ GL	6421	0.242
GL ⟶ MG	9588	0.007

- **Simulation Specifications**

The process simulation software, Aspen Plus11.1 is used here. Because oleic acid is the major fatty acid in canola oil (Lawson, 1995), triolein ($C_{57}H_{104}O_6$) is chosen to represent canola oil in the simulation. Accordingly, methyl oleate ($C_{19}H_{36}O_2$) is taken as the resulting biodiesel product. In an addition, diolein ($C_{39}H_{72}O_5$) is chosen for diglycerides, monoolein ($C_{21}H_{40}O_4$) for monoglycerides.

Due to the presence of the highly polar components, methanol and glycerol, the non-random two liquid (NRTL) thermodynamic/activity models is suggested to predict the activity coefficients of the components in a liquid phase. A combination of NRTL and RK-Soave (NRTL-RK) thermodynamic properties were used in the simulation.

Sodium hydroxide is used as catalyst with a concentration of 1.0 wt % based on the mass of the canola oil, here represented by triolein.

➢ **Simulation Results**

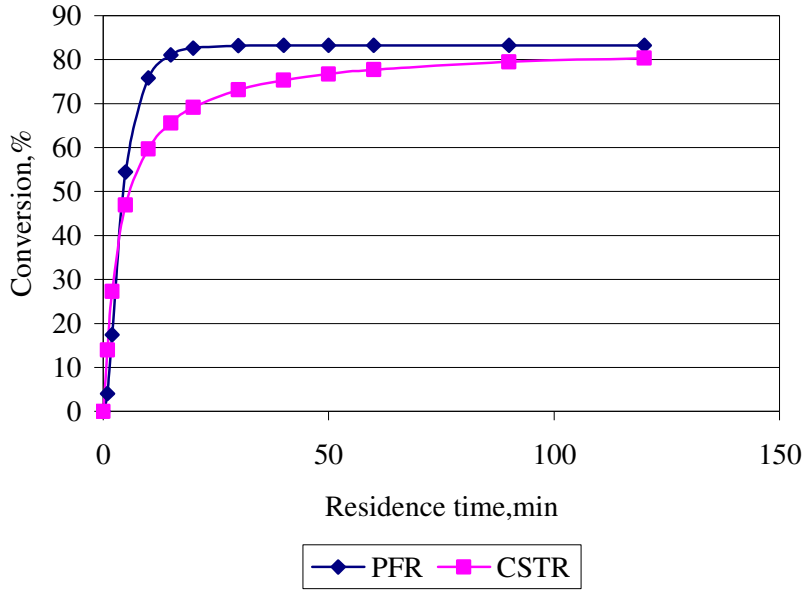

Figure A.1 Comparison of conversions of triglyceride versus residence time in two reactors at 25℃ for 6:1 of molar ratio

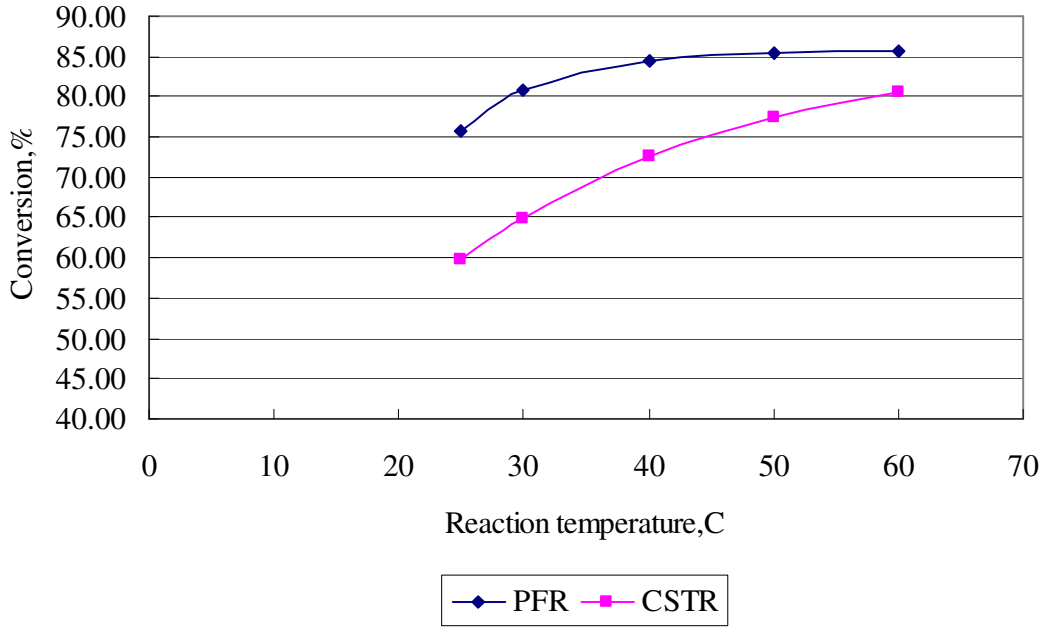

Figure A.2 Comparison of conversions of triglyceride versus reaction temperature in two reactors for 10min of residence time and 6:1 of molar ratio

Part A.2 CFD Simulation of the Two-disc Spinning Disc Reactor

➢ **Dimensions of the Two-disc Spinning Disc Reactor**

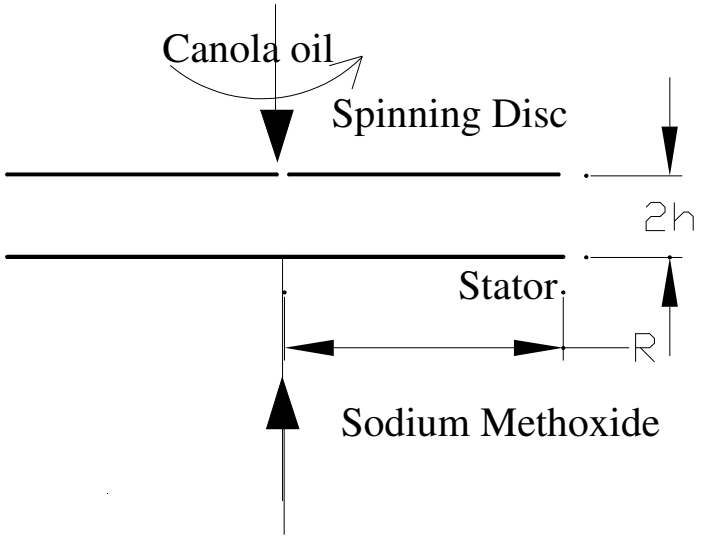

Figure A.3 Dimensions of the two-disc spinning disc reactor for biodiesel production

➢ **Modelling Development**

- **Continuity Equation:**

$$\frac{1}{r}\frac{\partial}{\partial r}(r\upsilon_r)+\frac{\partial}{\partial z}(\upsilon_z)=0 \tag{1}$$

or

$$\frac{\partial}{\partial r}(r\upsilon_r)+\frac{\partial}{\partial z}(r\upsilon_z)=0 \tag{2}$$

- **Momentum Equations:**

r direction:

$$\rho\left(\upsilon_r\frac{\partial\upsilon_r}{\partial r}+\upsilon_z\frac{\partial\upsilon_r}{\partial z}-\frac{\upsilon_\theta^2}{r}\right)=-\frac{\partial P}{\partial r}+\mu\left[\frac{\partial}{\partial r}\left(\frac{1}{r}\frac{\partial}{\partial r}(r\upsilon_r)\right)+\frac{\partial^2\upsilon_r}{\partial z^2}\right] \tag{3}$$

θ direaction:

$$\rho\left(\upsilon_r\frac{\partial\upsilon_\theta}{\partial r}+\upsilon_z\frac{\partial\upsilon_\theta}{\partial z}+\frac{\upsilon_r\upsilon_\theta}{r}\right)=\mu\left[\frac{\partial}{\partial r}\left(\frac{1}{r}\frac{\partial}{\partial r}(r\upsilon_\theta)\right)+\frac{\partial^2\upsilon_\theta}{\partial z^2}\right] \tag{4}$$

z direction:

$$\rho\left(v_r\frac{\partial v_z}{\partial r}+v_z\frac{\partial v_z}{\partial z}\right)=-\frac{\partial P}{\partial r}+\mu\left[\frac{1}{r}\frac{\partial}{\partial r}\left(r\frac{\partial v_z}{\partial r}\right)+\frac{\partial^2 v_z}{\partial z^2}\right]+\rho g \tag{5}$$

• **Nondimensionization**

$$G=\frac{H}{R} \tag{6}$$

$$\mathrm{Re}=\frac{\Omega H^2}{\nu} \tag{7}$$

$$r=r^* H \tag{8}$$

$$z=z^* H \tag{9}$$

$$v_r=v_r^*\Omega H \tag{10}$$

$$v_\theta=v_\theta^*\Omega H \tag{11}$$

$$v_z=v_z^*\Omega H \tag{12}$$

$$P=P^*\rho\Omega^2 H^2 \tag{13}$$

where H is the gap size between discs.

Continuity:

$$\frac{\partial}{\partial r^*}\left(r^* v_r^*\right)+\frac{\partial}{\partial z^*}\left(r^* v_z^*\right)=0 \tag{14}$$

Momentum:

r direction:

$$v_r^*\frac{\partial v_r^*}{\partial r^*}+v_z^*\frac{\partial v_r^*}{\partial z^*}-\frac{v_\theta^{*2}}{r^*}=-\frac{\partial P^*}{\partial r^*}+\frac{1}{\mathrm{Re}}\left[\frac{1}{r^*}\frac{\partial}{\partial r^*}\left(r^*\frac{\partial v_r^*}{\partial r^*}\right)+\frac{\partial^2 v_r^*}{\partial z^{*2}}-\frac{v_r^*}{r^{*2}}\right] \tag{15}$$

θ direction:

$$v_r^* \frac{\partial v_\theta^*}{\partial r^*} + v_z^* \frac{\partial v_\theta^*}{\partial z^*} + \frac{v_r^* v_\theta^*}{r^*} = \frac{1}{\mathrm{Re}}\left[\frac{1}{r^*}\frac{\partial}{\partial r^*}\left(r^* \frac{\partial v_\theta^*}{\partial r^*}\right) + \frac{\partial^2 v_\theta^*}{\partial z^{*2}} - \frac{v_\theta^*}{r^{*2}}\right] \tag{16}$$

z direction:

$$v_r^* \frac{\partial v_Z^*}{\partial r^*} + v_z^* \frac{\partial v_Z^*}{\partial z^*} = -\frac{\partial P^*}{\partial z^*} + \frac{1}{\mathrm{Re}}\left[\frac{1}{r^*}\frac{\partial}{\partial r^*}\left(r^* \frac{\partial v_z^*}{\partial r^*}\right) + \frac{\partial^2 v_z^*}{\partial z^{*2}}\right] \tag{17}$$

• Boundary Conditions

At the bottom stationary disc ($z^* = 0$),

$$v_r^* = v_\theta^* = v_z^* = 0 \tag{18}$$

At the top rotating disc ($z^* = 1$),

$$v_r^* = v_z^* = 0\,,\ v_\theta^* = r^* \tag{19}$$

At the center of discs ($r^* = 0$),

$$v_r^* = v_\theta^* = 0 \tag{20}$$

At the edge of discs ($r^* = 1$),

$$\frac{\partial v_r^*}{\partial r^*} = \frac{\partial v_\theta^*}{\partial r^*} = \frac{\partial v_z^*}{\partial r^*} = 0 \tag{21}$$

➢ **Preliminary CFD Simulation Results**

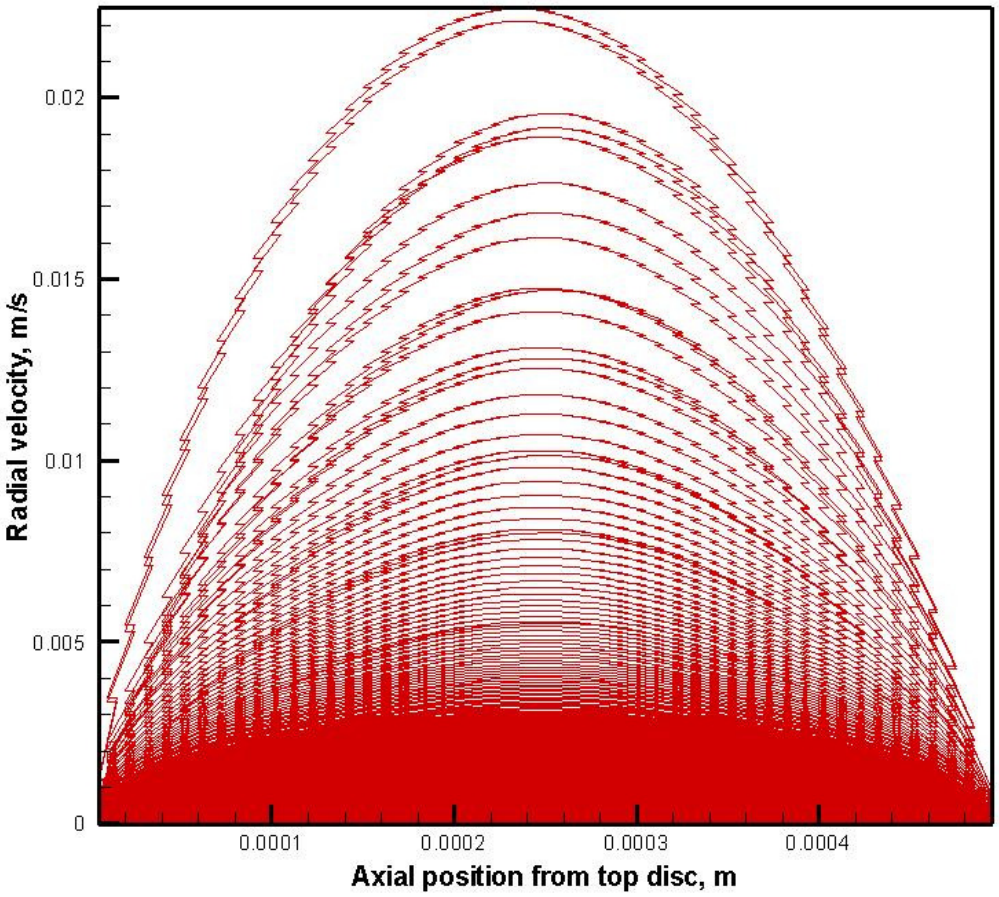

Figure A.4 Radial velocity distribution in the gap when gap size is 0.5mm and rotational speed is 0rpm

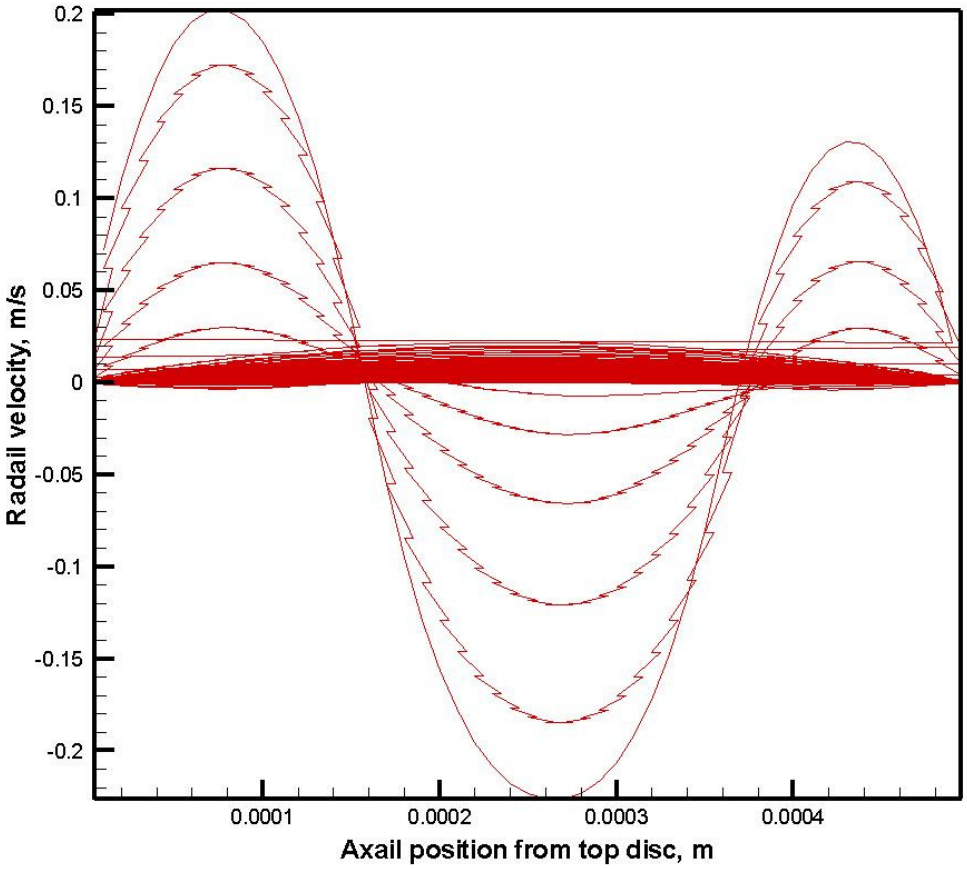

Figure A.5 Radial velocity distribution in the gap when gap size is 0.5mm and rotating speed is 1000rpm

References

1. H. Noureddini and D. Zhu, Kinetics of transesterification of soybean oil, J. of the American Oil Chemists' Society, 74 (1997) 1457-1463.